A Mechanistic Investigation of Nitrogen Evolution and Corrosion with Oxy-Combustion

Report Type:
Final Technical Report

Reporting Period Start Date: September 1, 2005
Reporting Period End Date: December 31, 2008

Principle Authors:
Dale R. Tree, Andrew J. Mackrory, Thomas Fletcher

Report Issue Date: February 1, 2009
DOE Award Number: DE-FG26-05NT42530

Submitting Organization:
Brigham Young University
A-285 ASB
Provo, Utah, 84602

Disclaimer:

Abstract

A premixed, staged, down-fired, pulverized coal reactor and a flat flame burner were used to study the evolution of nitrogen in coal contrasting differences in air and oxy-combustion. In the premixed reactor, the oxidizer was staged to produce a fuel rich zone followed by a burnout zone. The initial nominal fuel rich zone stoichiometric ratio (S.R.) of 0.85 selected produced higher NO reductions in the fuel rich region under oxy-combustion conditions. Air was found to be capable of similar NO reductions when the fuel rich zone was at a much lower S.R. of 0.65. At a S.R. of 0.85, oxy-combustion was measured to have higher CO, unburned hydrocarbons, HCN and NH_3 in the fuel rich region than air at the same S.R. There was no measured difference in the initial formation of NO. The data suggest devolatilization and initial NO formation is similar for the two oxidizers when flame temperatures are the same, but the higher CO_2 leads to higher concentrations of CO and nitrogen reducing intermediates at a given equivalence ratio which increases the ability of the gas phase to reduce NO. These results are supported by flat flame burner experiments which show devolatilization of nitrogen from the coal and char to be similar for air and oxy-flame conditions at a given temperature. A model of premixed combustion containing devolatilization, char oxidation and detailed kinetics captures most of the trends seen in the data. The model suggests CO is high in oxy-combustion because of dissociation of CO_2. The model also predicts a fraction (up to 20%, dependent on S.R.) of NO in air combustion can be formed via thermal processes with the source being nitrogen from the air while in oxy-combustion equilibrium drives a reduction in NO of similar magnitude. The data confirm oxy-combustion is a superior oxidizer to air for NO control because NO reduction can be achieved at higher S.R. producing better char burnout in addition to NO from recirculated flue gas being reduced as it passes back through the flame.

Table of Contents

Executive Summary

This work consists of experiments on two facilities designed to investigate the evolution of nitrogen from its origin in coal to NO_X emissions during combustion processes in air and O_2/CO_2 mixtures or oxy-combustion. A model of detailed kinetics, devolatilization, and char oxidation in a simple plug flow was also developed and used to interpret the data.

The first facility was a premixed, down-fired, staged reactor where the first stage was fuel rich followed by a burnout oxidizer stage. The oxidizer was varied from air (23% O_2 by mass in N_2) to two different mixtures of O_2 and CO_2 (25% and 30% O_2 by mass). Three coals were investigated including Pittsburgh #8, Illinois #6, and Powder River Basin (PRB). Similarities and differences in the air and oxy-fired cases were as follows. Both cases produced a very rapid initial formation of NO with similar amounts of total fuel nitrogen converted to NO. In air combustion, NO can be either formed or reduced by thermal equilibrium forces dependent on the local equivalence ratio. At an initial or primary zone stoichiometric ratio (S.R.) of 0.82, air combustion appeared to produced thermal NO while at S.R. = 0.65 no evidence of thermal NO is seen. In oxy-combustion, initial NO formation produced concentrations above equilibrium, creating a situation where NO was being destroyed by thermal processes at all measured S.R. In the fuel rich region, destruction of NO for both oxidizers is dependent on stoichiometry with lower S.R. producing higher NO_X destruction. At a fixed S.R., oxy-fuel combustion produced a more rapid reduction of NO than air. However, the lower the S.R. the higher the rate of NO formation at the point of tertiary air injection. The competition between NO destruction in the fuel rich region and NO formation at the point of oxidizer injection creates an effluent out NO minimum for each oxidizer. The magnitude of the minimum was similar for air and oxy-fuel combustion but the S.R. at the minimum was higher for oxy-fuel combustion. This suggests oxy-fuel combustion does not require as deep of a staging environment to achieve NO_X reduction and can therefore achieve higher burnout.

The second facility used was a flat flame burner with particle and gas sampling. This experiment also produced a similar temporal history for single coal particles to that experienced in the fuel rich zone of a staged, full-scale boiler. Char particles were sampled after passing through either air and oxy-flames. In oxy-flames, the normal diluent of N_2 was replaced with CO_2. The ratio of O_2/CO_2 was varied in order to produce different flame temperatures. Little difference was seen between air and oyx-fuel pyrolysis of coals. The oxy-fuel cases produced a slightly faster heating rate and devolatilization began earlier which was attributed to the higher heat capacity and specific heat of CO_2 but volatile yields and rates of devolatilization were not different enough to be measurable.

A model of the combustion process was completed consisting of fuel devolatilization, a detailed gas phase kinetic mechanism, and char oxidation. The model predicted with unreasonable accuracy the initial formation of NO. The model suggested magnitudes of NO formation due to prompt NO pathways was insignificant, but thermal NO formation can be significant on the order of 10-20% in air combustion, while in oxy-combustion, thermal processes can destroy NO on the order of 10-20%. The model was unable to predict a fuel rich region containing unburned hydrocarbons and nitrogen intermediates as were measured in experiments. This appears to be due to the monodisperse size distribution assumed for particles and the fact that devolatilization and char oxidation are can not occur simultaneously in the model. Thus volatiles are not released under fuel rich conditions in the model. The model does capture trends seen with NO formation and amount of burnout oxidizer.

The work was completed on time and on budget with a three month no-cost extension granted to accommodate student work schedules. To date, this work has resulted in three conference publications with an additional two conference papers and two journal articles in preparation. The computer program that has been created is based in Matlab and utilizes an open source kinetics code, Cantera. Air Liquide, an industrial partner throughout the project has been meeting regularly with BYU to understand an interpret results from this work. A FLUENT based model of the experimental facility was given to Air Liquide and follow-on work has been solicited by Air Liquide in the area of oxy-combustion modeling. Babcock and Wilcox has also solicited a proposal for oxy-combustion work to be done at BYU.

One Ph.D. student, Andrew Mackrory was supported entirely by this funding and is now employed at Babcock and Wilcox research center. Partial support of another Ph.D student, Shrinivas Lokare was received who is now at Reaction Engineering, a combustion consulting company. At least four undergraduate research assistants also participated in this work.

Background

NO_X Formation in Coal Flames

In conventional wall-fired boilers utilizing low-NO_x burners, the contributions of thermal-, prompt-, and fuel-NO_x formation have been studied in some detail. Most of the NO_x emissions from these air-fired boilers (~80%) are fuel-NO_x with ~95% being NO (Zevenhoven and Kilpinen, 2002). The contributions of thermal- and prompt-NO_x are relatively small under typical operating conditions. Nitrogen, originating in the fuel, passes through four distinct zones in this type of combustion process in a temporally separated sequence. In zone 1, premixed combustion of the volatiles with the primary air and any air entrained upstream of the flame occurs. During this process NO_x is formed rapidly but fuel nitrogen is in competition with volatile hydrocarbons for oxygen, which is in short supply. In the second zone, the atmosphere is reducing causing fuel nitrogen in the volatiles, typically in the form of HCN and NH_3, to be reduced to N_2 while NO formed in zone 1 can be reduced to N_2 through reburning reactions with unburned hydrocarbons, HCN and NH_3. Zone 3 is the oxidation of the rich products of combustion and volatiles that have been evolved in zones 1 and 2. This can occur as primary stream oxidizer is mixed into the fuel rich recirculation zone or mixing of products with secondary or tertiary air. In zone 3, the remaining HCN, NH_3 and gaseous hydrocarbon bound nitrogen can be oxidized to produce NO_x. Zone 4 consists of char burnout and cooling of the combustion products from peak reaction temperatures to effluent temperatures. In zone 4, NO_x is rapidly frozen and typically remains constant; however heterogeneous reactions with coal char may produce or destroy NO_x and high temperatures may create thermal-NO_x.

In oxy-fuel combustion where atmospheric nitrogen in the combustion chamber is replaced with recycled flue gas, the potential exists to alter temperature and species concentrations in each of these zones and thereby influence NO_x formation and destruction mechanisms. Experimental work has demonstrated that oxy-fuel combustion can produce lower NO_x emissions than comparable combustion in air, which was unexpected given the relative insignificance of thermal and prompt NO_x. A number of possible reasons for NO_x reduction in oxy-fuel combustion are as follows:

1. Near-elimination of thermal- and prompt-NO_x
2. More attached flame reducing oxygen entrainment and mixing
3. Elevated NO concentrations during the formation period
4. Reduction of recycled NO_x in the flue gas passing through the fuel-rich flame zone
5. Temperature increases driving thermal NOx to zero more rapidly in oxy-flames
6. Increased residence times in fuel-rich regions
7. Equilibrium considerations
8. Reduced NO formation from char
9. Enhanced heterogeneous reburning
10. Increased importance of gasification reactions

In addition to the potential explanations for NO_x reduction listed above, the potential exists for decreased NO_x formation during the initial premixed burn period in zone 1. The higher temperatures anticipated in oxy-fuel combustion would increase the reaction rates of both hydrocarbon and nitrogen containing volatiles such as HCN. The competition for oxygen

between these two groups may be altered both by temperature and oxygen concentration, potentially changing NO_x formation during this first stage of combustion.

To date the mechanisms of NO_x formation in oxy-fuel combustion are not well understood. An objective of this work is to gain increased understanding of the relative importance of the mechanisms listed leading to an increased ability to model and/or optimize oxy-fuel combustion for NO_x abatement. A further objective is to gather information that may indicate the potential of oxy-fuel combustion to cause increased corrosion.

Review of NO_X Formation in Oxy-combustion

Oxy-fuel experiments are reported as early as 1992 by Nakayama et al. who reported reduced NO_X emissions under oxy-fuel conditions.

Kimura et al. (1995) performed a study of combustion characteristics under oxy-fuel conditions using a swirl-stabilized burner firing 100 kg/hr coal. They used positive gage pressure in their furnace to prevent air infiltration, and reported NO_X in terms of a NO_X conversion ratio defined as conversion of fuel-N to NO_X assuming all NO_X is fuel-derived. It was observed that:

Higher oxygen concentrations (by volume) than in air were required in oxy-fuel combustion to match flame temperatures.

NO_X in oxy-fuel combustion was reduced to about one fifth the levels in air combustion for conditions where unburned carbon was similar. This improvement was attributed to reburning of recycled NO_X.

Nozaki et al. (1997) in a follow up paper report that NO_X in the flame (mostly recycled NO_X) was reduced rapidly to HCN or NH_3 in the early stages of coal combustion. Oxygen injection at the burner centerline raised near burner gas temperatures, causing increased devolatilization. Formation of NO_X in the flame was concluded to be lower under oxy-fuel conditions.

Okazaki and Ando (1997) are widely referenced in the oxy-fuel literature. Their paper is one of very few that documents a correction made to the NO_X measurement to account for CO_2 interference in a chemiluminescent analyzer (Zabielski et al., 1984). They studied three mechanisms of NO_X reduction in oxy-fuel combustion relative to air and used analytical methods to separate the effects of the mechanisms and quantify the significance of each pathway. The three mechanisms were:

NO_X reduction by char enhanced by high CO concentrations which themselves come from high CO_2 concentrations. Less than 10% of oxy-fuel NO_X reduction was attributed to this mechanism. The relative insignificance of it was concluded to be due to low particle density in pulverized coal conditions (particle spacing > 40 diameters).

Interactions between recycled NO_X and nitrogen released from the fuel. 10-50% of the NO_X reduction effect of oxy-fuel was attributed to this mechanism.

Reduction of recycled NO_X was determined to be the dominant effect responsible for 50-80% of NO_X reduction relative to air-firing.

While the conclusion that reduction of recycled NO_X is dominant is probably sound, certain aspects of the experiment differed from practical burners and it is possible that mechanisms that may have been unimportant in their work may still be important in oxy-fuel generally. Specifically, these points should be considered:

Coal volatiles were simulated with CH_4 and NH_3 despite, as noted by the authors, coal volatiles consist of many hydrocarbons. Smoot (1993) suggests (not referring to this experiment) that the presence of CH_4 may exaggerate the prompt NO_X and reburning reactions. In addition, NH_3 is probably not the major nitrogen species from coal pyrolysis. HCN was not used for safety reasons.

The gases used to simulate volatiles combustion were premixed, removing mixing and transient effects of coal pyrolysis that lead to local variation in stoichiometry.

Char was simulated with anthracite which is expected to have much lower active surface area than an industrial char (Smith et al., 1994).

Hu et al. (2001) studied the reduction of recycled NO and NO_2 in a high-volatile bituminous coal flame under low recycling ratio (high O_2 concentration in the oxidizer). Less recycled NO was reduced when oxygen concentrations were higher which according to their discussion may be due to consumption of CH fragments by the high O_2 concentration leaving less CH fragments for NO reduction. HCN concentration decreased with increases in recycled NO concentration. This is consistent with a pathway where HCN reacts with NO to form N_2, but from the literature they referenced it appeared that the reaction between CH fragments and NO were more important to the reduction of recycled NO than the HCN + NO pathway. No obvious effect of temperature was found, which may be due to competing effects: increased production of NO with temperature vs. increased volatiles yield with temperature providing more species for reduction of NO. Recycled NO_2 followed similar trends to NO consistently for this bituminous coal, but in a later work (Hu et al., 2003) a semi-anthracite coal exhibited lower reduction efficiency for NO_2 than NO. Most (95% or greater) NO_X emissions from combustion of pulverized coal in air are NO (Zevenhoven and Kilpinen, 2002).

Sangras et al. (2004) report on oxy-fuel performance in a 1.5 MW_{th} plant where 70% reduction in NO_X was achieved relative to air combustion. They note advantages to oxy-fuel such as reduced flue gas flow rates, less sensible heat loss to the stack, and easier capture of CO_2. The lower NO_X emissions were achieved with air infiltration of about 5% of the total boiler gas flow rate indicating that small amounts of N_2 may not affect the NO_X performance greatly.

Farzan et al. (2005), using the same facility as Sangras et al. (2004), used oxygen and recycled flue gas flow rates to achieve combustion conditions suitable for existing boiler technology. With overall combustion characteristics comparable to air firing, the NO_X emissions were reduced almost 65%. The burner was a scaled-down B&W DRB-4Z low-NO_X burner modified for oxy-fuel combustion. Flame temperatures were prevented from exceeding conventional boiler flame temperatures by more than 60 K to prevent thermal NO_X. It is noted that there is less thermal NO_X because there is less N_2 available, but N_2 was entering the boiler with the oxygen (purity < 100%) and air ingress. The boiler parameters (including burner SR) were optimized for NO_X reduction while maintaining heat transfer similar to the air-fired baseline case. Recycled flue gas ranged from 80-90% of total flue gas. They observed that NO_X emissions decreased with recycled flue gas flow rate, but this was only a slight effect. This trend is opposite to that reported by Hu et al. (2001) from experiments at much lower recycling ratio. These two results indicate that there may be an optimum level of recycling (or oxygen concentration) for minimum NO_X.

Flame temperatures measured by Farzan et al. (2005) using two-color pyrometry were 1572 and 1633 K for air and oxy-fuel at burner SR's of 0.86 and 1.05 respectively. Flame spectral

emittance measurements were also made and the air and oxy-fuel cases were similar with the exception of small regions of the spectrum corresponding to emission from CO_2. The results indicate that the radiation heat transfer from the flame was dominated by soot, coal, and ash particles and the increased CO_2 (and H_2O) concentrations were relatively unimportant.

In furnace areas other than the flame, CO_2 and H_2O may become more important radiators as ash emittance decreases with increased carbon conversion (Nozaki et al., 1997). There is some difference in gas emittance between wet and dry recycled oxy-fuel flue gas, and air-fired flue gas (Khare et al., 2005).

Buhre et al. (2005) review oxy-fuel combustion technology. Oxygen purity of 95-99.5% purity has been used in full-scale testing. Lower oxygen purity requires less energy for the air separation unit, but low levels of N_2 are potentially undesirable. They quote combined modeling and experimental work performed at CANMET in Canada where small amounts of N_2 (3%) significantly decreased the difference in NO_X between air and oxy-fuel combustion. This conclusion may be burner-specific as others (Andersson et al., 2007) have observed only modest increases in NO with air ingress of 4% of feed gas flow.

Khare et al. (2005) reviewed the oxygen levels used by various groups. They note that some of the O_2 required for combustion will come from the recycle stream. The choice between wet and dry recycle streams affects the required oxygen concentration as the heat capacity of the flue gas changes significantly with water content. Flame temperatures depend on mixing rates and other factors beyond oxygen concentration. For the furnace designs they considered, required oxygen concentrations through the burner were estimated to range from 25 to 38% by volume.

Shaddix (2007) and Molina and Shaddix (2007) explain that due to the competing effects of increased oxygen concentration, and lower diffusion coefficients in CO_2 relative to air, O_2 and CO_2 effects on ignition and devolatilization approximately cancel each other out for 30 vol. % O_2 in CO_2.

Tan and Croiset (2005) note that even though unrecycled flue gas is ideally destined for CO_2 sequestration; NO_X in this stream will probably be released to the atmosphere when the CO_2 is compressed, dehydrated and cooled. It is also possible that a plant may need to temporarily increase power to the grid by shutting down the CO_2 capture train and venting all unrecycled flue gas through the stack. These possibilities underscore the importance of designing the combustion system for low NO_X. They point out that lower NO_X is not automatic or inherent in oxy-fuel combustion and that low-NO_X burner designs should be used. In contrast, Allam et al. (2005) and Sarofim (2007) refer to a process proposed by Air Products and Chemicals, Inc. where high NO_X levels might be beneficial. Increased concentrations of trace species in oxy-fuel (including SO_X, HCl, and mercury) will increase the acid dew point temperature. SO_X and NO_X would be condensed in the CO_2 purification unit as sulfuric and nitric acids and the nitric acid will react with the mercury to allow its removal with the acids. Regardless of the choice of CO_2 processing method, understanding of the NO_X chemistry is important to produce the desired level of NO_X.

In the experiments of Tan and Croiset (2005) the conversion ratio of SO_2 to SO_3 did not change from air to oxy-fuel combustion, but the accumulation of recycled SO_2 did result in increased SO_3 concentrations. They suspected that higher SO_3 concentrations would threaten boiler integrity and therefore most boiler systems (particularly those that fire high-sulfur coal) would have the flue gas recycled from a point downstream of SO_2 removal.

Scheffknecht et al. (2007) performed unstaged oxy-fuel combustion experiments and report that fuel NO_X emissions increased with O_2 partial pressure. For oxidizer-staged experiments, trends in NO_X with burner SR were the same for air and oxy-fuel combustion. They also achieved effectively 100% reduction of recycled NO_X with a staged combustion test. They measured higher CO near the burner in oxy-fuel relative to air and attributed this to enhanced water-shift and CO_2-shift reactions. Peak measured in-flame CO in air was about 15 vol. % and oxy-fuel about 18 vol. %.

Dhungel et al. (2007) determined that the pathways of NO reduction in oxy-fuel in their experiment were similar to those in air combustion. They present a pathway for NO_X where recycled NO_X is reduced to HCN by reaction with hydrocarbon radicals. It was observed that reduction of recycled NO_X was lower when some of it went through an overfire air port. If the furnace is deeply staged this becomes more of an issue and may be one reason why the optimum burner stoichiometry was higher in oxy-fuel than air in the work reported by Farzan et al. (2005).

Andersson et al. (2007) performed oxy-fuel experiments with associated modeling. Their model made use of the gas-phase fuel-N model of De Soete (1975) and one NO destruction reaction:

$$NO + CO \longleftrightarrow \tfrac{1}{2} N_2 + CO_2 \qquad \text{[Reaction 1]}$$

The nitrogen-containing reactions were modeled with kinetic rate expressions while most other species were assumed to be in chemical equilibrium. CO and O_2 were controlled to agree with experimentally measured values because of their importance to the nitrogen containing reactions.

The model parameters were tuned to match one air and one oxy-fuel case, and thereafter the model correctly predicted a minimum in NO concentration at a point inside the flame for a different oxy-fuel case with higher oxygen concentrations and temperatures. This minimum in the NO profile did not exist in the air and oxy-fuel cases used for model tuning. At the location of the minimum in NO the reported in-flame CO data exhibit dramatic differences in CO (by 7 vol. %) between the two oxy-fuel flames that differ in temperature by only 58 K (1476 and 1534 K) at the point of interest. CO_2 dissociation to form CO becomes significant at about 1500 K which is consistent with the measurements, but another factor is that O_2 was lower when CO was higher and vice versa. Thermal dissociation of CO_2 may therefore not be the only factor in the high CO values. Since CO in the model was controlled to fit measured values it is not clear to what extent CO trends could be predicted, but CO would be critical to predict if Reaction 1 is to be used. It was concluded that the reduction of NO_X in oxy-fuel is due to increased destruction of NO_X, both recycled and otherwise. Stoichiometry was varied and oxy-fuel was found to be fairly insensitive to stoichiometry in terms of NO_X emissions. As mentioned above, simulated air ingress had only a small effect on NO_X formation.

In the discussion by Skreiberg et al. (2004) Reaction 1 is not believed to be important as an elementary reaction. The more recently published large mechanisms have used lower rates for reaction of NO with CO to form N atoms and so Reaction 1 should be considered a global reaction. In addition, Skreiberg et al. (2004) state that they do not expect that CO under reducing conditions causes a significant reduction in NO below 1400 K.

Hjärtstam et al. (2007) reporting on the same experiments as Andersson et al. (2007) note that stack CO emissions were comparable between air and oxy-fuel cases even when very high levels of CO existed in the oxy-fuel flames. They also report improved attachment of the flame with increasing oxygen concentration in the oxy-fuel cases. Oxygen concentration in the flames was

lower when the flame was better attached which is presumably a combined effect of less entrainment of oxygen from the secondary stream and more rapid consumption of the primary oxygen by the fuel.

Method

Pulverized coal was burned in a refractory-lined, laminar flow reactor referred to as the Multi-fuel Flow Reactor or MFR (Figure 1). The MFR has inside dimensions of 0.12 m x 2 m. It uses a non-swirling, water-cooled, honeycomb, premixed burner.

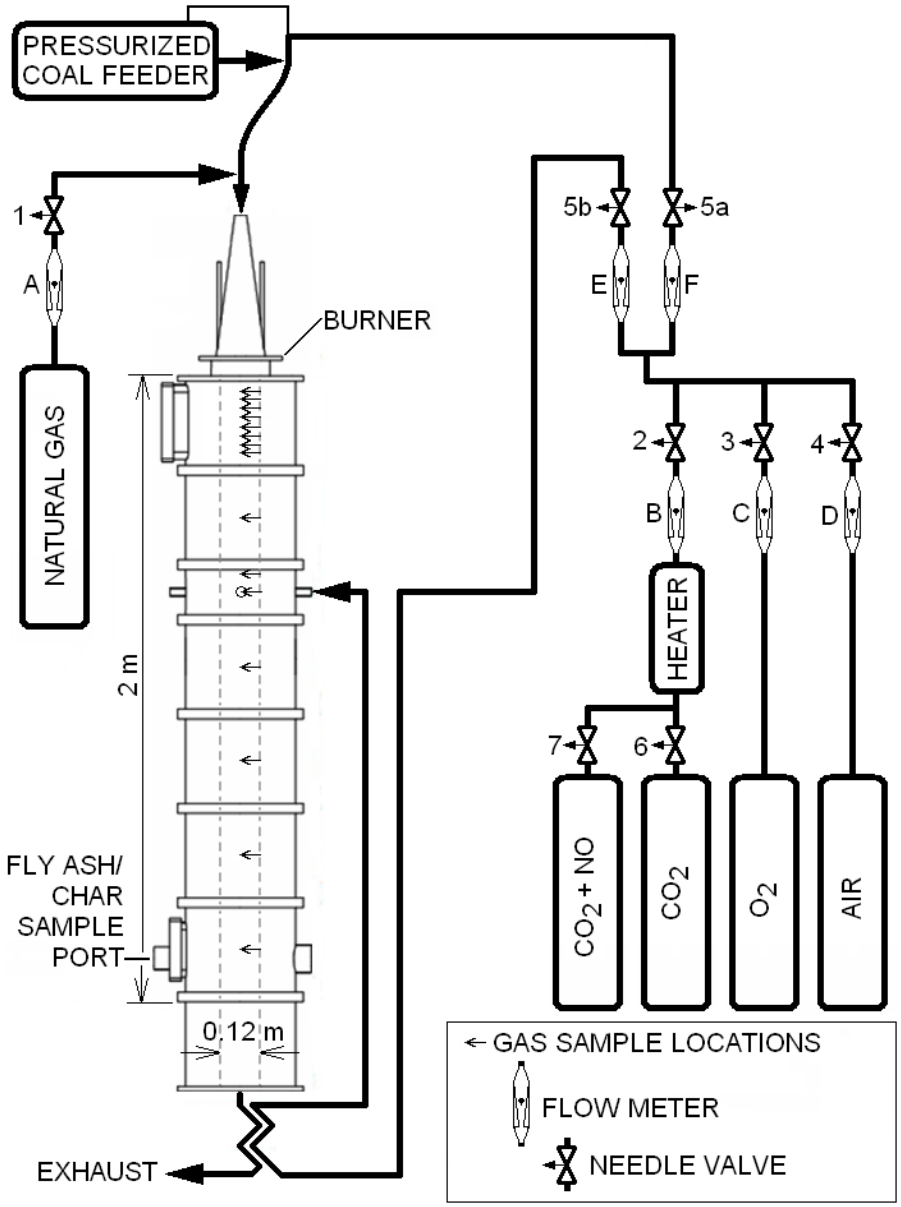

Figure 1. Schematic of the Multi-fuel Flow Reactor (MFR).

Natural gas and pulverized coal are premixed with the primary air or primary CO_2/O_2 oxidizer. The natural gas produces a stable flame at each of the 5 mm diameter holes in the burner through which the coal passes. The reactor can be run in two configurations, with and without oxidizer staging. The primary zone can therefore be operated overall lean or rich. When the primary zone is run overall rich, burnout air or oxidizer was added 0.67 m from the burner. Regularly spaced

ports allow sampling of wall temperatures and product gases at the arrow point locations shown in the figure.

The oxidizer (air or O_2/CO_2 mixtures) is metered from compressed gas sources and then mixed prior to splitting the primary and burnout streams. The reaction chamber is operated at slight positive pressure to prevent air infiltration. Reactor pressure is controlled with a variable speed induced-draught exhaust fan.

A window and flange has been removed from the top reactor section and replaced with eight sampling ports. Previously the probe length (Figure 2) had restricted gas sampling in this section to near-wall locations only. The removal of the window and flange allowed the gas sample probe to reach the reactor centerline.

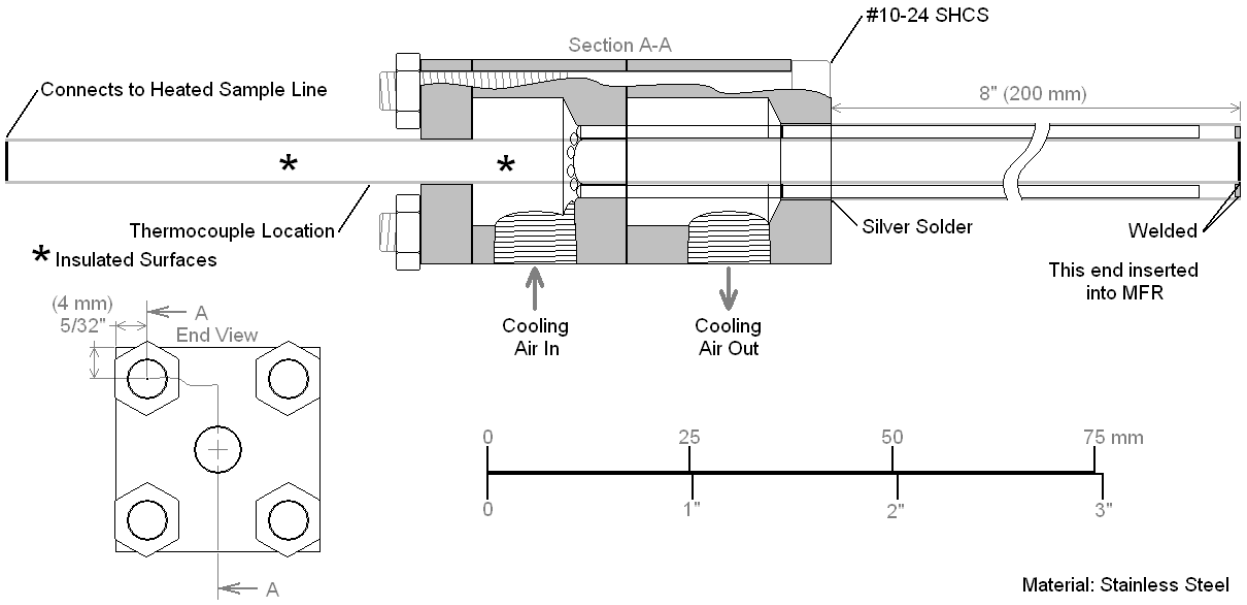

Figure 2. Diagram of the air-cooled gas sampling probe.

The simulated dry recycled flue gas (CO_2) can be doped with NO to study the effect of mechanisms involving NO in the recycle stream.

O_2 (vol. %, dry), and CO and NO_x (ppm, dry) are measured using a Horiba PG-250 portable gas analyzer using the chemiluminescence principle for NO_x. Testing has shown that this particular analyzer does not suffer from significant CO_2 interference with the NO_x measurement. This is largely due to the analyzer diluting the sample 12:1 with room air prior to analysis. The O_2 measurement has previously been obtained using a zirconium oxide sensor and a galvanic cell. A galvanic cell used earlier suffered from CO_2 interference.

An FTIR gas analyzer manufactured by MKS was used for additional gas species measurements including NO, NO_2, N_2O, CO, CO_2, H_2O, SO_2, HCN, and NH_3. To prevent condensation of the sample for this gas analyzer the sample line and probe were maintained at 180 °C.

To allow a fair comparison between air cases and oxy-fuel cases with varying amounts of diluent (CO_2 or N_2) the NO_x results are converted to a nitrogen conversion efficiency, η_N. This is the

ratio of mass flux of nitrogen in NO_x to the mass flux of fuel-N coming into the MFR. Equation 1 provides the relationship necessary to convert the measured molar concentration of NO_x on a dry basis ($X_{NO,dry}$) to nitrogen conversion efficiency. Ash is considered inert and the mass flux rates ($\dot{m}_{prod,wet}$ and $\dot{m}_{coal}$) are calculated from the measured reactant flow rates. All of the terms in the equation are known or measured except the molecular weight of the product gases being sampled ($MW_{prod,dry}$), and the mass fraction of condensed liquids (H_2O and H_2SO_4) in the cooled sample ($Y_{moist,prod,wet}$). These values were estimated from an equilibrium calculation. These calculations are performed using 70% of the coal for sampling points upstream of secondary oxidizer injection. This accounts for the incomplete conversion of the coal in the fuel-rich region of the reactor.

$$\eta_N \approx \frac{\dot{m}_{prod,wet}\left(1 - Y_{moist,prod,wet}\right) X_{NO,dry} \dfrac{MW_N}{MW_{prod,dry}}}{\dot{m}_{coal} Y_{N,coal}} \qquad \text{Equation 1}$$

Fuel Properties

Three coals were used in this work: Illinois #6, Pittsburgh #8, and a sub-bituminous coal originating from Wyoming's Powder River Basin (PRB). All coals were pulverized and samples were sent for analysis to an independent laboratory. Selected coal properties are shown in Table 1. Particle size distributions determined using US Standard sieves are shown in Figure 3.

Table 1. Selected properties of the coals.

	Sub-bituminous	Illinois #6	Pittsburgh #8
Proximate Analysis	**DAF wt%**	**DAF wt%**	**DAF wt%**
Volatile Matter	49.72	44.17	41.96
Fixed Carbon	50.28	55.83	58.04
Ash (wt%, dry)	6.42	9.31	10.67
Higher Heating Value (Btu/lb, DAF)	11981	14226	14785
ASTM Rank	Sub-bituminous A	High-volatile C bituminous	High-volatile A bituminous
Ultimate Analysis	**DAF wt%**	**DAF wt%**	**DAF wt%**
C	70.56	81.88	85.19
H	4.18	4.37	4.87
O	23.63	7.83	4.70
N	1.04	1.27	1.38
S	0.59	4.64	3.86
	100	100	100

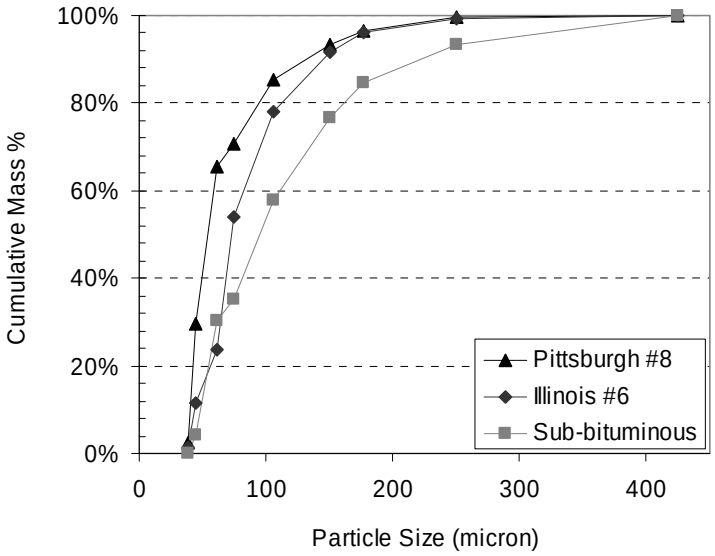

Figure 3. Coal particle size distributions.

Due to continual drying of the coal, moisture analysis was performed just prior to each run to properly calculate stoichiometry based on coal mass flow rate. After most runs an ash sample from the exhaust system was used to determine the level of burnout achieved.

The laboratory natural gas system receives gas from the city natural gas supply. Gas is compressed and stored in tanks connected by a manifold. Although daily gas quality reports are available from the utility, there is uncertainty as to when the gas in the tanks was compressed. Typical gas properties obtained by averaging the gas quality report over the time when most data for this work was taken are listed in Table 2.

Table 2. Approximate composition of the natural gas (Source: Questar Gas Quality Information).

Component	%
N_2	0.44
CO_2	0.87
C1	92.82
C2	4.07
C3	1.13
IC4	0.22
NC4	0.23
IC5	0.08
NC5	0.05
C6	0.05
C7	0.03
C8	0.01
C9	0
Specific Gravity	0.607
Btu/Cu Ft	1067

Experiment Conditions

A number of different experiments were performed using different oxidizers, different coals, and different ratios of primary to burnout oxidizer. The experiment conditions are detailed in Table 3 through Table 9. Each experiment has a unique name consisting of the coal used and the nominal oxidizer composition (Air, O25, O30), followed by a notation for special conditions (if any). The standard experiment was oxidizer-staged i.e. enough oxidizer was diverted from the burner to the burnout oxidizer ports to result in a nominal primary zone SR of 0.75. The notations for special conditions are as follows:

- Unstaged: Unstaged experiments had all reactants flow through the burner.
- Staging: In these experiments the ratio of primary to burnout oxidizer was varied to determine the effect on effluent NO_X concentration.
- (Opt): These experiments were conducted at the ratio of primary to burnout oxidizer that produced minimum effluent NO_X.
- (x ppm NO): To investigate the effect of recycled NO_X, an experiment was conducted using CO_2 doped with 525 ppm NO. The data obtained just prior to the switch from pure CO_2 to doped CO_2 make up the (0 ppm NO) experiment, and that taken with the doped CO_2 make up the (525 ppm NO) experiment.

Table 3. Experiment conditions for unstaged experiments.

Experiment Name: **Illinois #6 Air Unstaged**			
	Flow Rates (kg/hr)		
Reactant	Burner	Burnout Oxidizer	Total
Coal	0.734	-	0.734
Natural Gas	0.373	-	0.373
Air	17.0	-	17.0
	Stoichiometric Ratio:	1.06	
	Coal Moisture (as fired):	~14 wt%	

Experiment Name: **Illinois #6 O25 Unstaged**			
	Flow Rates (kg/hr)		
Reactant	Burner	Burnout Oxidizer	Total
Coal	0.737	-	0.737
Natural Gas	0.374	-	0.374
O_2	3.92	-	3.92
CO_2	11.6	-	11.6
	Stoichiometric Ratio:	1.04	
	Coal Moisture (as fired):	~14 wt%	

Experiment Name: **Illinois #6 O30 Unstaged**			
	Flow Rates (kg/hr)		
Reactant	Burner	Burnout Oxidizer	Total
Coal	0.737	-	0.737
Natural Gas	0.378	-	0.378
O_2	3.93	-	3.93
CO_2	9.15	-	9.15
	Stoichiometric Ratio:	1.04	
	Coal Moisture (as fired):	~14 wt%	

Table 4. Experiment conditions for standard experiments performed with Illinois #6 coal.

Experiment Name: **Illinois #6 Air**			
Reactant	Flow Rates (kg/hr)		
	Burner	Burnout Oxidizer	Total
Coal	0.732	-	0.732
Natural Gas	0.372	-	0.372
Air	11.87	7.13	19.0
Oxidizer to Burnout Oxidizer Ports:	37.5 %		
Primary Stoichiometric Ratio:	0.75		
Burnout Stoichiometric Ratio:	1.21		
Burnout Oxidizer Temperature:	502 K		
Coal Moisture (as fired):	11.3 wt%		

Experiment Name: **Illinois #6 O30**			
Reactant	Flow Rates (kg/hr)		
	Burner	Burnout Oxidizer	Total
Coal	0.729	-	0.729
Natural Gas	0.375	-	0.375
O_2	2.8	1.66	4.46
CO_2	6.5	3.85	10.35
Oxidizer to Burnout Oxidizer Ports:	37.2 %		
Primary Stoichiometric Ratio:	0.76		
Burnout Stoichiometric Ratio:	1.21		
Burnout Oxidizer Temperature:	461 K		
Coal Moisture (as fired):	11.3 wt%		

Table 5. Experiment conditions for experiments performed using pure CO_2 and NO-doped CO_2.

Experiment Name: **Illinois #6 O30 (0 ppm NO)**			
Reactant	Flow Rates (kg/hr)		
	Burner	Burnout Oxidizer	Total
Coal	0.736	-	0.736
Natural Gas	0.376	-	0.376
O_2	2.84	1.63	4.47
CO_2	6.5	3.72	10.22
NO in CO_2:	0 ppm		
Oxidizer to Burnout Oxidizer Ports:	36.4 %		
Primary Stoichiometric Ratio:	0.77		
Burnout Stoichiometric Ratio:	1.21		
Burnout Oxidizer Temperature:	436 K		
Coal Moisture (as fired):	11.7 wt%		

Experiment Name: **Illinois #6 O30 (525 ppm NO)**			
Reactant	Flow Rates (kg/hr)		
	Burner	Burnout Oxidizer	Total
Coal	0.736	-	0.736
Natural Gas	0.377	-	0.377
O_2	2.83	1.61	4.44
CO_2	6.43	3.67	10.10
NO in CO_2:	525.4 ppm		
Oxidizer to Burnout Oxidizer Ports:	36.3 %		
Primary Stoichiometric Ratio:	0.76		
Burnout Stoichiometric Ratio:	1.2		
Burnout Oxidizer Temperature:	435 K		
Coal Moisture (as fired):	11.7 wt%		

Table 6. Experiment conditions for standard experiments with Pittsburgh #8 coal.

Experiment Name: **Pittsburgh #8 Air**			
Reactant	Flow Rates (kg/hr)		
	Burner	Burnout Oxidizer	Total
Coal	0.645	-	0.645
Natural Gas	0.372	-	0.372
Air	10.99	6.51	17.5
Oxidizer to Burnout Oxidizer Ports:	37.2 %		
Primary Stoichiometric Ratio:	0.76		
Burnout Stoichiometric Ratio:	1.2		
Burnout Oxidizer Temperature:	466 K		
Coal Moisture (as fired):	1.51 wt%		

Experiment Name: **Pittsburgh #8 O30**			
Reactant	Flow Rates (kg/hr)		
	Burner	Burnout Oxidizer	Total
Coal	0.644	-	0.644
Natural Gas	0.372	-	0.372
O_2	2.59	1.49	4.08
CO_2	5.80	3.71	9.51
Oxidizer to Burnout Oxidizer Ports:	36.6 %		
Primary Stoichiometric Ratio:	0.76		
Burnout Stoichiometric Ratio:	1.2		
Burnout Oxidizer Temperature:	425 K		
Coal Moisture (as fired):	1.51 wt%		

Table 7. Experiment conditions for standard experiments with sub-bituminous coal.

Experiment Name: **Sub-b Air**			
Reactant	Flow Rates (kg/hr)		
	Burner	Burnout Oxidizer	Total
Coal	0.877	-	0.877
Natural Gas	0.373	-	0.373
Air	11.16	7.24	18.4
Oxidizer to Burnout Oxidizer Ports:	39.3 %		
Primary Stoichiometric Ratio:	0.75		
Burnout Stoichiometric Ratio:	1.23		
Burnout Oxidizer Temperature:	522 K		
Coal Moisture (as fired):	8.46 wt%		

Experiment Name: **Sub-b O25**			
Reactant	Flow Rates (kg/hr)		
	Burner	Burnout Oxidizer	Total
Coal	0.874	-	0.874
Natural Gas	0.373	-	0.373
O_2	2.63	1.65	4.28
CO_2	7.9	4.94	12.84
Oxidizer to Burnout Oxidizer Ports:	38.5 %		
Primary Stoichiometric Ratio:	0.76		
Burnout Stoichiometric Ratio:	1.23		
Burnout Oxidizer Temperature:	522 K		
Coal Moisture (as fired):	8.46 wt%		

Experiment Name: **Sub-b O30**			
Reactant	Flow Rates (kg/hr)		
	Burner	Burnout Oxidizer	Total
Coal	0.878	-	0.878
Natural Gas	0.377	-	0.377
O_2	2.63	1.66	4.29
CO_2	6.18	3.91	10.09
Oxidizer to Burnout Oxidizer Ports:	38.8 %		
Primary Stoichiometric Ratio:	0.75		
Burnout Stoichiometric Ratio:	1.23		
Burnout Oxidizer Temperature:	495 K		
Coal Moisture (as fired):	8.46 wt%		

Table 8. Experiment conditions for the Staging-type experiments.

Experiment Name: **Sub-b Air Staging**			
Reactant	Flow Rates (kg/hr)		
	Burner	Burnout Oxidizer	Total
Coal	0.872	-	0.872
Natural Gas	0.378	-	0.378
Air	Oxidizer split between burner and burnout oxidizer ports was varied		18.4
Oxidizer to Burnout Oxidizer Ports:	18.9, 25.0, 31.9, 34.2, 35.8, 39.6, 42.9, 49.0, 53.8 %		
Primary Stoichiometric Ratios:	1.00, 0.92, 0.84, 0.81, 0.79, 0.74, 0.70, 0.63, 0.57		
Burnout Stoichiometric Ratio:	1.23		
Burnout Oxidizer Temperature:	492, 514, 527, 519, 520, 534, 535, 532, 525 K		
Coal Moisture (as fired):	8.46 wt%		

Experiment Name: **Sub-b O25 Staging**			
Reactant	Flow Rates (kg/hr)		
	Burner	Burnout Oxidizer	Total
Coal	0.878	-	0.878
Natural Gas	0.373	-	0.373
O_2	Oxidizer split between burner and burnout oxidizer ports was varied		4.29
CO_2			12.88
Oxidizer to Burnout Oxidizer Ports:	20.5, 24.8, 31.1, 36.4, 39.3, 46.4 %		
Primary Stoichiometric Ratio:	0.98, 0.93, 0.85, 0.78, 0.75, 0.66		
Burnout Stoichiometric Ratio:	1.23		
Burnout Oxidizer Temperature:	475, 494, 510, 520, 523, 526 K		
Coal Moisture (as fired):	8.46 wt%		

Experiment Name: **Sub-b O30 Staging**			
Reactant	Flow Rates (kg/hr)		
	Burner	Burnout Oxidizer	Total
Coal	0.873	-	0.873
Natural Gas	0.373	-	0.373
O_2	Oxidizer split between burner and burnout oxidizer ports was varied		4.29
CO_2			10.05
Oxidizer to Burnout Oxidizer Ports:	18.8, 25.2, 32.8, 36.0, 39.0, 43.0, 47.1 %		
Primary Stoichiometric Ratio:	1.00, 0.92, 0.83, 0.79, 0.75, 0.70, 0.65		
Burnout Stoichiometric Ratio:	1.24		
Burnout Oxidizer Temperature:	445, 464, 483, 490, 493, 497, 494 K		
Coal Moisture (as fired):	8.46 wt%		

Table 9. Experiment conditions for minimum effluent NO_X.

Experiment Name: **Sub-b Air (Opt)**			
Reactant	Flow Rates (kg/hr)		
	Burner	Burnout Oxidizer	Total
Coal	0.875	-	0.875
Natural Gas	0.373	-	0.373
Air	9.33	9.07	18.4
Oxidizer to Burnout Oxidizer Ports:	49.3 %		
Primary Stoichiometric Ratio:	0.63		
Burnout Stoichiometric Ratio:	1.23		
Burnout Oxidizer Temperature:	514 K		
Coal Moisture (as fired):	8.46 wt%		

Experiment Name: **Sub-b O30 (Opt)**			
Reactant	Flow Rates (kg/hr)		
	Burner	Burnout Oxidizer	Total
Coal	0.876	-	0.876
Natural Gas	0.377	-	0.377
O_2	2.89	1.4	4.29
CO_2	6.77	3.27	10.04
Oxidizer to Burnout Oxidizer Ports:	32.6 %		
Primary Stoichiometric Ratio:	0.83		
Burnout Stoichiometric Ratio:	1.23		
Burnout Oxidizer Temperature:	467 K		
Coal Moisture (as fired):	8.46 wt%		

Computational Methods

General Description of the Detailed Model

The approach taken for detailed kinetic modeling was to simulate the MFR using existing sub-models available in the literature. In order to produce a model that required little adjustment to match experimental data, the emphasis was on fundamental over empirical methods. An advantage of such a model is that it may be used to investigate the relative importance of various NO_X mechanisms by enabling and disabling them and determining which features of the model are most important to correctly predicting the nitrogen evolution observed experimentally.

A conceptual diagram of the model is shown in Figure 4. The MFR was represented as a plug flow reactor divided into a series of 875 slices (each 2 mm in the axial direction). Each slice was modeled as a continuously-stirred tank reactor (CSTR). In the limit, a series of infinitely-small CSTR's is a plug flow reactor. The size of 2 mm was chosen as the smallest size where the model would predict ignition of the incoming reactants. Grid independence was verified by comparing results from a 4 mm and 2 mm grid spacing model.

The open-source kinetic code Cantera (Goodwin, 2003) was used to integrate the gas-phase reactions in each CSTR. Three gas-phase mechanisms were tested: SKG03 (Skreiberg et al., 2004), GRI-Mech 3.0 (Smith et al., 2000), and GRI-Mech 3.0 + B96 which is the GRI-Mech 3.0 mechanism with advanced reburning reactions from Bowman (1997) added following a similar approach to Xu et al. (2001).

Devolatilization was modeled using the CPD-NLG model (Grant et al., 1989; Fletcher et al., 1992; Genetti and Fletcher 1999) which includes prediction of nitrogen and light gas species release from the coal. Genetti's correlations to estimate the required ^{13}C NMR parameters for the coal based on proximate and ultimate analyses were employed.

MATLAB was chosen for the main program as Cantera functions can be called from MATLAB. The CPD-NLG model was translated from FORTRAN source code to MATLAB and modified to replace built-in correlations for gas properties (that assumed N_2) with gas mixture properties evaluated by Cantera.

A char oxidation and gasification (by CO_2) model described in Smoot and Smith (1985) using the data of Goetz et al. (1982) was included. This char reaction model only becomes active after devolatilization is completed.

Each CSTR was solved sequentially with the exception of the first 5 CSTR's which had to be solved simultaneously to model thermal feedback from the natural gas flame necessary for ignition. After each CSTR the gas mixture was altered to account for production of volatiles by the coal or consumption of oxidant and production of CO by the char. The new mixture was then passed downstream to the next CSTR.

Convective heat transfer between gas and particles was modeled as well as radiation between particles and the walls. Measured wall temperatures were used as an input. Radiation heat transfer from the gases was neglected on account of the small reactor cross section (Wall et al., 1979). Convective losses from the gases to the walls and other heat transfer such as radiation from soot and char are handled with an empirically-adjusted factor that was based on matching gas temperature data from a well-characterized natural gas MFR experiment, and gas species measurements (CO) from this work indicative of gas temperature.

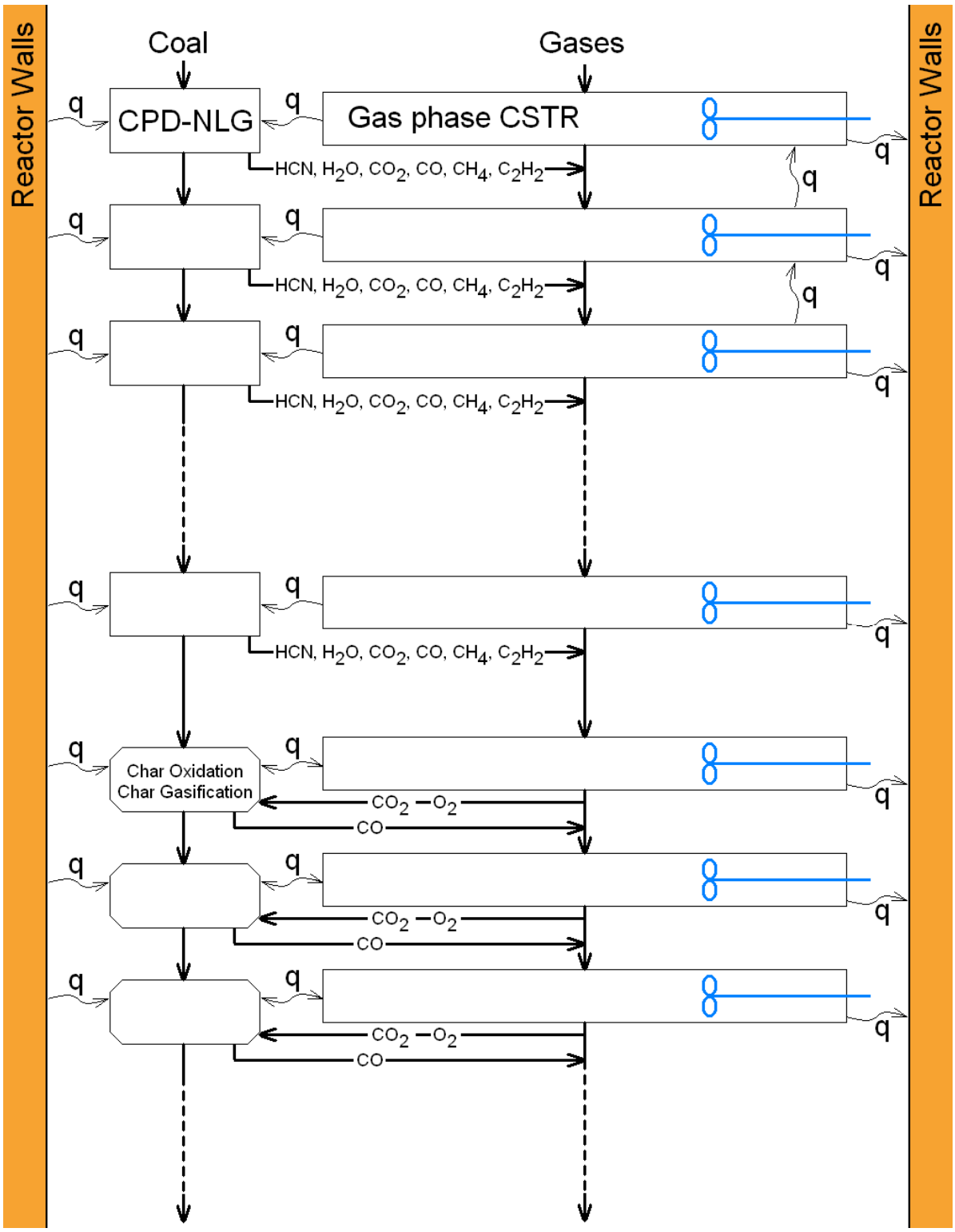

Figure 4. Schematic diagram of the detailed kinetic model. The letter "q" indicates heat transfer.

Simplifying Assumptions

Key assumptions made in the model were largely based on the literature and included the following:

- Coal particles were spherical and entrained (i.e. particle velocity was equal to gas velocity). A calculation was performed to estimate the terminal velocity of a 115 μm diameter coal particle in hot combustion gases. The result was a predicted velocity of 0.17 m/s for a Reynolds number of 0.07. The estimated gas velocity was much higher at 1.42 m/s. This assumption greatly simplifies the model.
- All gas products from the coal consisted of species in the kinetic mechanism. Secondary pyrolysis of coal char results in soot and light gases such as H_2, CO, C_2H_2, C_2H_4, and single ring aromatics (Glarborg et al., 2003). The CPD-NLG model predicts some light gases as indicated in Figure 4, and other volatiles were assumed to consist of CH_4 and C_2H_2 in proportions that closed the carbon and hydrogen balances. These balances were based on carbon release being proportional to burnout and hydrogen mass release being a function of burnout as described by Equation 2 and Equation 3. Equation 2 was generated by curve-fitting data from Asay (1982) for a bituminous coal. The equation had an r^2 value of 0.95 for the bituminous data and was a good visual match to a set of sub-bituminous data. This is a significant assumption and is based on assuming that all tars are cracked to form light gases. Soot is therefore neglected, but most, if not all, published NO_X mechanisms in the literature are based on light gases. Bose et al. (1988) concluded that homogeneous chemistry dominated NO_X destruction.

$$\%H_{released} = -0.5597 \times Burnout^2 + 1.5651 \times Burnout \qquad \textbf{Equation 2}$$

$$Burnout = 1 - \frac{Char\ Mass\ Flux\ (DAF)}{Initial\ Coal\ Mass\ Flux\ (DAF)} \qquad \textbf{Equation 3}$$

- Oxygen was assumed to be completely contained in the CPD predictions of CO, H_2O, and CO_2 in accordance with the findings of Niksa (1996).
- Natural gas was modeled as 100% CH_4 as done by Xu et al. (2001). Approximate natural gas composition is given in Table 2 and is mostly methane.
- All nitrogen in the volatiles was in the form of HCN. This matches the majority of observations in the literature as discussed in the literature review.
- Char consisted of C(s) and burned with a shrinking core of constant density and constant ash content with CO as the surface product. These assumptions were used in deriving the rate constants sourced from Goetz et al. (1982) and so needed to be used when applying said constants. Diffusion-limited vs. kinetic-limited char burning did not therefore need to be considered in this model. The experiments of Goetz et al. (1982) were performed at 1 atm over the temperature range of 1250-1730 K with chars prepared in 1750 K N_2 from 200-400 mesh coals, which is applicable to pulverized coal conditions. NO_X formation from char was not included in the model. CO from the char reactions was oxidized to CO_2 by the gas-phase kinetics.
- Sulfur species are neglected.

- No fluid mechanics were modeled as the focus of the model was the devolatilization and gas-phase kinetics. Mixing of burnout oxidizer was assumed to occur in one CSTR. This was initially tried for simplicity in coding and when it did not introduce any model instabilities it was retained.
- For coding simplicity the coal particles were represented with one particle diameter based on the mean diameter for a Rosin-Rammler distribution fit to the measured size distributions.

The full MATLAB source code is available for distribution to any interested party.

Gas-Phase Mechanisms

Skreiberg et al. (2004) recommend a mechanism known as SKG03 for modeling the reduction of NO by primary measures in biomass combustion, and combustion of coal syngas. It was validated under conditions similar to those in staged combustion.

GRI-Mech 3.0 (Smith et al., 2000) is a collection of 325 elementary reactions involving 53 species. It has been optimized for methane and natural gas combustion over the range 1000-2500 K, 10 Torr to 10 atm, and equivalence ratios from 0.1-5 for premixed systems. Some species such as ethane and propane are included in the species list because they are found in natural gas, but the authors state that the mechanism should not be used for modeling of fuels other than methane and natural gas, even if these species are on the species list. NO formation and reduction (thermal and prompt NO_X, and reburning reactions) are included in the mechanism with the notable exception of the chemistry involved in SNCR. Soot formation is also not described.

Xu et al. (2001) modeled advanced reburning with a reduced mechanism that was derived from the earlier GRI-Mech 2.11 mechanism with advanced reburning reactions from Bowman (1997) added. This advanced reburning model was used in the PCGC-3 CFD code. The model was activated at the location of NH_3 injection, and upstream of this a global fuel-N mechanism was employed. Agreement with experimental data was determined to be *"reasonably good"*. Given their success it was decided for this work to try the newer GRI-Mech 3.0 mechanism with Bowman's reaction set added. This mechanism is referred to as GRI-Mech 3.0 + B96.

Char Reactions

Both char oxidation by O_2 and char gasification by CO_2 were modeled. Typically in combustion modeling, gasification by CO_2 is neglected because the reaction rate is much slower than oxidation, but in this work it was included because the CO_2 concentrations in oxy-fuel combustion are much higher and the effect of increased CO_2 was of interest. Shaddix and Murphy, 2003 (as referenced by Buhre et al., 2005) found that in oxygen-enriched combustion, CO_2 gasification of the char becomes important at practical temperatures.

The only product considered for the char reactions was CO. Molina et al. (2000) in reviewing char combustion modeling note that while some workers have modeled heterogeneous production of both CO_2 and CO from char, it is known that the major pathway at combustion temperatures is production of CO, and that most CO_2 comes from homogeneous oxidation of CO.

The char reactions were modeled using rates measured by Goetz et al. (1982) for coals from the same US regions as used in this work. The parameters were sourced from Brown et al. (1988) and Smoot and Smith (1985) and are shown in Table 10. Figure 5 shows a visual comparison of

the rates of reaction on an Arrhenius plot. It can be seen from the figure that oxidation is a faster process than gasification, and that rates generally increase with decreasing rank.

Table 10. Char oxidation and gasification parameters used in the model (Goetz et al., 1982).

Coal	Oxidation Rate Parameters		Gasification Rate Parameters	
	A g/(cm^{2}s atmO_2)	E (cal/gmol)	A g/(cm^{2}s atmCO_2)	E (cal/gmol)
Sub-bituminous	145	19970	1040	42470
Illinois #6	60	17150	12973	56370
Pittsburgh #8	66	20360	1390	53700

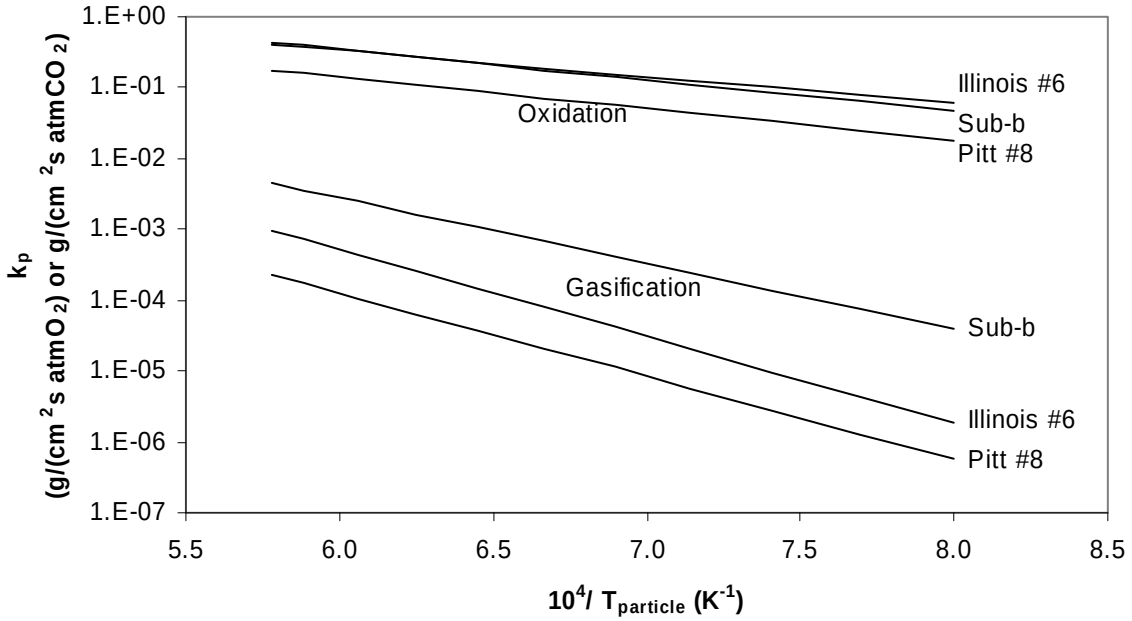

Figure 5. Comparison of rates of char reaction with O_2 (oxidation) and CO_2 (gasification).

Kajitani et al. (2006) studied CO_2 gasification of char in entrained flow gasification and concluded that CO can inhibit the CO_2 gasification, but high partial pressures of CO were required (>0.4 MPa) and the effect is less at high temperatures (> 1400°C). Based on these results this possible effect was neglected in the model and the values from Goetz et al. (1982) were used without modification.

Shaddix and Molina (2007) determined that char combustion rates were lower in a CO_2-based gas. As the surface kinetic rates were nominally the same as in air, the difference was attributed to slower diffusion of O_2 through the CO_2-rich boundary layer. The char model used here is based on bulk gas concentrations and therefore this knowledge could not be incorporated into the model. The error due to this is however minimal as the reported decrease in burning rate is only about 10%.

Experimental Results

Experimental results are presented here but discussion is delayed until after a presentation of the modeling results shown in the next section.

Unstaged Combustion Experiments

The unstaged experiments were conducted by introducing all reactants (premixed) through the burner with an overall SR of 1.04–1.06. CO_2 data for the air case shown in Figure 6 indicate that most reaction occurs in the upper half of the MFR.

Figure 7 presents the wall temperature data that indicate comparable heat release profiles for the Air and O25 oxidizers. The higher wall temperature near the burner for the O30 oxidizer suggests earlier heat release and probably higher particle heating rates. As is the case for all figures in this chapter, the lines connecting data points are to assist in visual association between widely spaced data points and do not imply that the plotted parameter follows that path.

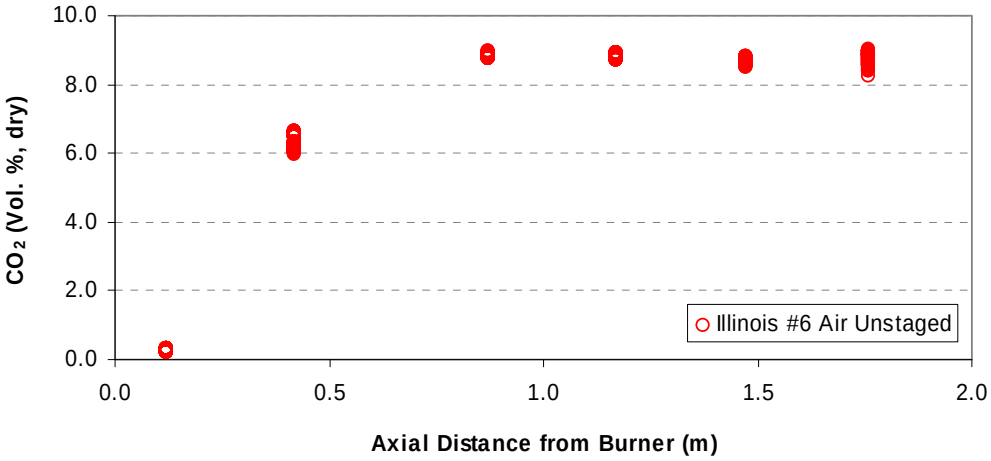

Figure 6. CO_2 data for the Illinois #6 Air Unstaged experiment.

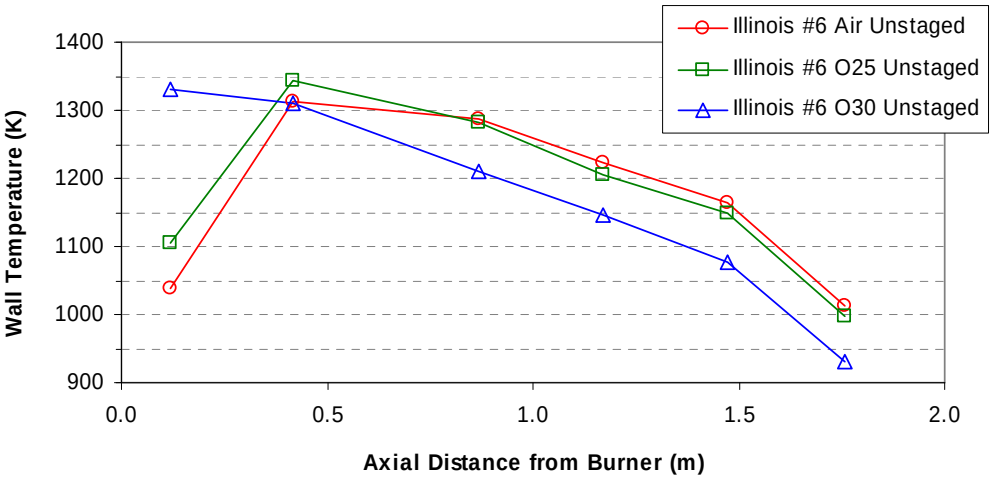

Figure 7. Wall temperature data for the Illinois #6 Unstaged experiments.

NO_X measurements in Figure 8 show higher NO_X concentrations in both oxy-fuel cases relative to the air case. The nitrogen conversion efficiency data removes the effect of the varying diluent and indicates that Air and O30 as oxidizers produce similar effluent NO_X with O25 producing slightly less.

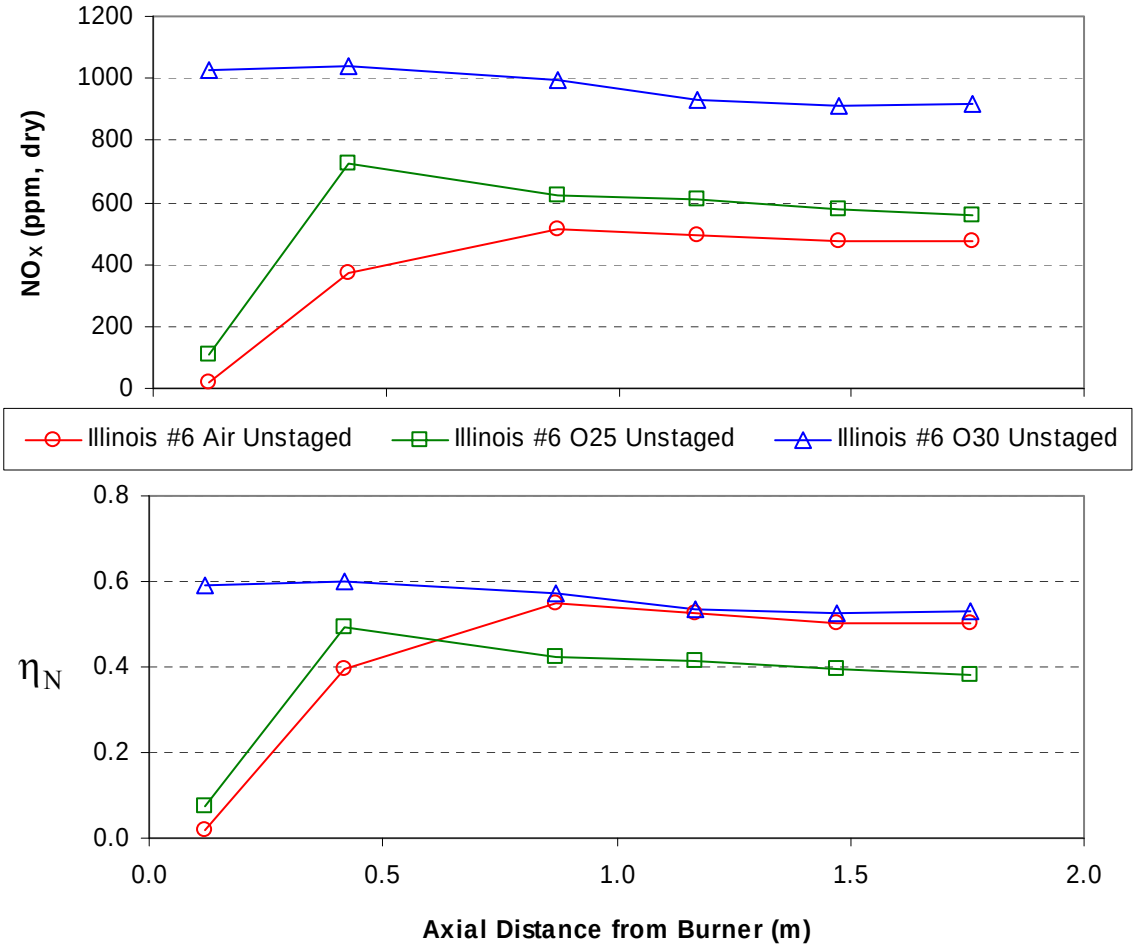

Figure 8. NO_X measurements and corresponding nitrogen conversion efficiency data for the Illinois #6 Unstaged experiments.

A slight decline in NO_X is observed for all cases in the lower half of the reactor. This drop was unexpected because NO reduction by reaction with char or by reverse thermal NO_X reactions was not expected to be significant in this section of the reactor. Other possible explanations include dilution by air leaking into the reactor or by CO_2 production during char oxidation. The CO_2 data in Figure 6 show little rise in this region of the reactor suggesting CO_2 dilution is not the cause. Although initially the reactor was found to leak air inward, the data shown were taken with a positive reactor gage pressure which eliminated this source of dilution. This leaves little explanation except to conclude that some reduction in NO_X due to char or the thermal mechanism is occurring.

The NO_X data for the O30 oxidizer show that peak NO_X values occur further upstream than for the Air and O25 oxidizers. This is consistent with more rapid combustion as indicated by the wall temperature data. The O25 oxidizer's lower effluent NO_X may also be due to differences in heating rates. A lower heating rate is expected to result in lower nitrogen release with the volatiles. Lower conversion efficiency of char-N to NO (relative to volatiles-N to NO conversion) could thereby cause lower overall NO production.

The slight decline in NO_X in the lower half of the reactor is insufficient to produce the low levels of nitrogen conversion efficiency required by emissions regulations. No notable difference in nitrogen evolution between air and oxy-fuel cases is noted beyond the initial NO_X formation, which may be simply due to differences in particle heating and combustion rates. The remainder of the work focused on oxidizer-staged combustion where a reducing zone was formed near the burner to simulate the performance of a low-NO_X combustion system.

Char and Fly Ash Analysis - Staged Combustion, Fixed Stoichiometry

For the oxidizer-staged experiments with three coals, an attempt was made to close the nitrogen balance by analyzing the char for residual nitrogen and using these data in combination with NO_X measurements. Figure 9 presents a summary of the results normalized by fuel-N entering the MFR (i.e. in terms of η_N). The figure is based on the assumption that all measured NO_X originates from fuel-N and that nitrogen not accounted for in the char and NO_X must have left the MFR in the form of N_2. Accuracy of the char-N and burnout measurements is not affected by this assumption. Burnout was determined by ashing particulate from the exhaust system filter and measuring the mass loss (i.e. ash was used as a tracer).

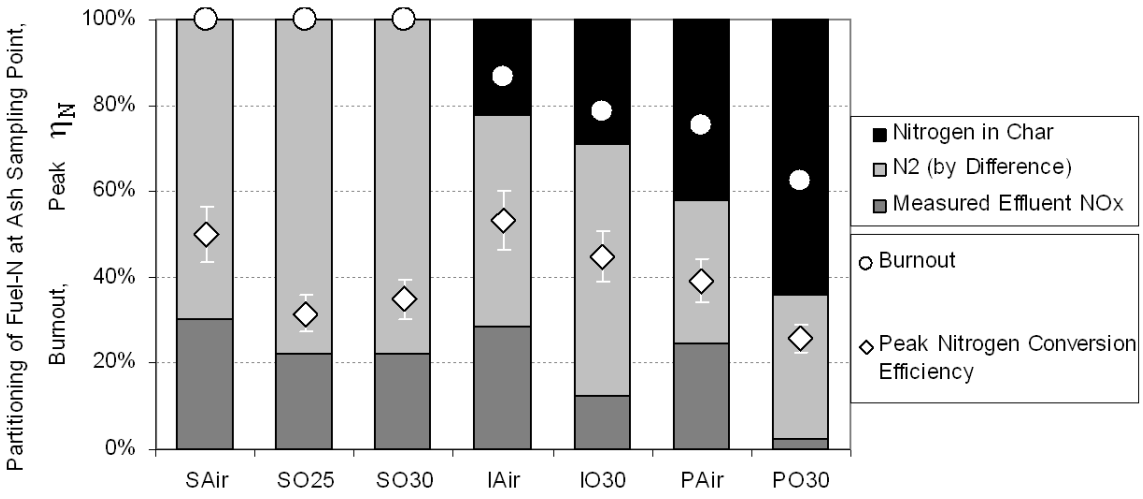

Figure 9. Summary of data showing the fate of fuel nitrogen in oxidizer-staged experiments (assuming all NO_X is fuel NO_X). All data are from the ash sampling location with the exception of the peak nitrogen conversion efficiency which is from the reactor centerline near the burner. The horizontal axis labels indicate the coal by the first letter: S, I, P for sub-bituminous, Illinois #6, and Pittsburgh #8 respectively, followed by the oxidizer type.

By comparing the burnout measurements to the char-N measurements in Figure 9 we see that for the two higher-ranked coals the percent of coal burned is greater than the percent of fuel-N converted. This is consistent with measurements made in developing the CPD-NLG coal devolatilization model that nitrogen release is slightly lower than volatiles release thus resulting in a char that is enriched in nitrogen relative to the parent coal (Genetti, 1999). Only the sub-bituminous coal achieved high burnout; which was the reason for it being the most extensively studied coal in this work. The O25 and O30 data in the figure for this coal show no difference in peak nitrogen conversion efficiency greater than the level of uncertainty.

Peak η_N in the air cases is higher than in the corresponding oxy-fuel cases for all three coals which may be due to thermal and prompt NO_X formation in addition to fuel NO_X. For all three coals the effluent NO_X emissions are lower in the oxy-fuel cases than the air cases and the higher the rank of the coal, the greater is the difference between the air and oxy-fuel NO_X emissions.

The high level of burnout achieved for the sub-bituminous coal made it possible to submit fly ash samples for mineral analysis without further thermal processing. Results are shown in Figure 10. As expected, the ash generated by combustion differs significantly from the ash prepared under laboratory conditions.

These data show the largest percentage change between air and oxy-fuel is in the sulfur content, with oxy-fuel being higher. Oxy-fuel ash was also higher in calcium by 17% and lower in silicon by 16%. Sarofim (2007) quotes multiple works that measured increased sulfur removal with the ash under oxy-fuel conditions, consistent with this result. The composition differences lead to changes in ash properties such as estimated ash fusion temperature.

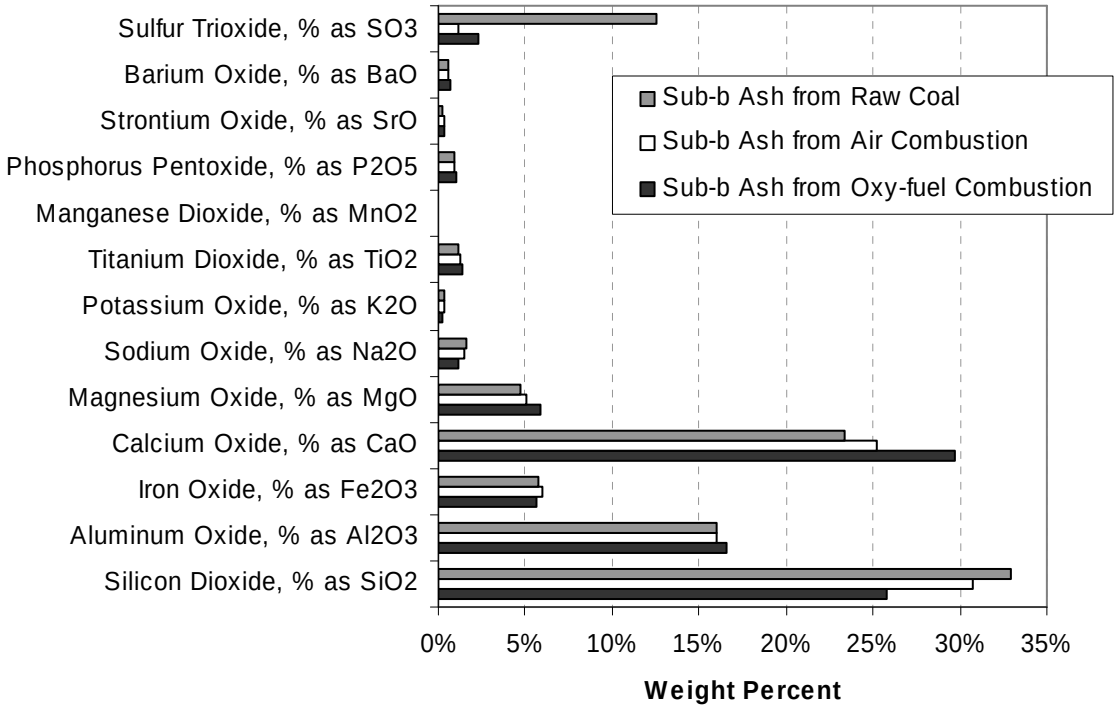

Figure 10. Mineral ash analysis from the parent sub-bituminous coal, and fly ash from air and oxy-fuel staged combustion. The fly ash was obtained from the exhaust system particulate filter. In the oxy-fuel case this was after both O25 and O30 experiments were conducted.

The causes of the NO_X evolution differences between air and oxy-fuel under oxidizer staged combustion were investigated through centerline measurements of NO_X formation and destruction along the length of the reactor. These data make up the remainder of this chapter.

Gas Species Measurements - Staged Combustion, Fixed Stoichiometry

Pittsburgh #8 Coal

Wall temperature measurements for the Pittsburgh #8 coal are shown in Figure 11. The oxy-fuel case has higher wall temperatures near the burner, lower temperatures further downstream in the reducing zone, and comparable temperatures to air combustion in the burnout zone.

The oxygen data in Figure 12 (which may be only qualitative) shows that consumption of oxygen in the primary combustion zone requires some distance downstream from the burner to occur. Some oxygen from burnout oxidizer injection is detected upstream of the injection point, and fairly rapid consumption occurs close to the burnout oxidizer injectors. It appears that little or no combustion occurs further downstream, and the final oxygen levels are consistent with the low level of burnout (Figure 9).

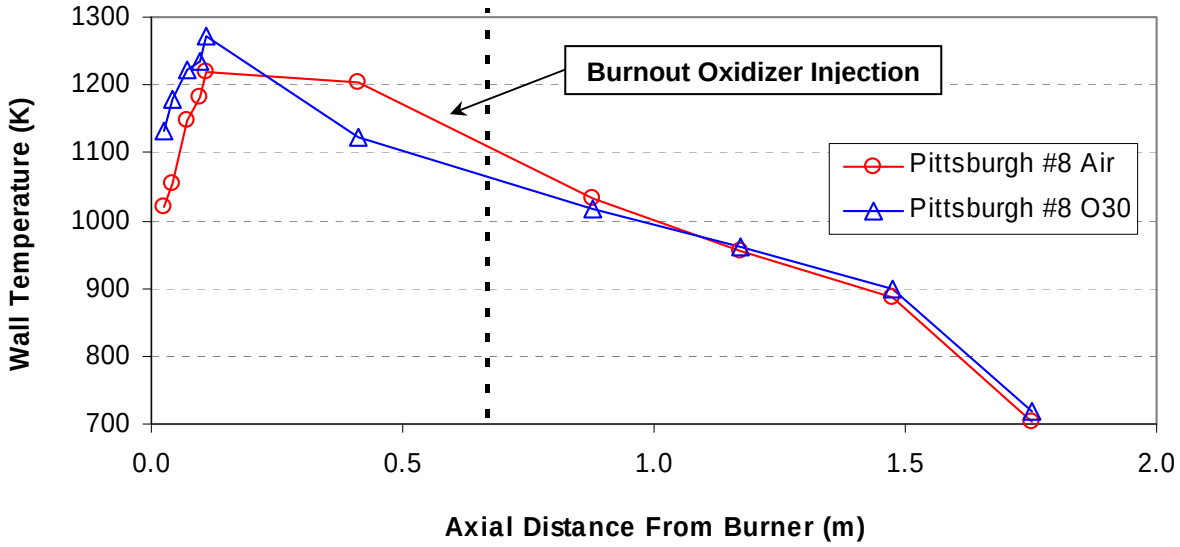

Figure 11. Wall temperature measurements for the Pittsburgh #8 staged combustion experiments.

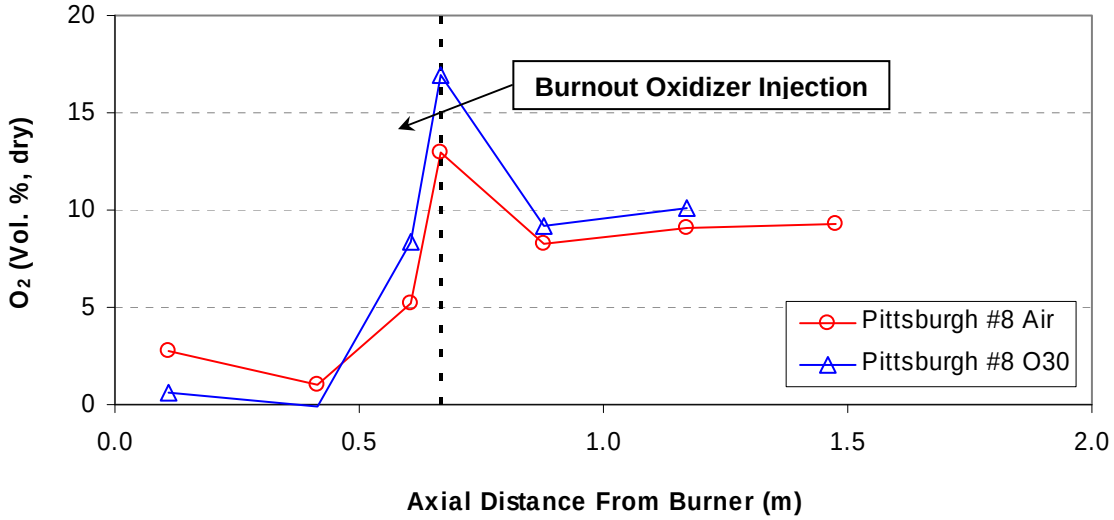

Figure 12. Oxygen measurements for the Pittsburgh #8 staged combustion experiments.

CO measurements (Figure 13) show very high levels of CO (beyond the HORIBA instrument's range of 5000 ppm) in the oxy-fuel reducing zone relative to air combustion. Data downstream of the burnout oxidizer injection are of limited value given the low level of fuel burnout.

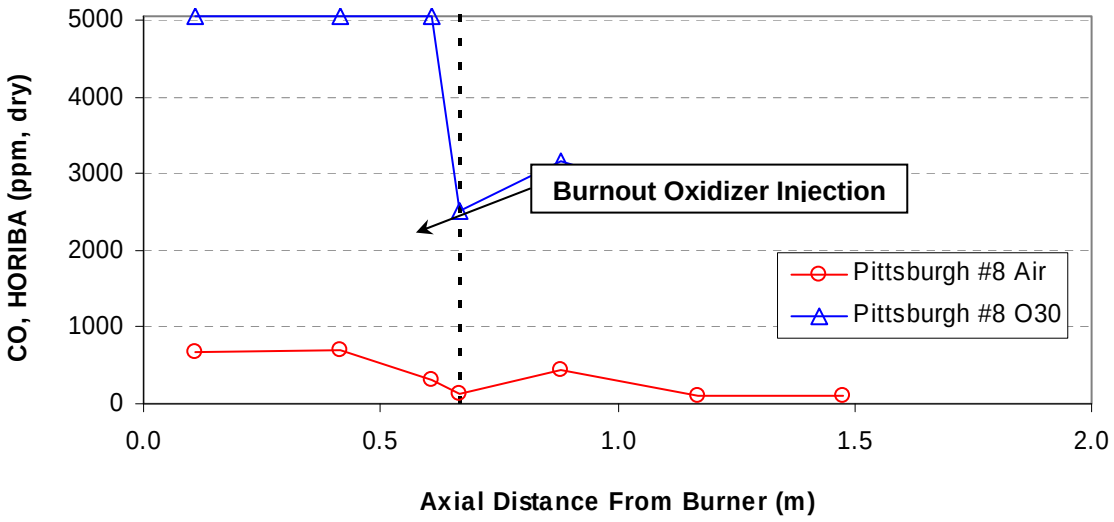

Figure 13. CO data for the Pittsburgh #8 staged combustion experiments.

Measurements of NO_X and corresponding η_N in Figure 14 indicate that the oxy-fuel case produced lower NO_X initially, and had more rapid NO_X destruction prior to burnout oxidizer injection. The air case produced more NO_X than the oxy-fuel case around the burnout injector location, and final NO_X levels were significantly higher than in the oxy-fuel case. The oxy-fuel char retained more nitrogen than the air char (see Figure 9).

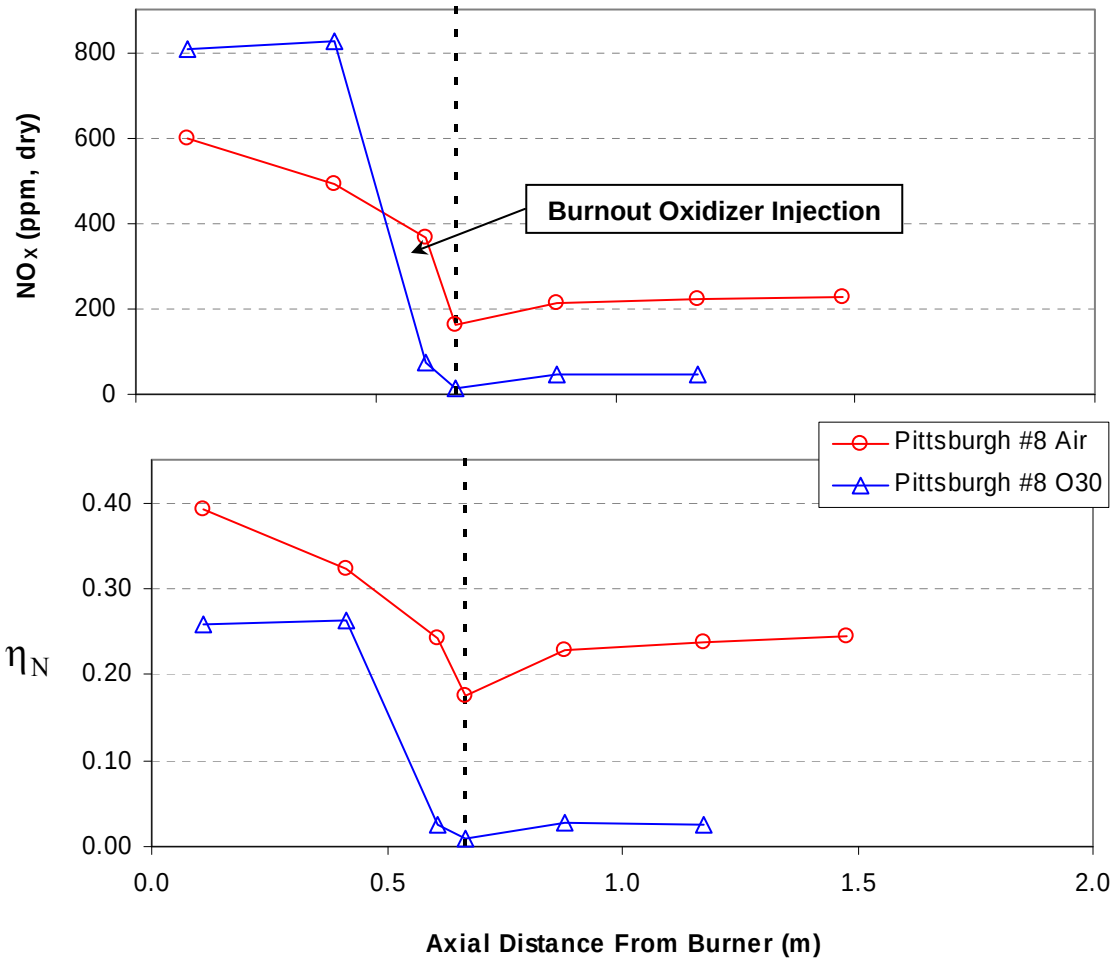

Figure 14. NO_X concentration measurements and corresponding nitrogen conversion efficiency for the Pittsburgh #8 staged combustion experiments (data from HORIBA instrument).

Illinois #6 Coal

Wall temperature profiles and major species (O_2, CO_2, and H_2O) measurements for the Illinois #6 Air and O30 experiments are shown in Figure 15. Like the Pittsburgh #8 wall temperature data the oxy-fuel case relative to air firing has higher temperatures near the burner, cooler temperatures later in the reducing zone and comparable temperatures in the burnout zone.

The O_2 measurements are constant for both air and oxy-fuel cases from 0.2–0.6 m from the burner. Again it is emphasized that these data are qualitative, and thus while the measured value is non-zero, the zero slope over this region in the reactor is believed to indicate that oxygen consumption has stopped due to oxygen being unavailable. Up to 0.2 m from the burner the O_2 appears to be consumed faster in the oxy-fuel case.

The oxy-fuel experiment has higher levels of CO_2 and H_20 as expected with the CO_2 diluent. In the lower half of the reactor the oxy-fuel data show an increase in CO_2 and H_20 while O_2 decreases, consistent with char oxidation. It is not known why the air experiment does not have

these characteristics. For oxy-fuel, the sum of O_2, CO_2, and H_2O concentrations is roughly 100% at the exit of the reactor.

Carbon combustion intermediate species (CO, CH_4, and C_2H_4) measurements are presented in Figure 16. The uppermost plot in the figure of CO data measured on a dry basis was limited by the HORIBA instrument to 5000 ppm, but this plot shows better resolution of lower CO levels in the burnout zone than can be seen in the second CO plot obtained from the MKS FTIR instrument. Effluent CO levels are comparable between air and oxy-fuel, but CO is significantly higher in the reducing zone for the oxy-fuel case, at nominally the same SR. CH_4 was only detected for the air case near the burner and could be methane from the natural gas supplied to the burner or from the coal volatiles. Ethylene (C_2H_4) was detected in higher concentrations in oxy-fuel over most of the reactor. With the exception of the data point at about 45 ppm there appears to be a trend of decreasing ethylene with distance from the burner in the reducing zone.

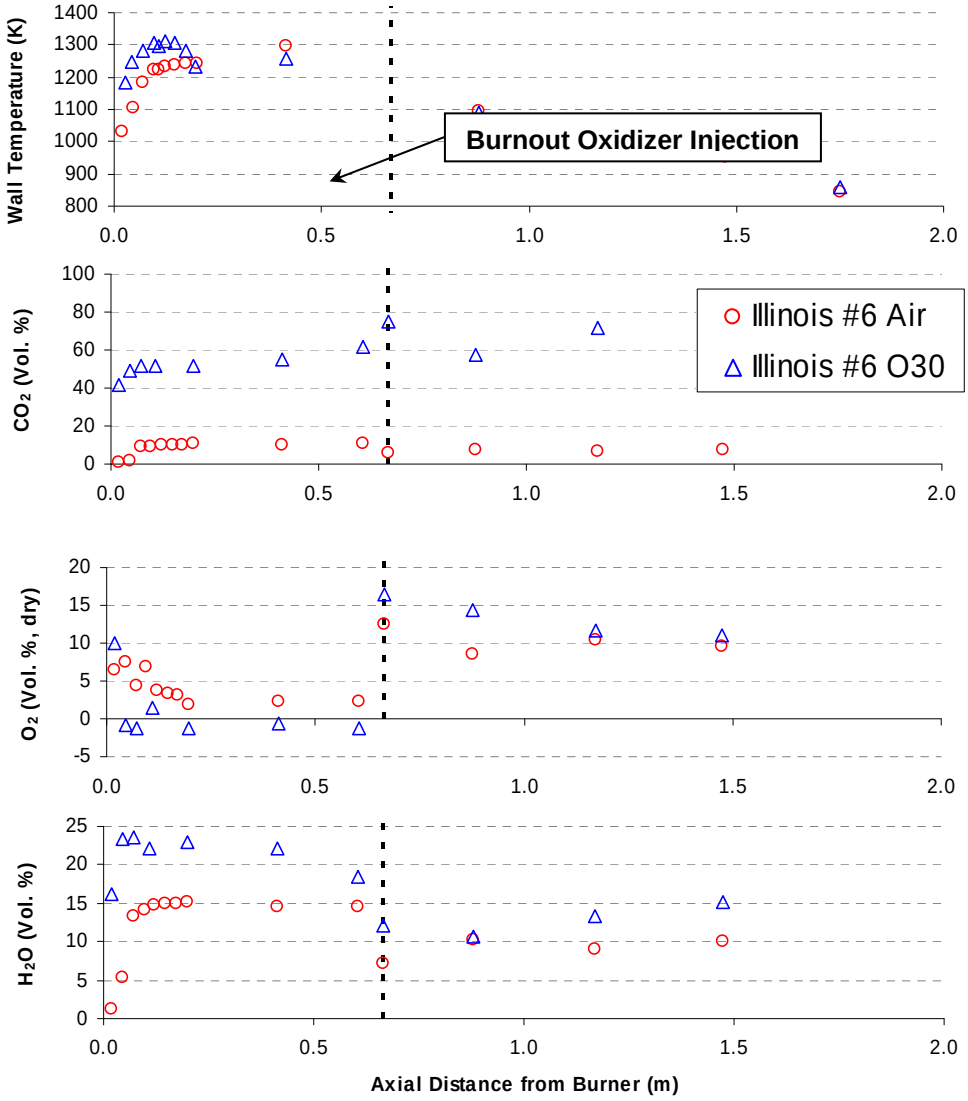

Figure 15. Wall temperatures and major species measurements for the Illinois #6 staged combustion experiments.

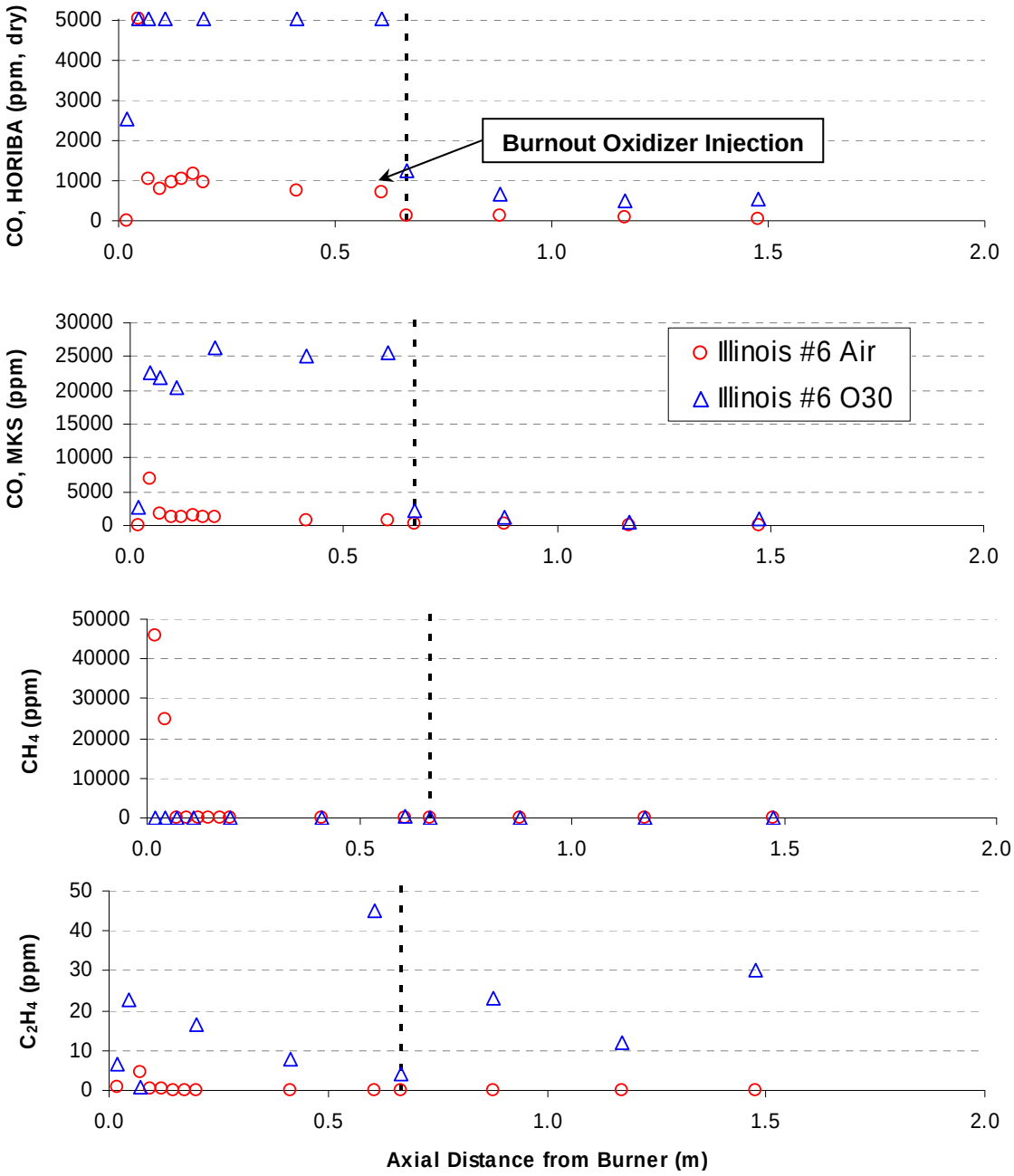

Figure 16. Carbon combustion species for the Illinois #6 staged combustion experiments.

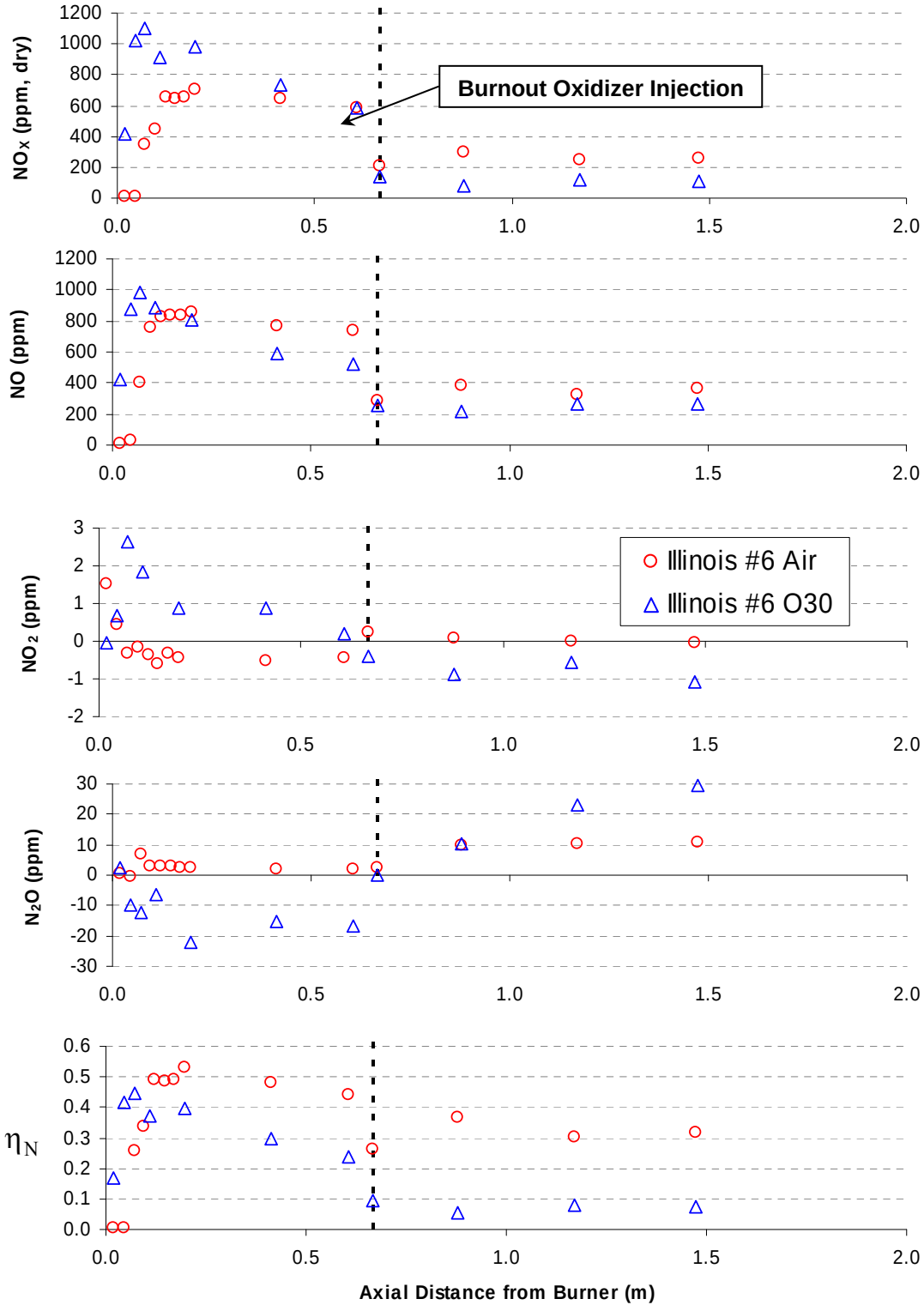

Figure 17. Nitrogen oxides measurements for the Illinois #6 experiments. Nitrogen conversion efficiency was calculated from the HORIBA NO_X data in the top plot.

Measurements of nitrogen oxides in Figure 17 show that the NO_X is predominantly NO. N_2O and NO_2 are in lower concentrations and the measurements have low signal-to-noise ratio as demonstrated by the negative values reported by the instrument. The NO_X data for air show a rapid rise in NO_X after the burner followed by a slower rise before the decline in NO_X associated with the reducing zone. The oxy-fuel case in contrast shows only the rapid rise followed by a decline that is more rapid than that observed for air. At the point of burnout oxidizer injection the air case forms some NO_X but the oxy-fuel case does not. With these differences the oxy-fuel case produced lower effluent NO_X despite the similarity in the initial rapid NO_X formation between air and oxy-fuel seen in the η_N plot at the bottom of the figure.

Concentrations of the nitrogen intermediate species HCN and NH_3 are plotted in Figure 18. Both species are in low concentrations although higher values were measured under oxy-fuel conditions. For the air case the highest values occur nearest the burner where as for oxy-fuel, HCN and NH_3 are found in measurable amounts throughout the region upstream of burnout oxidizer injection.

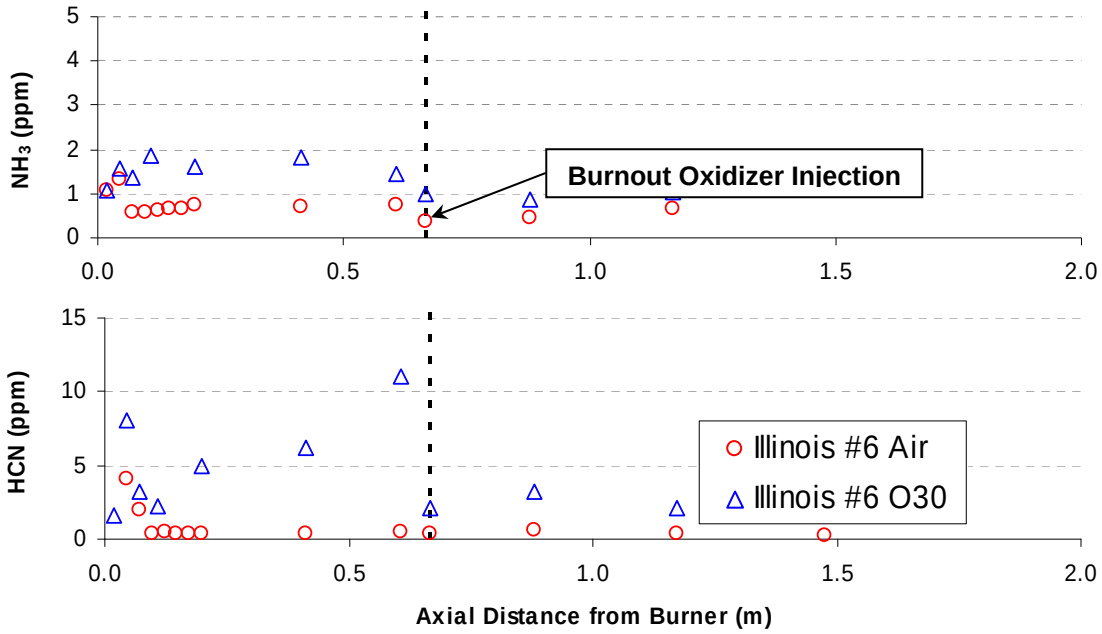

Figure 18. Nitrogen intermediates NH_3 and HCN for the Illinois #6 staged combustion experiments.

SO_2 concentrations were slightly higher in the oxy-fuel case as shown in Figure 19. It should be noted that these experiments were performed with oxidizer from bottled gases rather than flue gas recycling and thus the values are not representative of SO_2 concentrations to be expected in an industrial situation with a true recycle stream. The increased concentrations are primarily due to lower volumes of diluent (CO_2) in oxy-fuel relative to the N_2 in air. It is noted that unlike NO_X, SO_2 is not reduced in the reducing zone. Because of this behavior SO_2 is not amenable to control by combustion modifications and flue gas treatment is necessary. The drop in SO_2 at 0.67 m from the burner is due to the dilution of the combustion gases with burnout oxidizer.

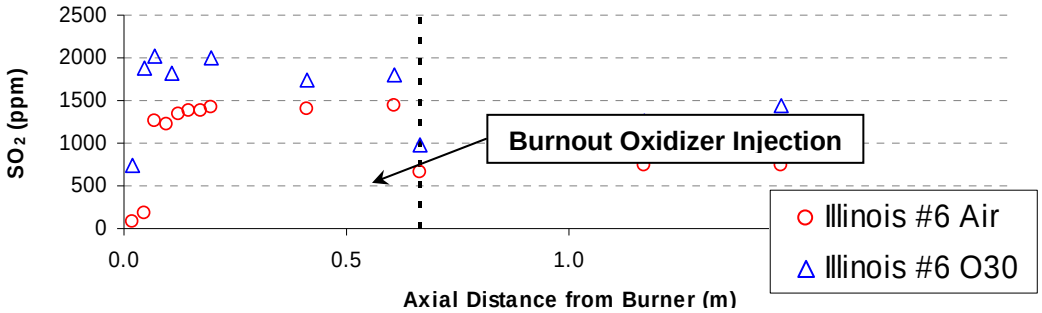

Figure 19. SO_2 concentrations measured in the Illinois #6 staged combustion experiments.

Illinois #6 Coal with NO in Reactants

The effect of recycled NO on nitrogen evolution was investigated by replacing the CO_2 in the oxidizer with a mixture of 525 ppm NO in CO_2. NO_X was measured with and without NO in the oxidizer with results shown in Figure 20. A line representing the difference between the two data has been added to assist in evaluating the data. As a result of dilution of the doped CO_2 with oxygen and natural gas, the gas mixture entering the reactor, has 308 ppm more NO than the pure CO_2-based mixture. At the first measurement location, the difference has decreased to only 253 ppm. Since the concentration of NO_X, at the first measurement position is higher than the incoming concentration it appears that NO_X formation is slower or inhibited by NO in the oxidizer. The difference continues to decrease monotonically during a period when both experiments show NO_X reduction. NO_X reduction therefore appears to increase with the presence of NO in the oxidizer. Both of these observed trends are consistent with the rate of NO_X destruction reactions being proportional to NO_X concentration. The rise in NO between 0.41 and 0.6 m from the burner is largely associated with transport of NO upstream from the burnout oxidizer.

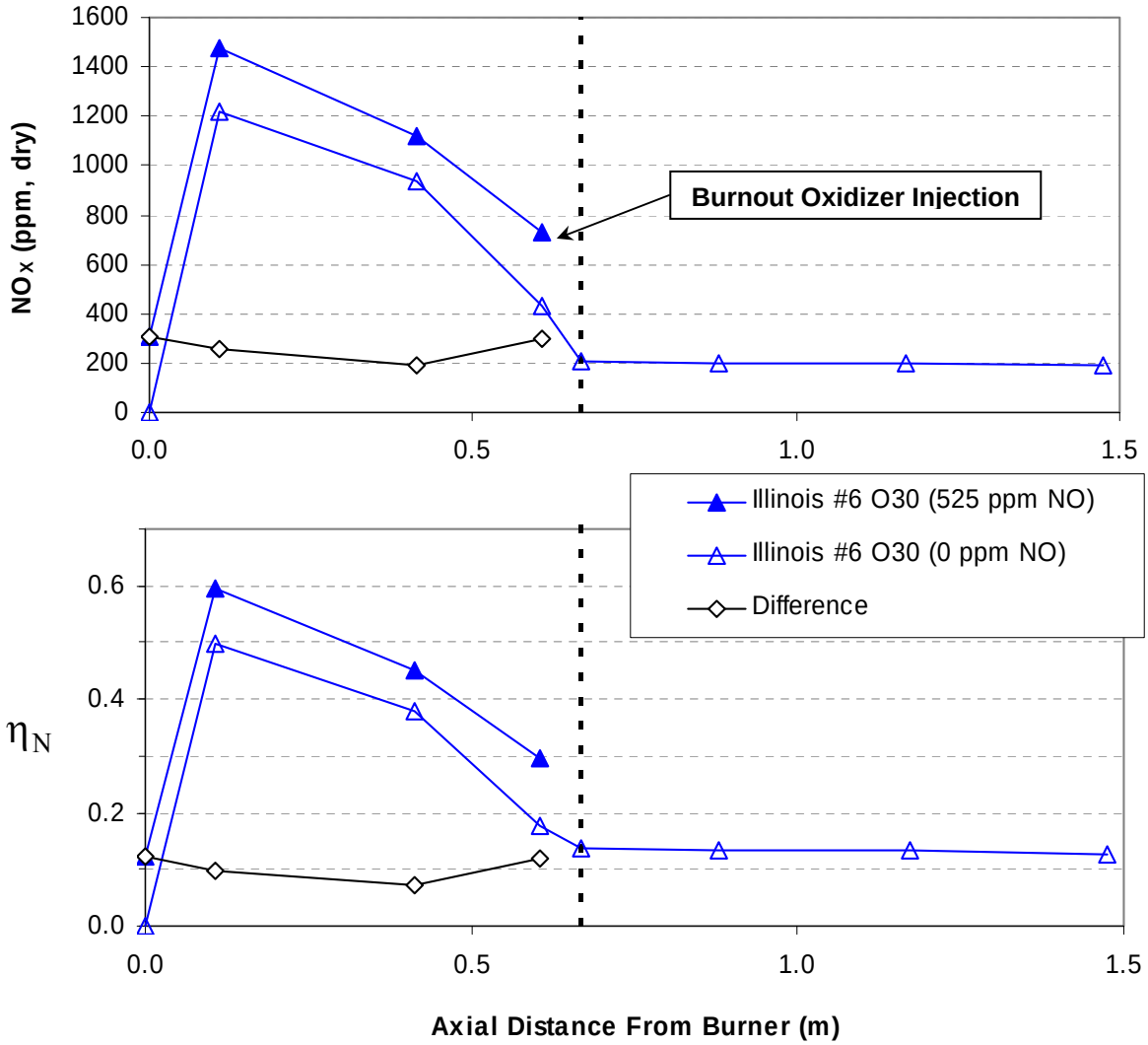

Figure 20. NO_X measurements and nitrogen conversion efficiency with and without NO in the reactants for Illinois #6 coal. Values at 0 m from the burner are calculated from the measured reactant flows as opposed to being directly measured. All data from the HORIBA instrument.

Sub-bituminous Coal

Wall temperature and major species data for the sub-bituminous coal staged combustion experiments are shown in Figure 21. Like the two other coals the wall temperatures near the burner are comparable or higher in oxy-fuel than air combustion, and lower in the reducing zone. Unlike the other two coals the oxy-fuel wall temperatures are higher than air combustion in the burnout region.

The O_2 data appear to indicate more rapid consumption of O_2 near the burner in the oxy-fuel cases. CO_2 and H_2O concentrations are higher in oxy-fuel than air cases. For all data the O25 and O30 oxy-fuel cases are more similar to each other than either is to the air case. Beyond these points there is nothing remarkable about the major species data.

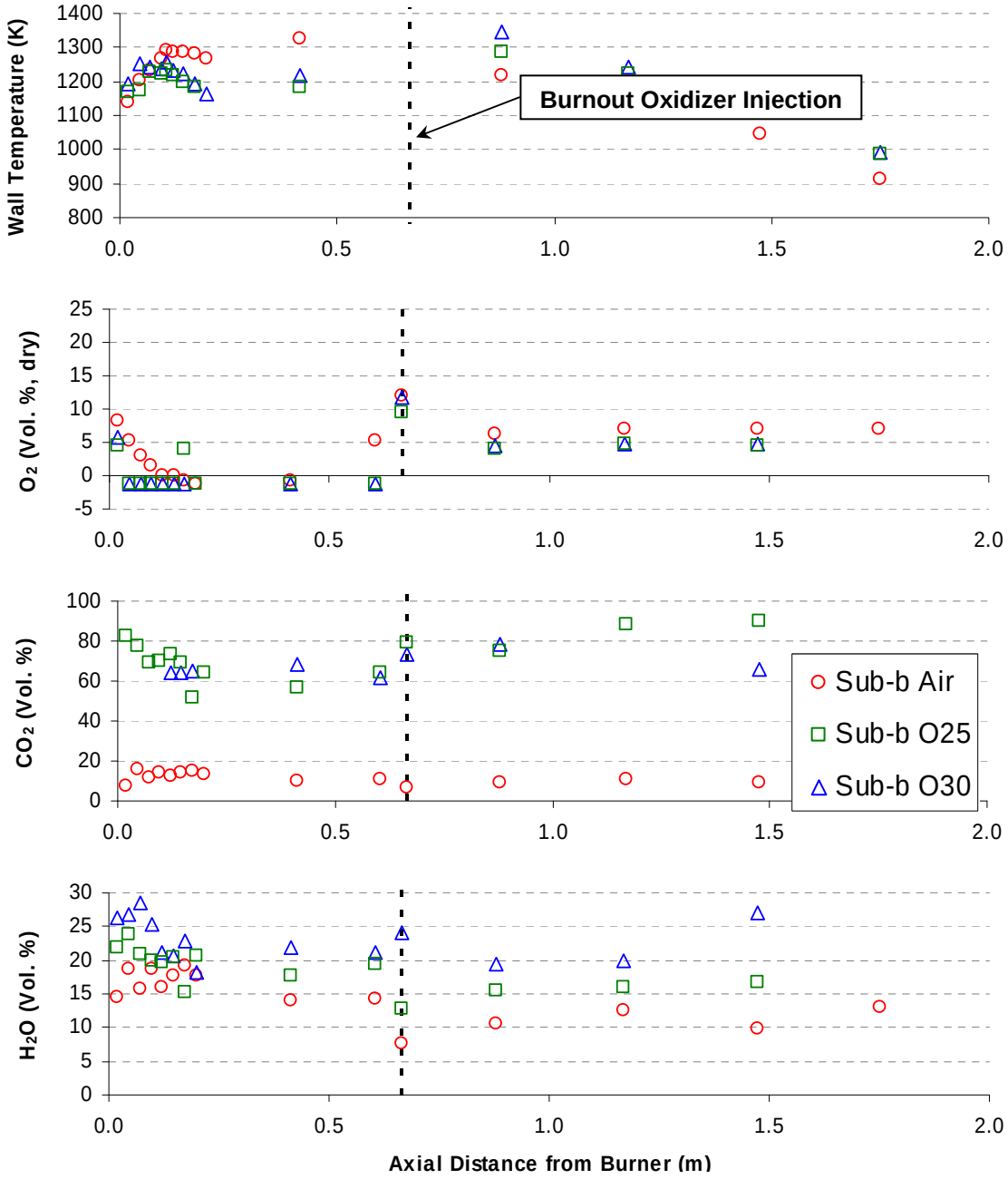

Figure 21. Wall temperatures and major species measurements for the sub-bituminous coal staged combustion experiments.

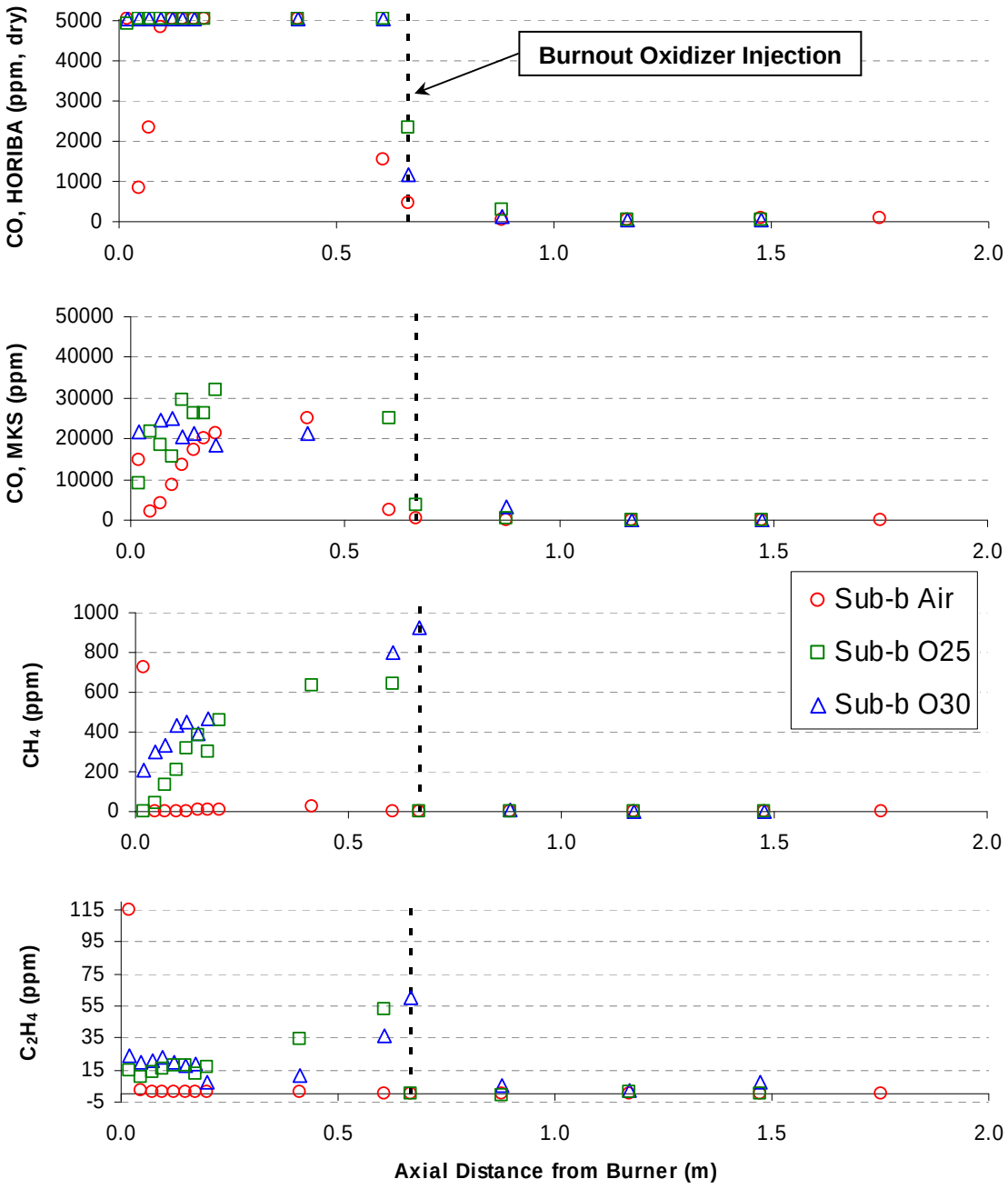

Figure 22. Carbon combustion species for the sub-bituminous coal staged combustion experiments.

CO, methane, and ethylene data are plotted in Figure 22. For the air case there is a peak in CO just downstream of the burner followed by a low value that rises to levels comparable to those in the oxy-fuel case. For the Illinois #6 coal the air case CO was quite low relative to the values shown here. The oxy-fuel cases have high CO levels throughout the primary combustion zone. All cases have very low effluent CO.

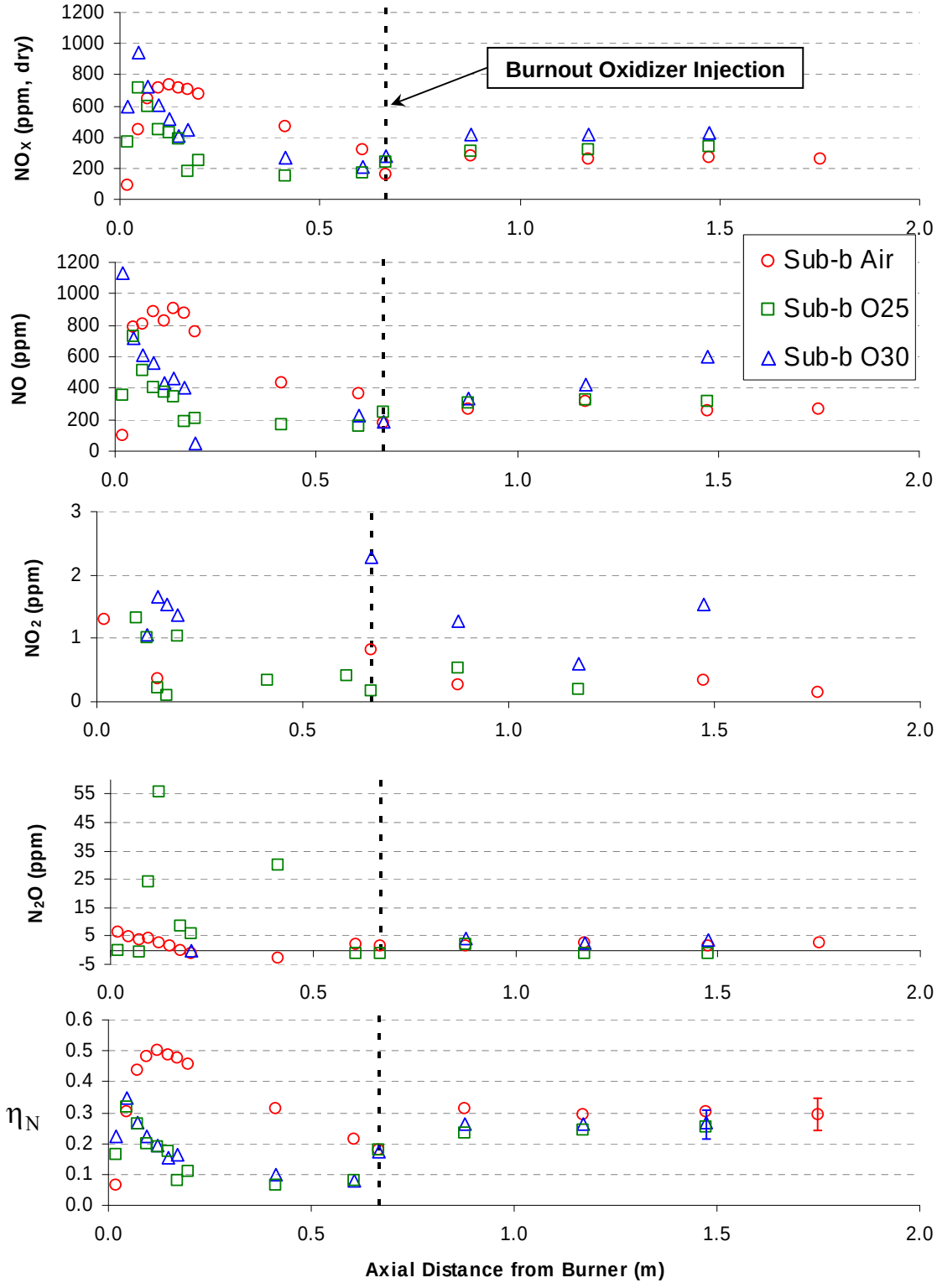

Figure 23. Nitrogen oxides measurements for the sub-bituminous coal experiments. Oxy-fuel data were not taken at 1.75 m from the burner due to experimental difficulties. η_N is calculated from NO_X data in the top plot.

Methane and ethylene are almost non-existent in the air case except very close to the burner. In contrast the oxy-fuel cases have significant amounts of both gases throughout the reducing zone.

Data for the oxides of nitrogen appear in Figure 23. Most features of the data are similar to those observed in the Illinois #6 experiments. The air case has rapid NO formation near the burner followed by slower formation. The oxy-fuel cases also have rapid formation initially, but this is followed by NO_X destruction that begins earlier than in the air case and has a faster rate. NO_X is dominated by NO and the initial levels of rapid NO formation are similar in terms of η_N. Several N_2O data points for the O30 case were discarded as the readings had a high noise to signal ratio, despite other species measurements being steady. This can be a result of interference from other gasses being larger than the absorption from N_2O.

Unlike the Illinois #6 coal, effluent NO_X levels for this coal are comparable between air and oxy-fuel. A key difference between the Illinois #6 η_N profile in O30 oxidizer and that of the sub-bituminous coal is the greater formation of NO_X in the sub-bituminous case as burnout oxidizer is injected. The uncertainty of η_N in Figure 23 is 18% suggesting the uncertainty is too large to conclusively state that the oxy-fuel cases produce lower η_N. However, when the data were later repeated in a sweep of primary zone stoichiometric ratios oxy-fuel again produced lower η_N.

Measurements of the nitrogen intermediates HCN and NH_3 in Figure 24 show that NH_3 is in much greater concentrations with sub-bituminous coal than for Illinois #6. NH_3 tends to increase with distance from the burner. Both HCN and NH_3 are more prevalent in oxy-fuel than air cases. Neither species was detected in significant amounts in the burnout region.

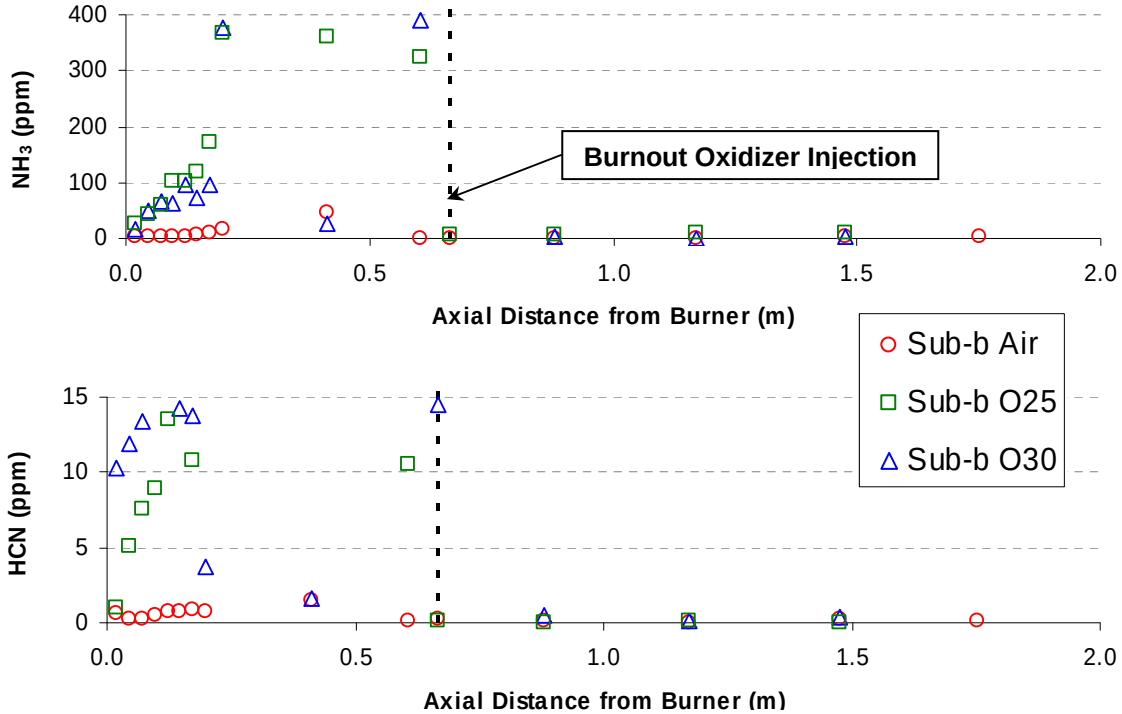

Figure 24. Nitrogen intermediates NH_3 and HCN for the sub-bituminous coal staged combustion experiments.

The results shown up to this point have compared air and oxy-fuel combustion on the basis of identical stoichiometry. In the next section the effect of primary (burner) SR on effluent NO_X was studied. This testing was done to find the conditions for lowest effluent NO_X in this reactor for air and oxy-fuel so that a detailed comparison could be made of the two combustion types operating under their optimum low-NO_X conditions.

Effluent NO_X Measurements – Staged Combustion with Varied Stoichiometry

Effluent NO_X as a function of primary zone SR is presented in Figure 25. Total oxidizer flow to the experiment was kept constant while the ratio of primary to burnout oxidizer was changed. As expected there was some level of staging (amount of oxidizer diverted from the burner) that produced minimum effluent NO_X. As primary zone SR decreases, O_2 availability to form NO_X initially is decreased and conditions for NO_X reduction are also created. There is some point however where combustion at the burnout injector location becomes so intense that significant NO_X begins to form and overall NO_X production increases.

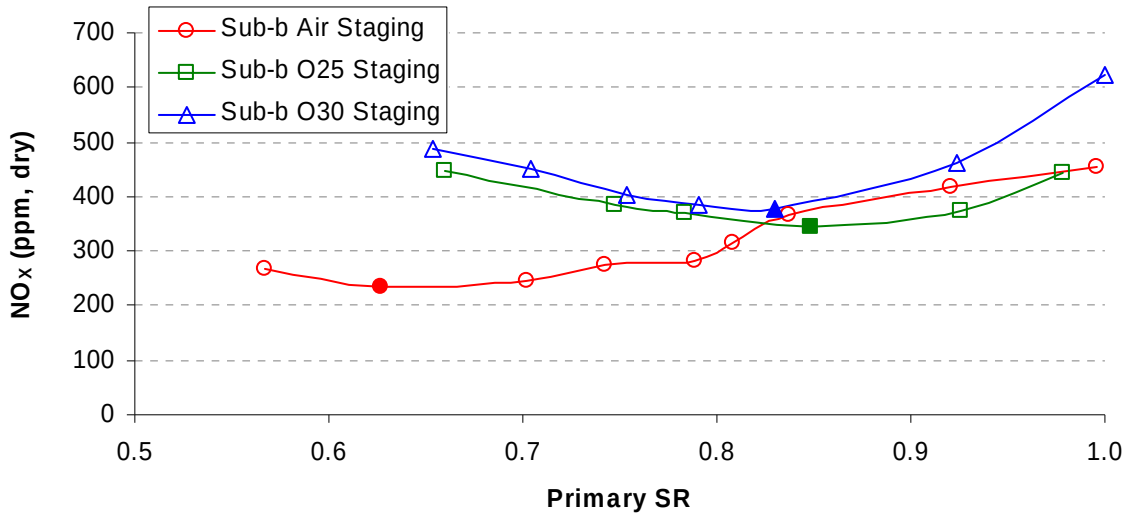

Figure 25. Effluent NO_X measurements for the sub-bituminous coal as a function of primary combustion zone SR.

Figure 26 shows that the primary zone SR for minimum NO_X in oxy-fuel was significantly higher than for air combustion consistent with the higher concentrations of intermediates and more rapid destruction of NO in the reducing zone measured at equal primary SR between air and oxy-firing shown earlier (see Figure 23 and Figure 24). This also suggests that oxy-fuel combustion produces a better reburning environment when NO_X is recycled through the flame in comparison to air combustion. Solid data point markers are used to indicate the conditions of minimum NO_X in the figures. While the minima are similar between oxidizers, at higher values of primary SR, η_N for the oxy-fuel cases are clearly lower than in air at the same primary SR. The data demonstrate that similar η_N can be achieved in air by deeply staging air combustion or staging oxy-fuel combustion to a lesser extent which also favors burnout in oxy-fuel. Note that

this is in the absence of recycled NO_X and shows that η_N reduction is favorable in oxy-fuel combustion independent of recycled NO_X. The air combustion NO_X is more sensitive to primary SR than the oxy-fuel cases at high values of primary SR consistent with trends observed by others. As with results already presented there is little difference between the characteristics of the O25 and O30 oxidizers.

Evidence of increased combustion intensity at the location of burnout oxidizer addition as primary SR decreases can be seen in the wall temperature data in Figure 27 through Figure 29. For all three oxidizers the minimum NO_X conditions are at or near the primary SR where wall temperature downstream of burnout oxidizer injection (0.88 m from burner) becomes higher than the wall temperature upstream (0.41 m from burner).

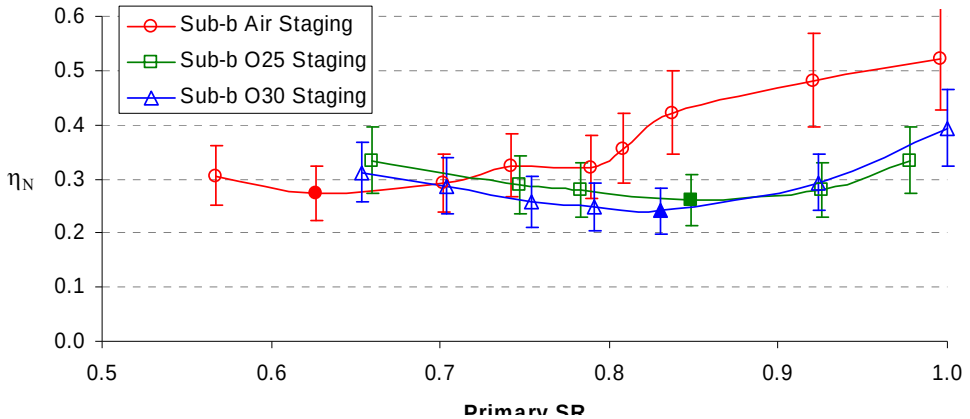

Figure 26. Effluent nitrogen conversion efficiency as a function of primary combustion zone SR. 18% error bars are shown for comparison between Air, O25, and O30. For comparisons within the same oxidizer experiment, the variability is an estimated 5%. An additional 5% uncertainty associated with nitrogen conversion efficiency calculation is not applicable here as the fuel was completely burned for these gas samples.

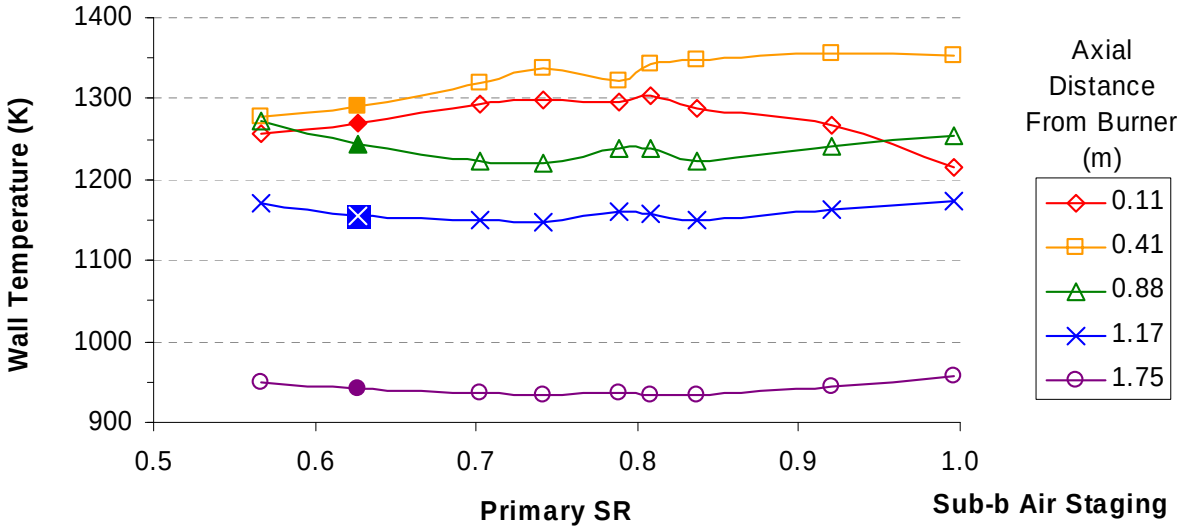

Figure 27. Wall temperature data at various axial locations as a function of primary zone SR for the Sub-b Air Staging experiment.

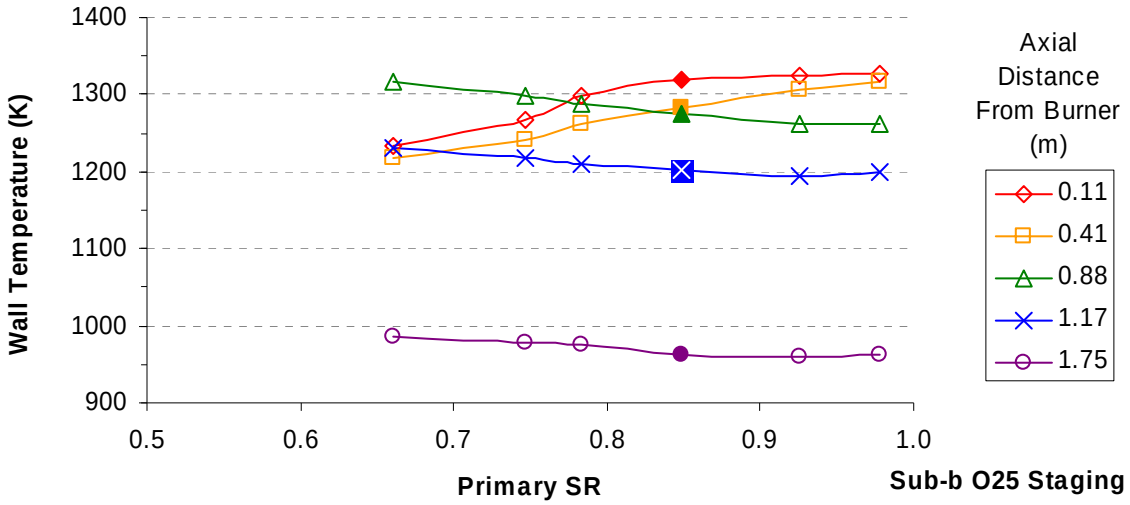

Figure 28. Wall temperature data at various axial locations as a function of primary zone SR for the Sub-b O25 Staging experiment

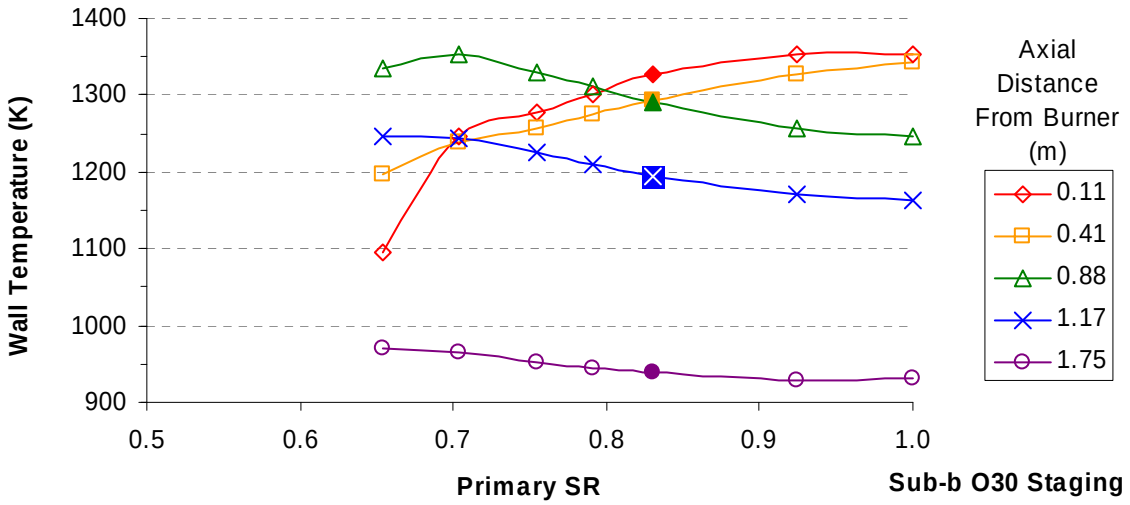

Figure 29. Wall temperature data at various axial locations as a function of primary zone SR for the Sub-b O30 Staging experiment.

Gas Species Measurements - Staged Combustion at Minimum NO_X Conditions

The primary SR's for minimum effluent NO_X that were determined from the results just presented were used to obtain the results reported in this section. High resolution gas sampling measurements and wall temperatures were obtained at these conditions to investigate details of NO_X formation and destruction. Wall temperatures are generally higher overall for the oxy-fuel case as seen in Figure 30. H_2O and CO_2 concentrations in the same figure are also higher for oxy-fuel relative to air combustion as expected. For both air and oxy-fuel the O_2 data near the burner seem inconsistent with neighboring data points and it is hard to tell where the O_2 concentration falls to zero. All of the species data appear to follow trends that do not follow

smooth curves but rather show significant scatter among what appears to be clear trends. The reason for this scatter is unexplained but the most likely cause is an unsteady fuel flow rate. From 0.25 m from the burner to the point of burnout oxidizer injection it appears that O_2 is unavailable in both cases.

CO, methane, and ethylene data in Figure 31 show similar trends for the air and oxy-fuel cases in the reducing zone. Oxy-fuel concentrations are typically lower for methane and ethylene, but considering both the differences in molecular weight of the oxidizers, and in primary SR, differences in total mass of CO, methane and ethylene are difficult to judge. The oxy-fuel conditions appear to produce NO_X reduction of a similar quantity to air combustion (Figure 32) even though species indicating the strength of the reducing environment are of similar or lower concentrations.

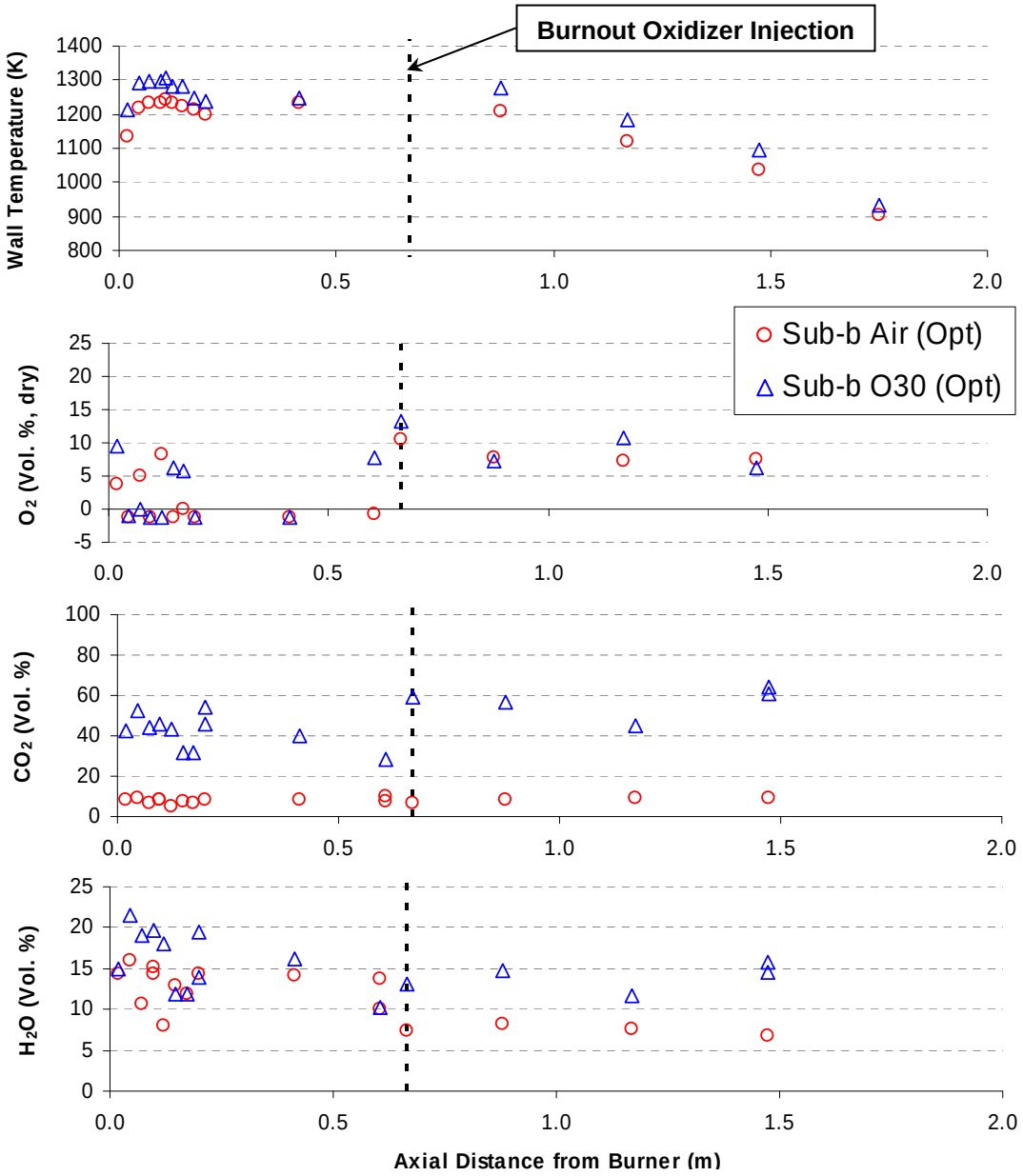

Figure 30. Wall temperatures and major species measurements for the sub-bituminous coal staged combustion experiments at minimum NO_X conditions.

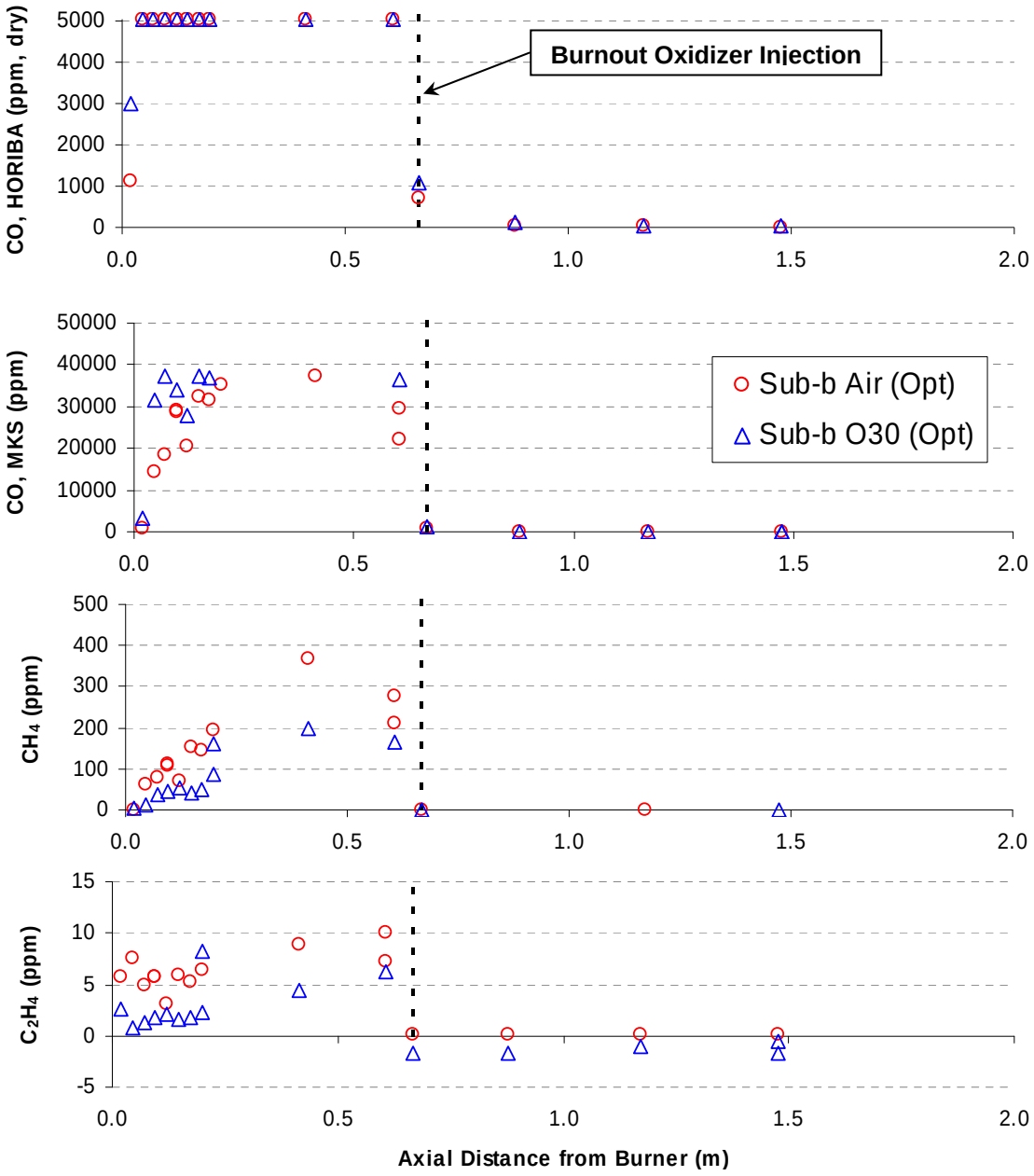

Figure 31. Carbon combustion species for the sub-bituminous coal staged combustion experiments at minimum NO_X conditions.

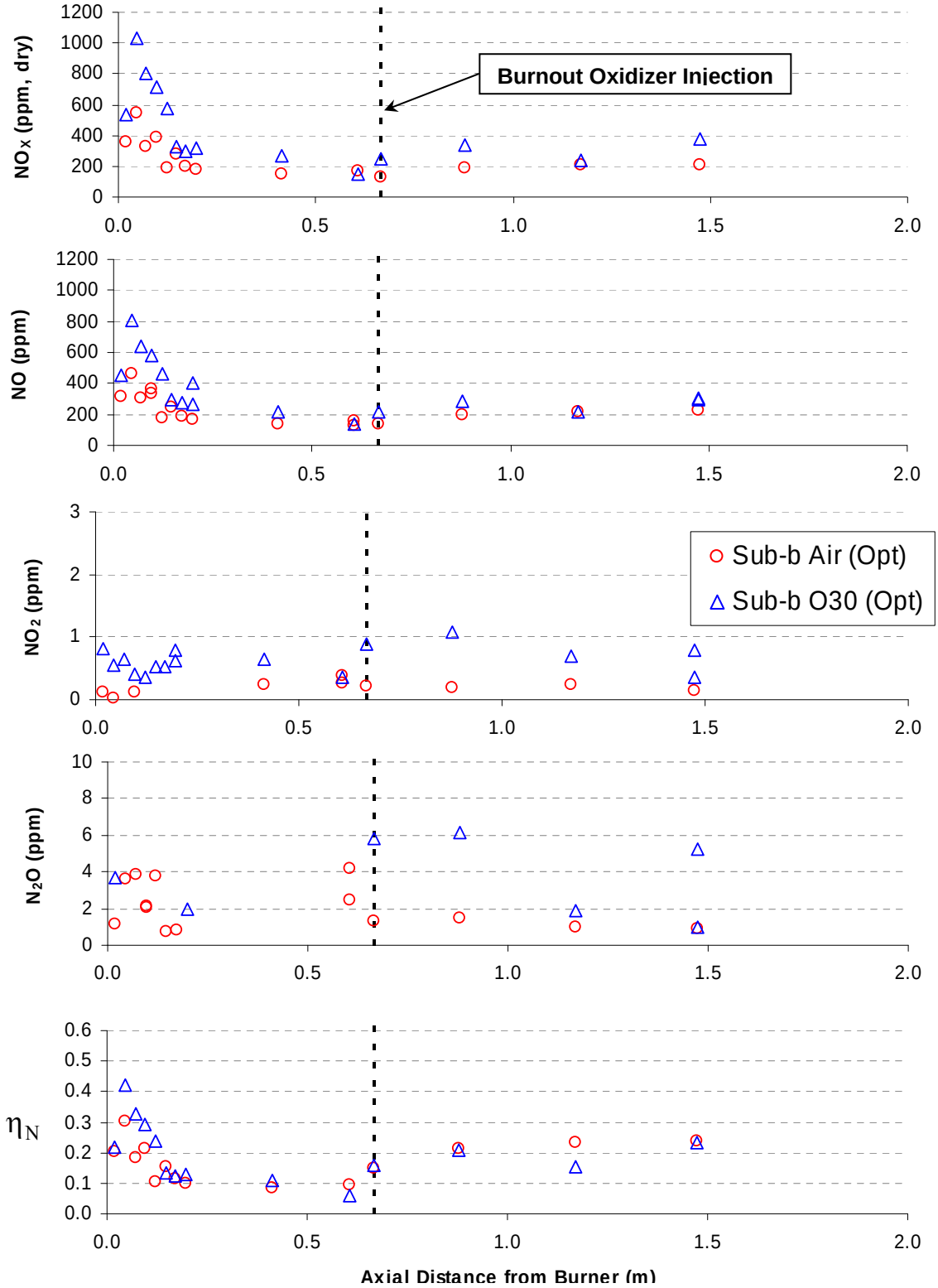

Figure 32. Nitrogen oxides measurements and associated nitrogen conversion efficiency for the sub-bituminous coal experiments at minimum NO_X conditions. Nitrogen conversion efficiency is calculated from the HORIBA NO_X data in the top plot. All other data are from the MKS FTIR.

As with data presented previously, the NO_X measurements in Figure 32 show NO to be the major nitrogen oxide product. Both air and oxy-fuel cases exhibit rapid initial NO_X formation followed by fairly rapid destruction. Any changes in η_N over the lower two-thirds of the reducing zone are much less significant. A notable difference between these data and those shown previously is that the air case here does not have the slow NO_X formation after initial rapid formation. Concentrations of NO are higher in the oxy-fuel case, but in terms of η_N the two cases are quite similar. It is also interesting to note that both cases appear to form some NO_X at the point of secondary oxidizer injection indicating the minimum NO_X occurs even though some NO_X is produced at this location.

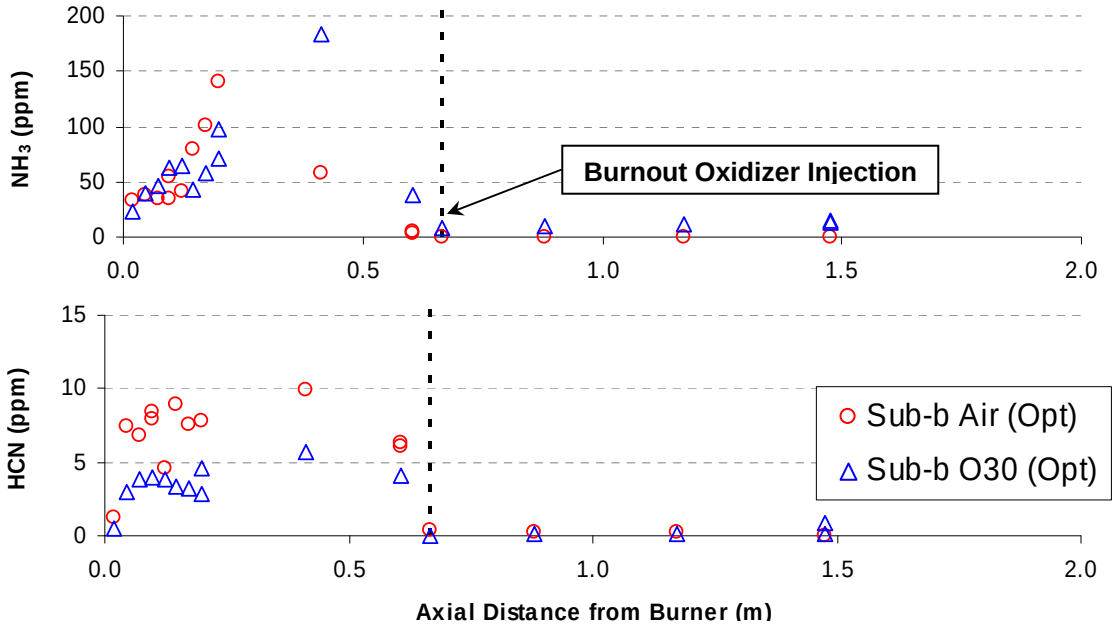

Figure 33. Nitrogen intermediates NH_3 and HCN for the sub-bituminous coal staged combustion experiments at minimum NO_X conditions.

NH_3 concentrations are also similar between air and oxy-fuel combustion as seen in Figure 33. The concentration of NH_3 increases as NO (Figure 32) decreases up to 0.2 m from the burner. Over this same space the HCN concentration is roughly constant. NH_3 is in higher concentrations than HCN (by a factor of 10). The HCN data show low levels between 5 and 10 ppm but they are about twice as high in the air case. As for other experiments these species are only detected upstream of burnout oxidizer injection.

Computational Modeling Results

Equilibrium Calculations

If the NO chemistry was sufficiently fast and radicals were available, the concentration of NO would reach equilibrium. Equilibrium NO_X levels therefore indicate a limit on NO_X reduction by alterations to stoichiometry and temperature. Figure 34 illustrates the trends in equilibrium NO_X as a function of SR and temperature for air and oxy-fuel mixtures. These results were calculated using the NASA-Glenn CEA2 equilibrium code.

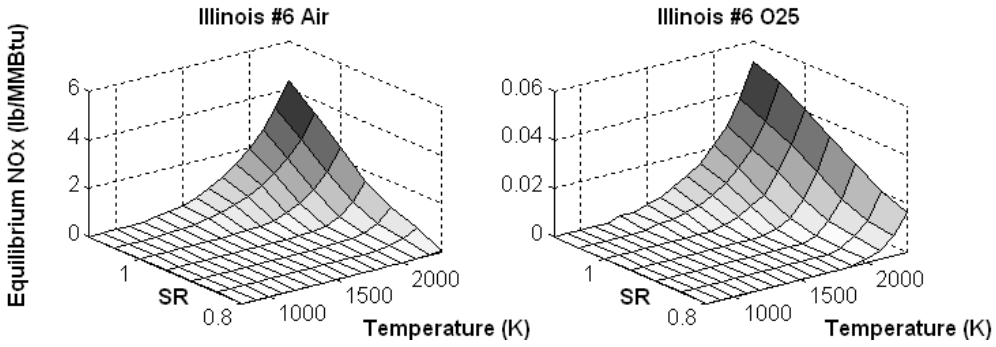

Figure 34. Equilibrium NO_X as a function of temperature and stoichiometry. Note the difference in the vertical scales.

As can be seen in the figure, high levels of NO_X are favored by high temperature, fuel-lean (high SR) conditions for both air and oxy-fuel combustion. The equilibrium levels however are almost two orders of magnitude lower in oxy-fuel than air.

Often in combustion modeling it is assumed that major combustion products have fast chemistry and react to equilibrium as rapidly as the reactants are mixed. NO_X formation on the other hand is characterized by finite rate chemistry and it is kinetic considerations that determine the level of NO_X. The computational model described above was used to calculate the concentrations of NO predicted by kinetics (using the GRI-Mech 3.0 mechanism) for the Sub-b Air and Sub-b O30 experiments. These predictions are compared to equilibrium NO values and experimental data in Figure 35 and Figure 36.

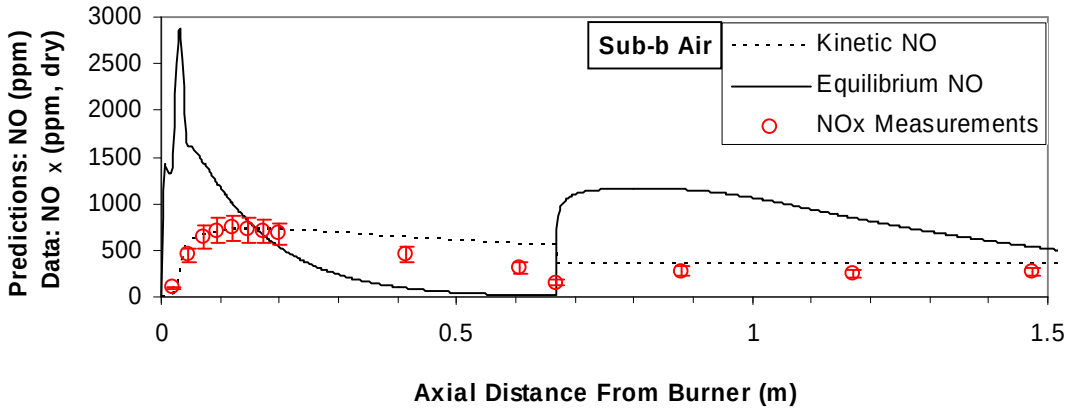

Figure 35. Comparison of experimental NO_X data (HORIBA) with finite rate chemistry model predictions (Kinetic NO) and associated equilibrium NO levels for staged air combustion.

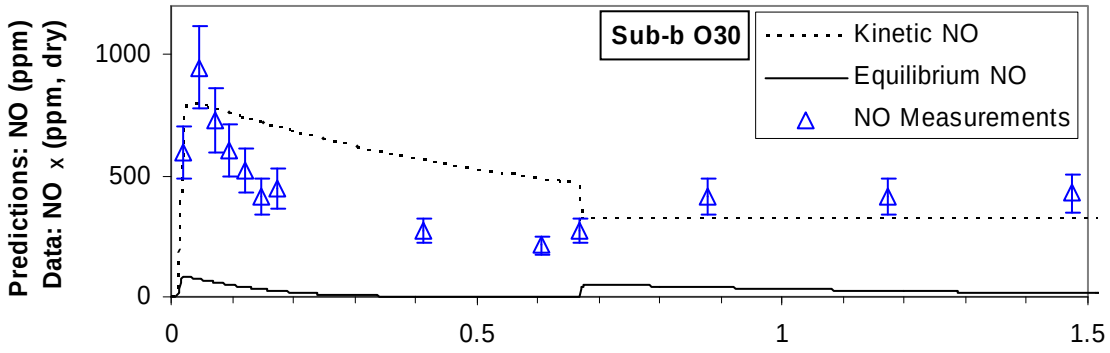

Figure 36. Comparison of experimental NO_X data (HORIBA) with finite rate chemistry model predictions (Kinetic NO) and associated equilibrium NO levels for staged oxy-fuel combustion.

In terms of the shape of the NO_X profile near the burner Figure 35 and Figure 36 show good agreement between kinetic predictions and experimental data. In the air case (Figure 35) the rapid initial NO formation and the slow NO formation that follows occur while NO is at sub-equilibrium levels. Once equilibrium NO levels fall below the actual concentration the decrease in NO begins. The model however suggests that NO reduction is limited by reaction rates and although there is a reduction in NO, it cannot follow the equilibrium curve and NO is frozen at super-equilibrium values for the latter part of the reducing zone.

In the oxy-fuel case the equilibrium NO is at all locations lower than the kinetically-computed and experimental values. This may partially explain why the slow formation of NO after rapid initial formation does not occur in the oxy-fuel cases. The initial formation of super-equilibrium NO is a result of the finite rate nitrogen chemistry. Some insight into the chemistry can be gained from the reaction pathway diagrams in Figure 37 and Figure 38. These diagrams were generated from the kinetic model predictions using the MixMaster application distributed with the Cantera software.

Figure 37 shows that modeled NO is being formed from N, NH, HNO, and NCO with NCO and HNO being the reactants with the dominant pathways as indicated by the uppermost value in the reaction details next to the respective pathway arrows. The relative width of the arrows also provides an indication of pathway importance.

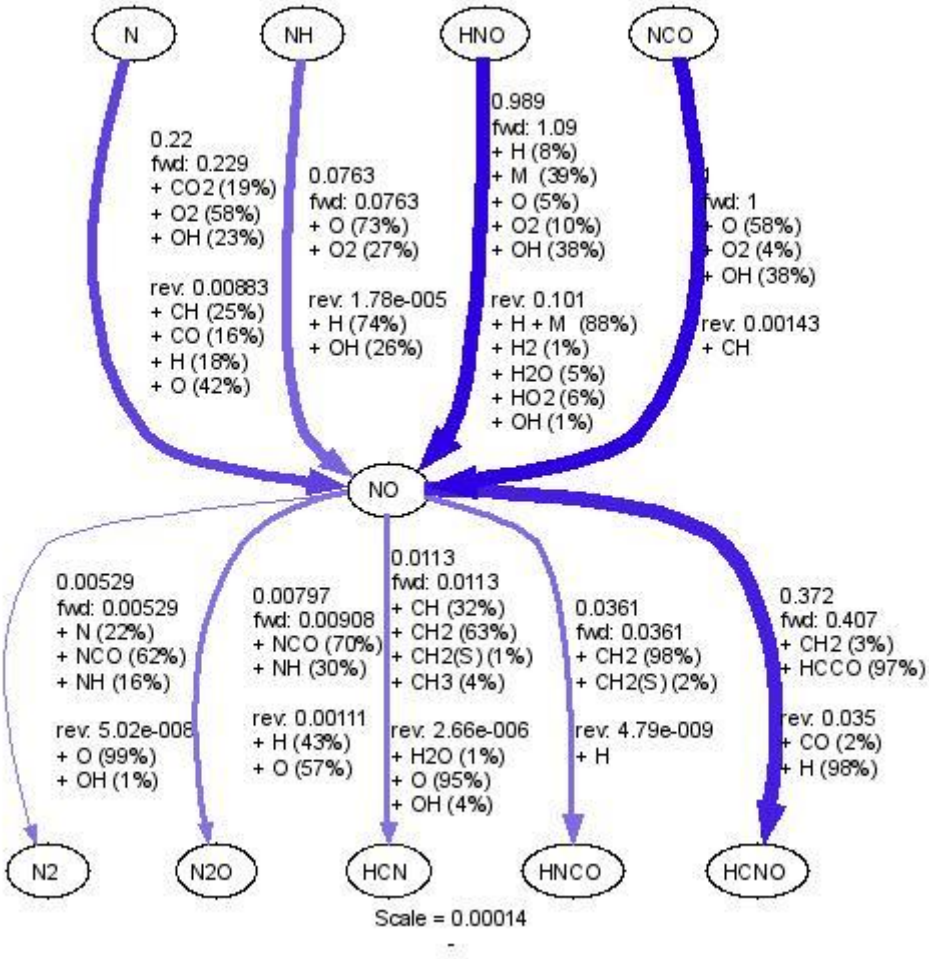

Figure 37. Reaction pathway diagram for NO formation and destruction in the Sub-b O30 model 14 mm from the burner (GRI-Mech 3.0 mechanism).

As indicated in the diagram, NO is also being consumed to form N_2, N_2O, HCN, HNCO, and HCNO. These pathways are of lesser significance at this point in the reactor than the NO formation pathways. In the near-burner region the NO formed is an intermediate species rather than a final product, but its concentration increases because the reactions producing NO are faster than the reactions that are consuming it. If both reaction sets were fast the NO concentration would remain low.

Figure 38 gives additional insight into the modeled NO formation pathways by showing important nitrogen species in the mechanism including HCN from the volatiles.

CO was another species of interest in this work. In contrast to NO, CO levels predicted by the kinetic calculations (GRI-Mech 3.0) closely matched equilibrium values as shown in Figure 39. Comparisons of model predictions with experimental data will be discussed in further detail below.

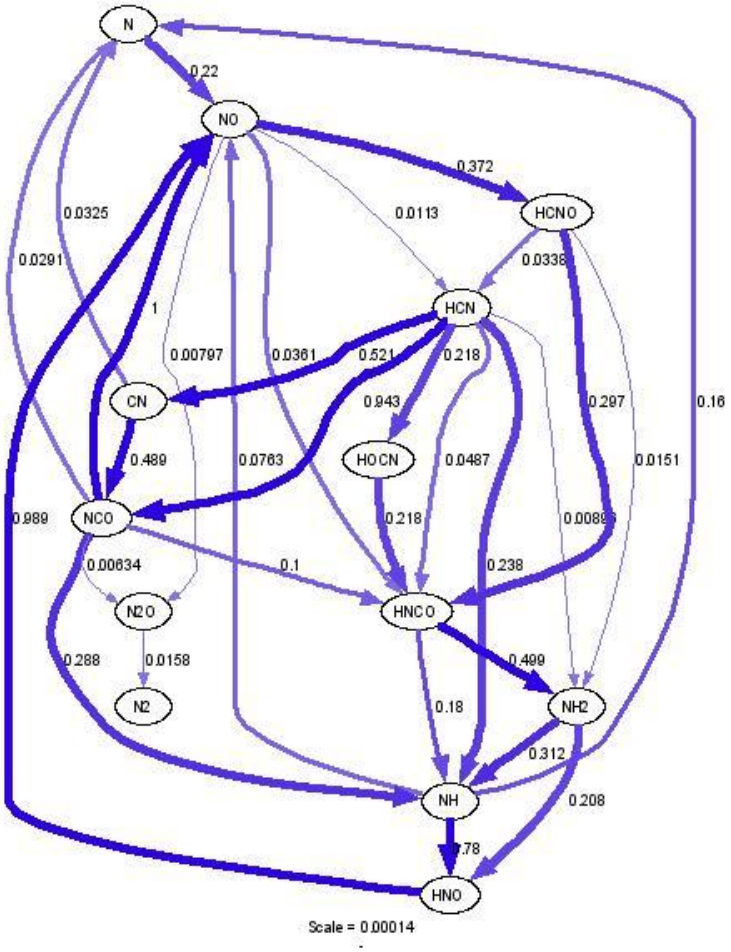

Figure 38. Reaction pathway diagram for N-containing species in the Sub-b O30 model 14 mm from the burner (GRI-Mech 3.0 mechanism).

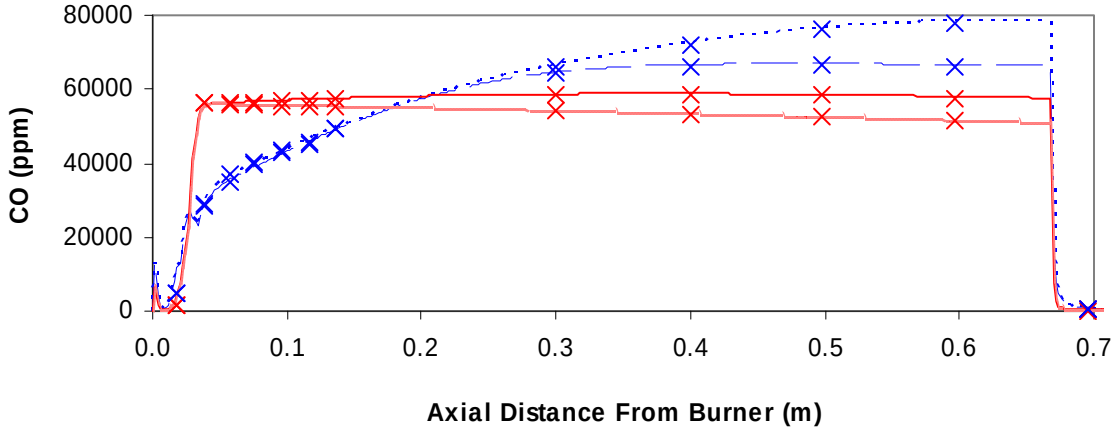

Figure 39. Comparison of CO levels for Sub-b Air and O30 (Opt) cases as calculated by kinetics (lines) and equilibrium (×'s). The purpose of this figure is only to illustrate the agreement between kinetic and equilibrium CO predictions. The specific cases shown are identified in Figure 61.

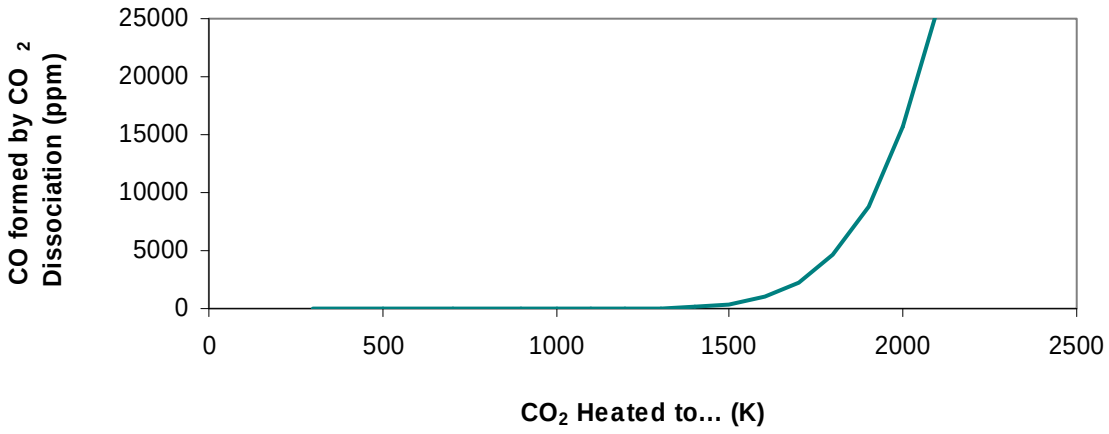

Figure 40. CO formation by thermal dissociation of CO_2 as calculated with NASA-Glenn CEA2 equilibrium code.

CO may be formed by thermal dissociation of CO_2 at high temperatures. Equilibrium calculation results in Figure 40 indicate that this process is extremely temperature sensitive and begins at about 1500 K.

Comparison of NO Data with Predictions from the Three Gas-Phase Mechanisms

With three gas-phase mechanisms, several experiment cases, and tens of species predicted by the model it is impractical to report predictions from all permutations. One gas-phase mechanism was selected by comparing predictions of η_N (the parameter of primary interest) to experimental data. Comparisons for selected experiments appear in Figure 41 through Figure 43.

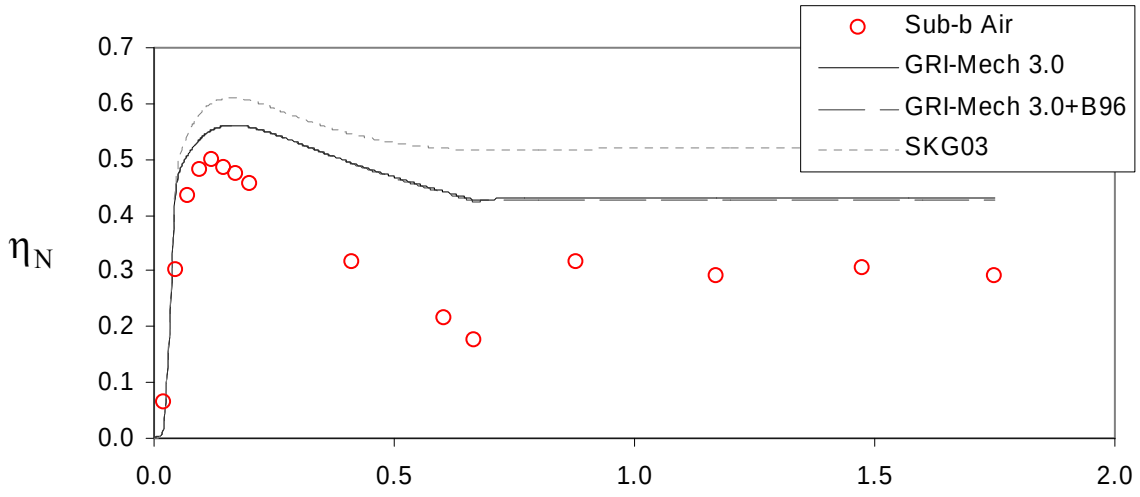

Figure 41. Comparison of nitrogen conversion efficiency predictions for all three gas-phase mechanisms for the Sub-b Air experiment.

The η_N data for the Sub-b Air experiment in Figure 41 exhibits slower NO_X formation following initial rapid formation near the burner. This characteristic is predicted by all three mechanisms,

as is the period of NO_X destruction that follows. All mechanisms predict similar levels of initial NO_X formation that are close to the experimental values. The two mechanisms with GRI-Mech reactions are closer to the experimental values than the SKG03 mechanism for this case. Advanced reburning reactions (B96) added to GRI-Mech 3.0 did not make any significant difference to the predictions for the conditions and assumptions in the model. The rate of NO_X destruction is under predicted by all three mechanisms, and the rise in NO_X as burnout oxidizer is added is very slight in the model predictions and well below the experimental values.

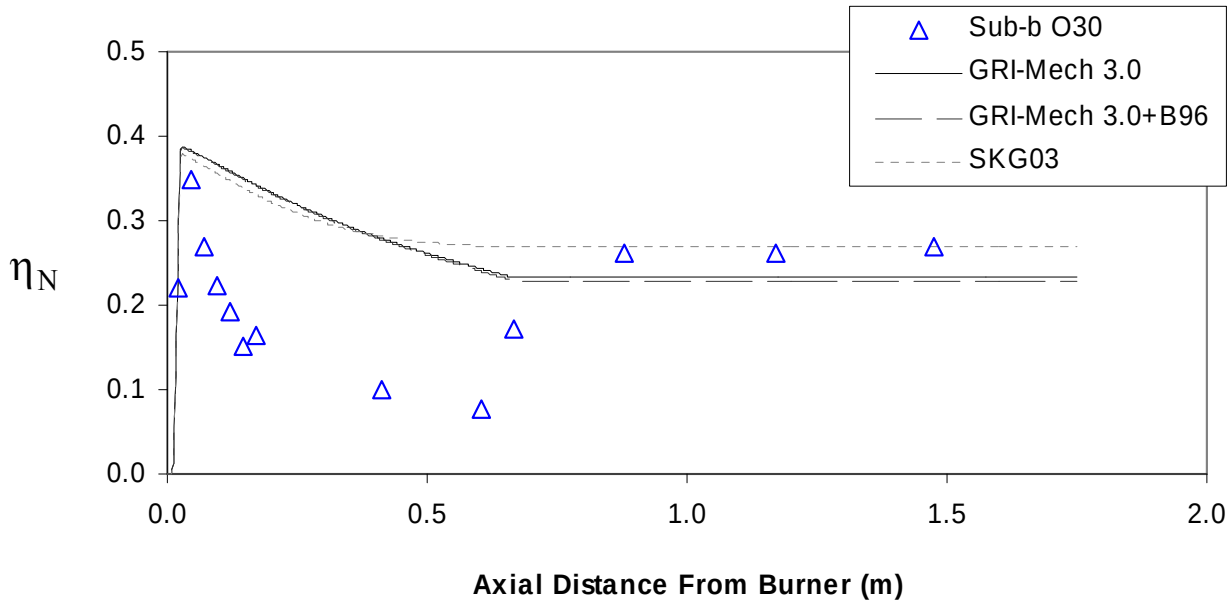

Figure 42. Comparison of nitrogen conversion efficiency predictions for all three gas-phase mechanisms for the Sub-b O30 experiment.

The qualitative agreement between model predictions and experimental data for initial NO_X formation in an oxy-fuel case is also good as shown in Figure 42. As in the air case the rate of NO_X destruction is under predicted as is the NO_X formation at burnout oxidizer injection. The addition of advanced reburning reactions to GRI-Mech 3.0 again does not change the predictions significantly.

Figure 41 and Figure 42 are typical of the model performance for air and oxy-fuel cases for all three coals and all oxidizers with the exception of one case shown in Figure 43. For the Sub-b Air (Opt) experiment the SKG03 mechanism predicted a similar initial rate of NO_X formation to the other mechanisms but this was followed by a rapid drop in NO_X unique to the SKG03 prediction in this case. This feature is discussed in more detail below.

The slight rise in NO_X predicted by the model at the location of burnout oxidizer injection is more noticeable in Figure 43 than previous figures, which is consistent with the more deeply-staged combustion, but lower than the experimentally observed rise.

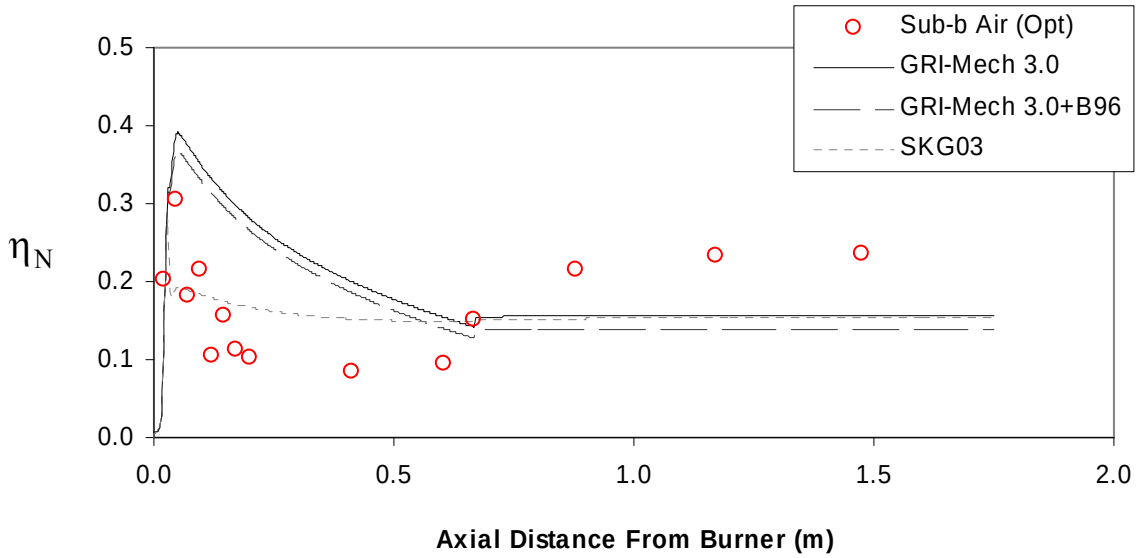

Figure 43. Comparison of nitrogen conversion efficiency predictions for all three gas-phase mechanisms for the Sub-b Air (Opt) experiment.

Choice of Gas-Phase Mechanism

In predictions of the shape and location of the NO_X formation profile near the burner, all three mechanisms were qualitatively accurate. The fact that the GRI-Mech 3.0-based mechanisms were often closer quantitatively is considered fortuitous and such may not be the case if the model assumptions were to change. All three mechanisms (in all cases but one) under predicted the rates of NO_X destruction such that no mechanism was clearly superior in this respect. Except where noted, the results in the remainder of this chapter are from the GRI-Mech 3.0 mechanism predictions. This mechanism was selected as it was the least computationally expensive.

Effect of Recycled NO

The model predictions for the experiments where NO was added to the reactants are shown with the experimental data in Figure 44. The apparently monotonic decrease in the modeled difference between 0 and 525 ppm NO tests would suggest that the initial formation of NO_X is somewhat suppressed in the model predictions by elevated NO concentrations, however the close up view shows that the modeled difference does not decrease much until the NO_X destruction zone begins. The experimental data have insufficient spatial resolution to fully investigate possible suppression of NO formation. Qualitatively the model captures the trends in the available experimental data, with the exception of upstream mixing of NO from the burnout oxidizer as fluid mechanics were not included in the model.

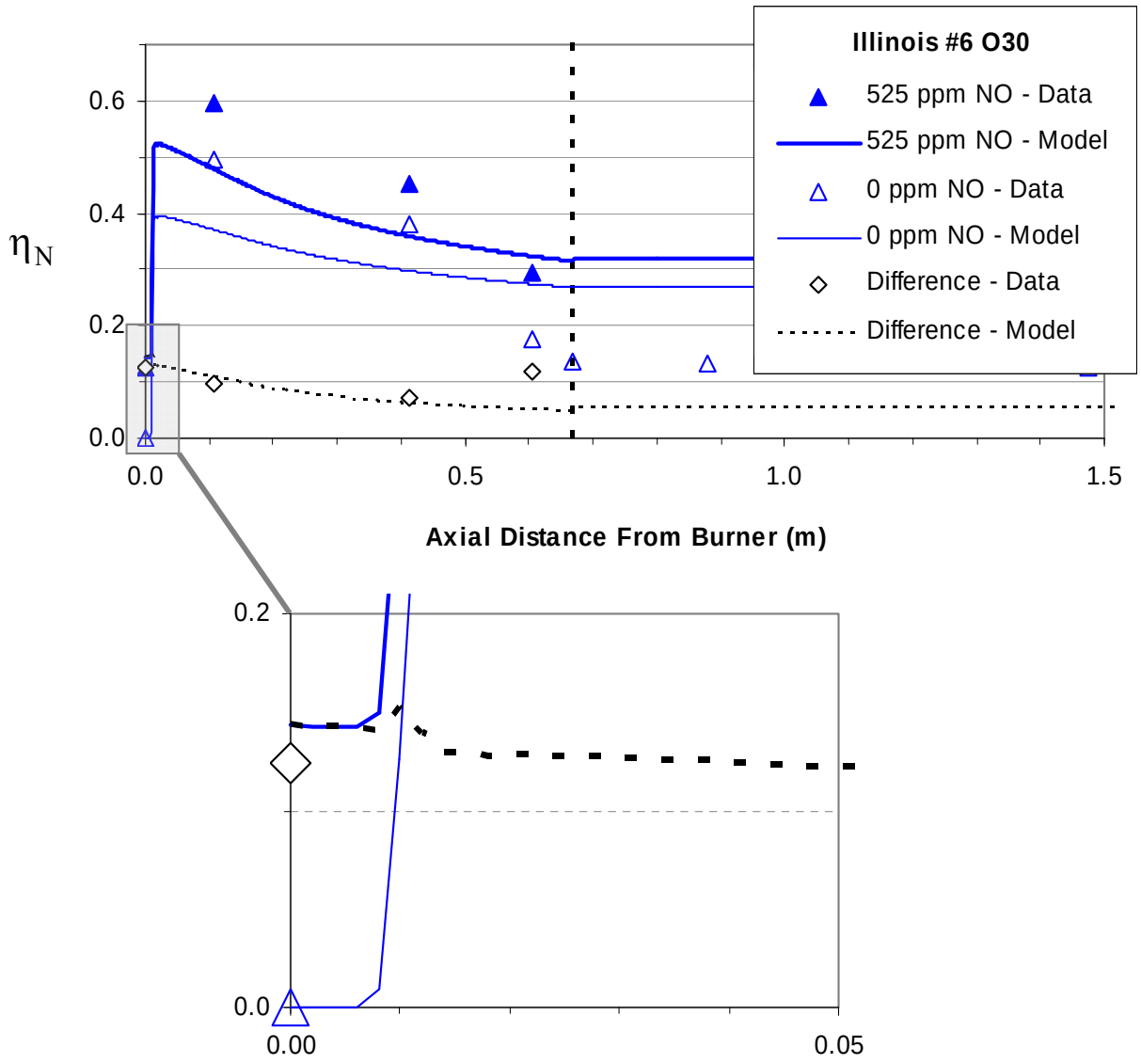

Figure 44. Comparison of model predictions and experimental data for experiments where NO was added to the reactor inlet to simulate recycled NO.

Effect of Air Infiltration

For practical systems it is expected that some air will enter the combustion space thus adding N_2 to the gas mixture. In the experiments the natural gas contained only about 0.44% N_2 (Table 2) and thus this N_2 was neglected in the modeling. To determine the predicted effect of air infiltration the model was run with and without N_2 in the reactants and results are shown in Figure 45.

The level of N_2 selected (2.6 vol. %) corresponds to air infiltration being 2.6% of total gas mass flow through the burner. As is seen in the figure, this air infiltration is not predicted to significantly increase NO_X. The small increase that is seen is predominantly formed by thermal NO_X reactions.

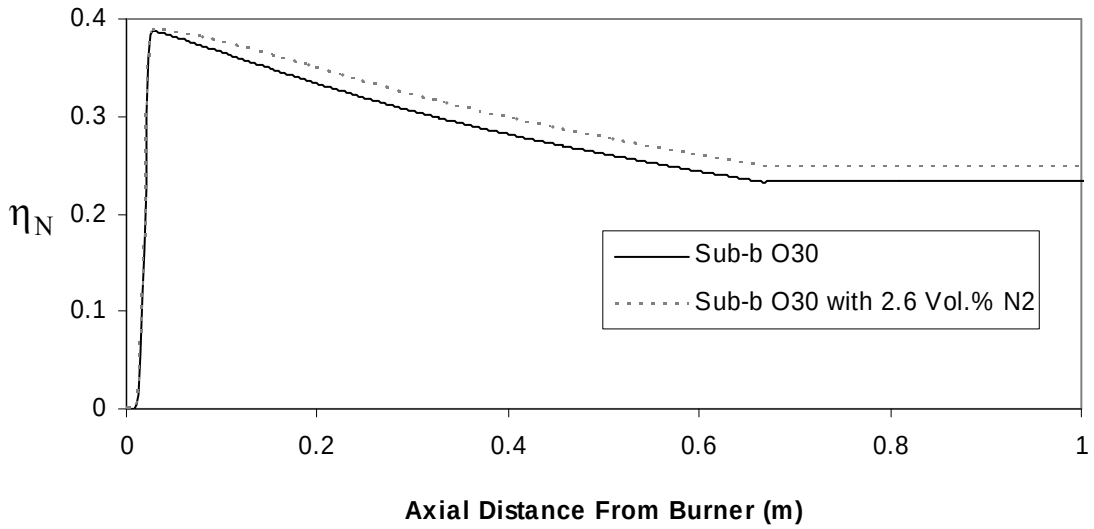

Figure 45. Modeled effect of 2.6 vol. % N_2 in the gaseous reactants for the Sub-b O30 experiment.

Relative Importance of Thermal, Prompt, and Fuel NO_X Mechanisms

A major advantage of a computational model is that individual chemical reactions may be disabled at will to determine the relative significance of different NO_X mechanisms.

For the Sub-b Air case the result of separating the thermal, prompt, and fuel NO_X contributions to NO_X is shown in Figure 46. This modeling exercise predicts that the rapid initial NO_X formation is due to fuel NO_X, and the slower formation thereafter is predominantly thermal NO_X. The model also predicts that thermal NO_X reactions are responsible for most of the predicted NO reduction. Reburning reactions (which are reflected in the fuel NO_X prediction) are of little significance to the modeled NO reduction. Prompt NO_X formation occurs rapidly, fairly close to the burner and is of minor importance compared to the other two mechanisms.

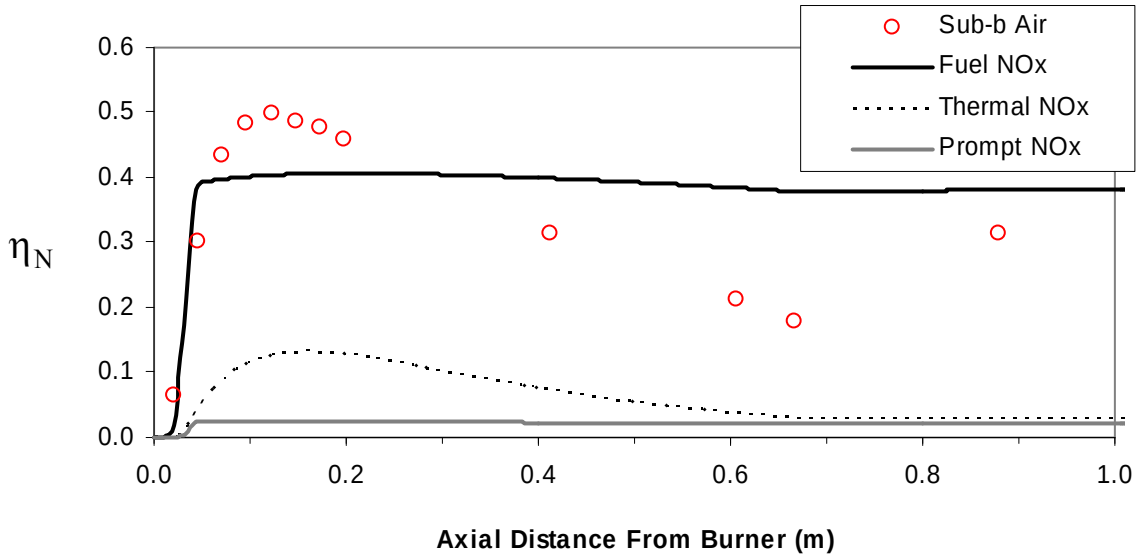

Figure 46. Separated contributions of thermal, prompt, and fuel NO_X predicted by the model for the Sub-b Air case. The experimental data are also plotted.

The same type of model predictions for the Sub-b O30 experiment appear in Figure 47. As with the air case the initial rapid rise in NO_X is attributed to fuel NO_X. The lack of N_2 results in negligible prompt NO_X, and as with the air case, the majority of predicted NO_X destruction is via thermal NO_X reactions.

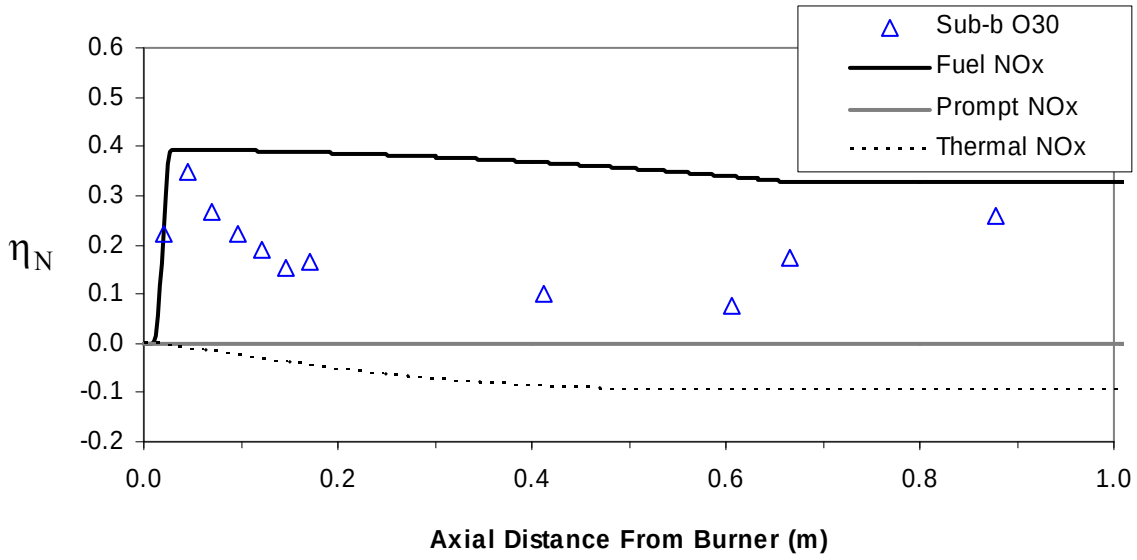

Figure 47. Separated contributions of thermal, prompt, and fuel NO_X predicted by the model for the Sub-b O30 case. Corresponding experimental data are also plotted.

Flame Characteristics in Devolatilization

Due to the transient release of coal volatiles, the gas-phase stoichiometry changes with distance from the burner. To gain insight into how this might affect nitrogen evolution the model was used to calculate the chemical equivalence ratio (Equation 4, Gordon and McBride, 1994) and this parameter was plotted with other relevant variables in Figure 48. The chemical equivalence ratio is based on elemental oxidation states and is 1 for stoichiometric gas mixtures, greater than 1 for reducing conditions, and less than 1 for oxidizing conditions.

$$r \equiv -\frac{\sum_{i=1}^{l} V_i^{+} \left(\sum_{j=1}^{k} a_{ij} \frac{Y_j}{MW_j} \right)}{\sum_{i=1}^{l} V_i^{-} \left(\sum_{j=1}^{k} a_{ij} \frac{Y_j}{MW_j} \right)} \qquad \textbf{Equation 4}$$

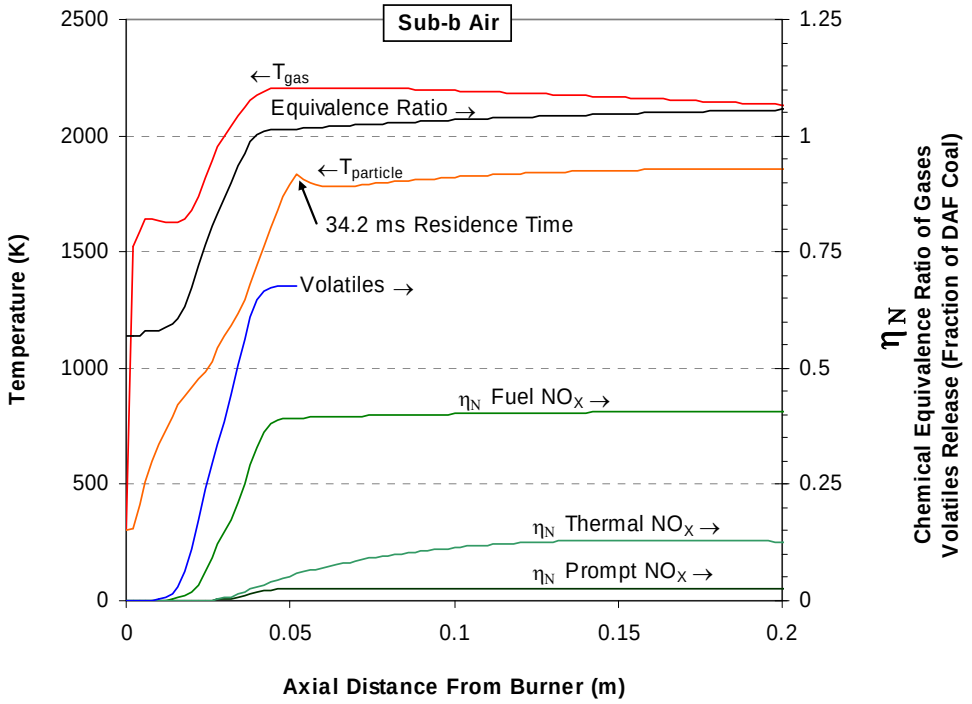

Figure 48. Plot of gas-phase chemical equivalence ratio in the Sub-b Air flame with other important variables.

The modeled gas temperature in Figure 48 has two distinct periods where temperature increases. The first is associated with the natural gas flame that provides heat for coal devolatilization and the second is from combustion of the coal volatiles. Particle temperature lags behind the gas temperature and as a result the coal volatiles are not released in the model until after the natural gas flame. Fuel NO_X formation begins with the release of volatiles, and thermal NO_X forms further downstream. Prompt NO_X only occurs over a small region corresponding to the location where chemical equivalence ratio changes from oxidizing to reducing values.

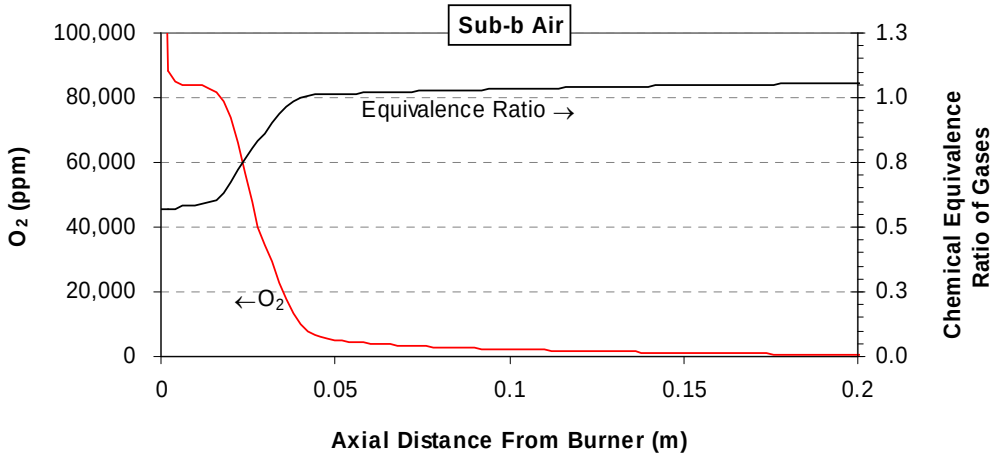

Figure 49. Modeled gas-phase chemical equivalence ratio for the Sub-b Air case plotted with predicted O_2 concentration.

Given the requirement for O_2, It may be somewhat surprising that thermal NO_X would form under chemical equivalence ratios greater than 1, but as seen in Figure 49 the modeled O_2 concentrations are low but non-zero over the region where the chemical equivalence ratio is greater than 1 and thermal NO_X is formed.

The most prevalent radical species predicted by the model are shown in Figure 50. The species profiles all have a valley between the methane and coal volatiles flames locations which indicates that in the model at least these two flames are largely independent. In the experiment the range of particle sizes is expected to cause some overlap, but the peak height (in some cases) and breadth (in all cases) of predicted volatiles flame radical species profiles is greater than for the methane flame. This may indicate that some overlap may not have a major influence in the volatiles flame radicals pool and resulting NO_X chemistry.

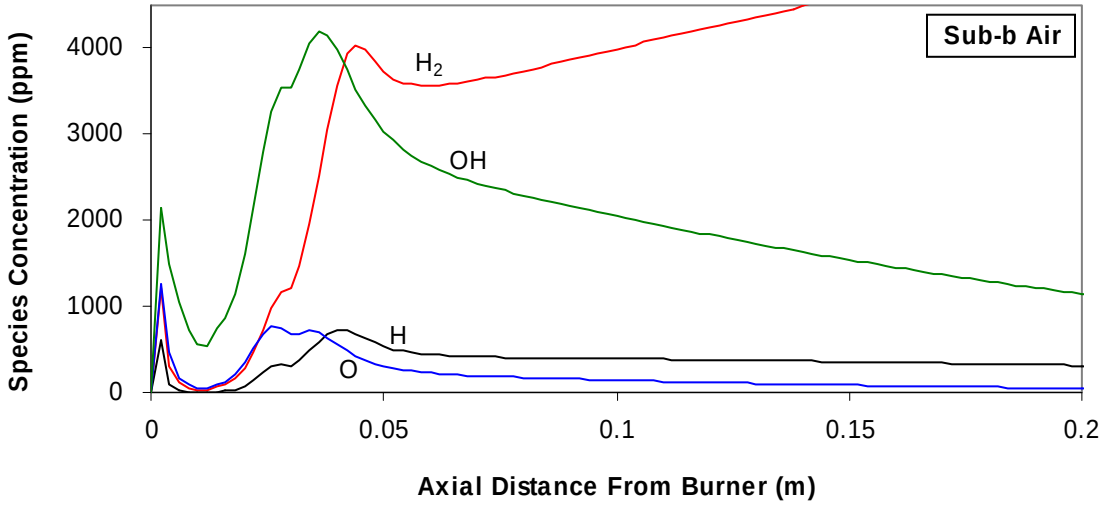

Figure 50. Major radicals species predicted in the Sub-b Air case near the burner.

Figure 51 shows the gas-phase chemical equivalence ratio and other predictions for the Sub-b O30 case. The values of chemical equivalence ratio in the oxy-fuel case are about the same as for the air case indicating that the diluent (N_2 or CO_2) does not affect this chemical measure of stoichiometry. The gas temperature increases occur slightly upstream of their locations in the air case, and particle heat up is slightly faster, but other than this there is little difference between the oxy-fuel and air cases. The dominant predicted radicals for this case are shown in Figure 52 and are also similar to the air case species profiles. Like the air case, some O_2 is predicted in the reducing zone where the chemical equivalence ratio is greater than 1 (Figure 53).

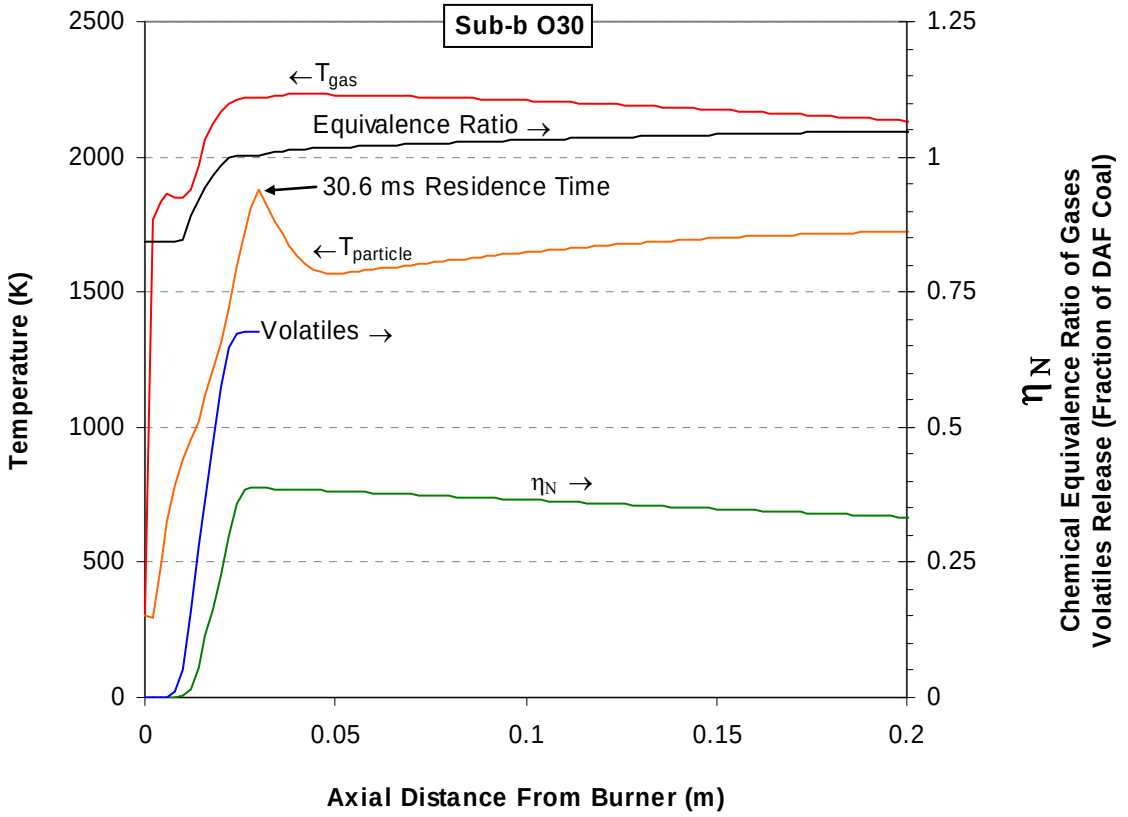

Figure 51. Plot of gas-phase chemical equivalence ratio in the Sub-b O30 flame with other important variables.

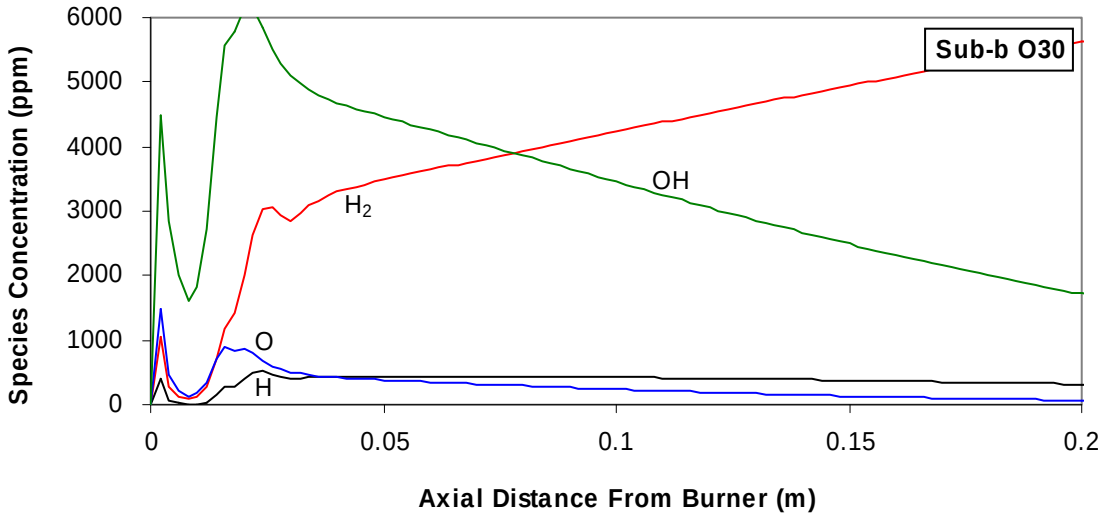

Figure 52. Major radicals species predicted in the Sub-b O30 case near the burner.

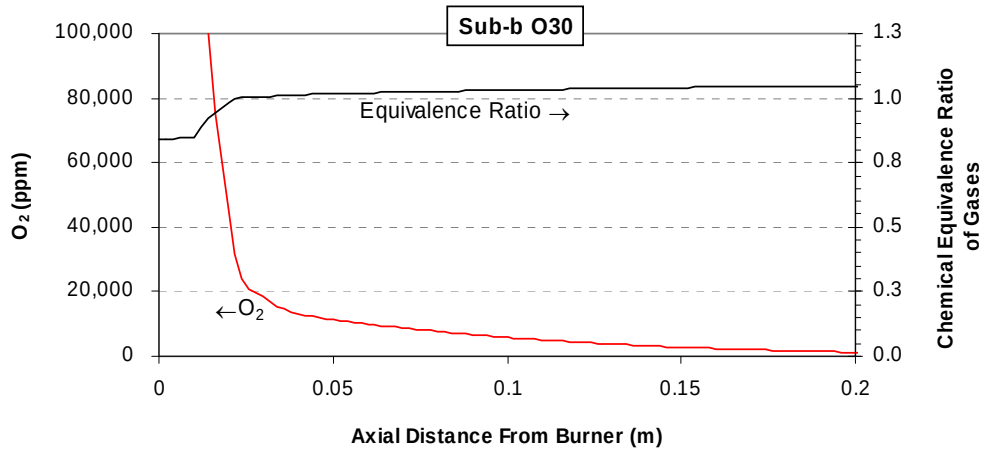

Figure 53. Modeled gas-phase chemical equivalence ratio for the Sub-b O30 case plotted with predicted O_2 concentration.

Effect of Varied Primary Stoichiometry

The model was used to examine the predicted trends in effluent NO_X with varied primary stoichiometry as was done in the Staging experiments. The model predictions and experimental data are compared in Figure 54. The most important result desired from a modeling study such as this is the primary SR for minimum NO_X. This was not identified by the model as the model results indicate that the minimums would occur at a primary SR below the lowest level tested. One aspect of the experimental data that is however correctly predicted is the greater sensitivity of air combustion NO_X to increases in primary SR.

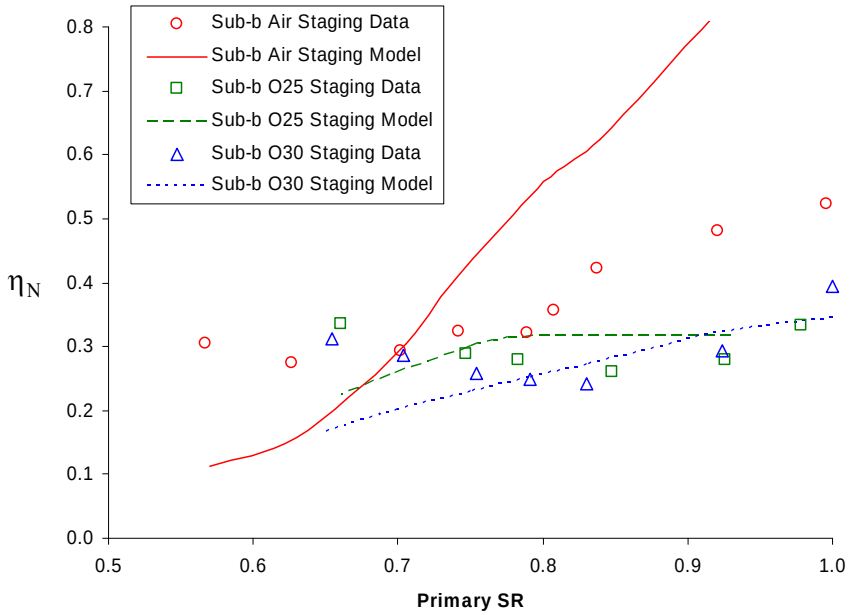

Figure 54. Predicted and measured trends in effluent η_N as a function of primary SR.

The predicted axial η_N profiles for each primary SR were plotted for air (Figure 55) and oxy-fuel (Figure 56). In the case of air it is seen that as primary SR decreases the slow formation of NO_X associated with thermal NO_X formation gradually disappears. The very significant contribution of thermal NO_X at high primary SR appears to explain the greater sensitivity of the air combustion NO_X to the stoichiometry.

Another trend visible in Figure 55 is that as primary SR decreases the predicted NO_X formation at the point of burnout oxidizer injection increases. This NO_X formation is under predicted as already shown in connection with Figure 43. If this NO_X formation were increased by the same multiplier for each stoichiometry, it can be seen that a minimum in final NO_X versus stoichiometry could be reached in the model as it is observed the data.

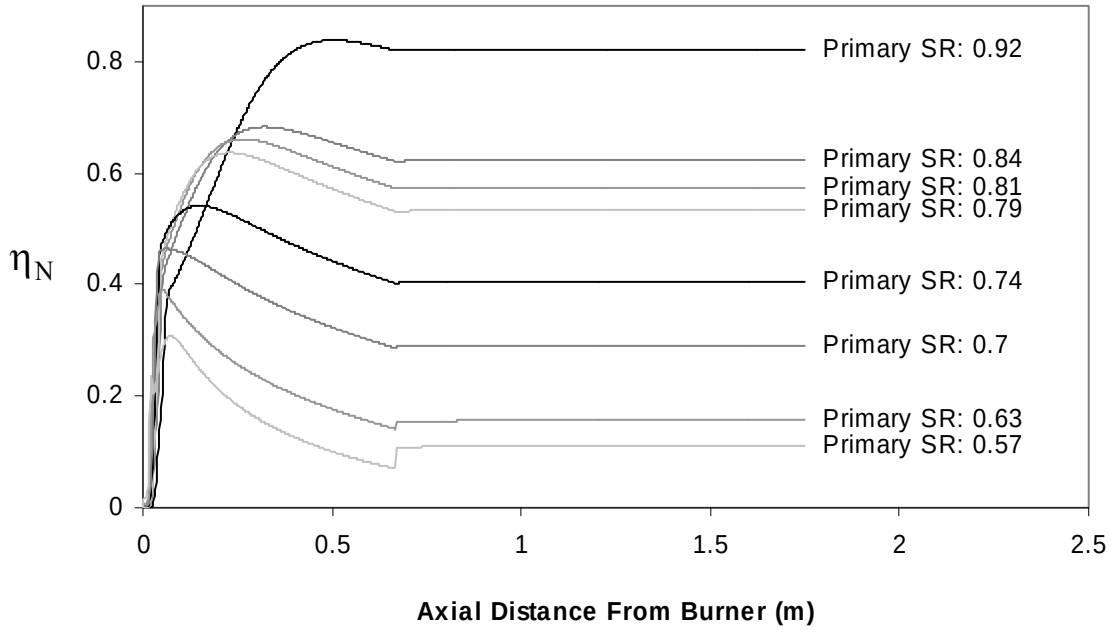

Figure 55. Axial profiles of predicted η_N in air combustion as a function of the depth of staging (or primary SR).

In the model predictions for oxy-fuel shown in Figure 56, the trend of increasing NO_X formation at burnout oxidizer injection with decreased primary SR is also apparent, and as shown previously in Figure 42 is also under predicted. Near the burner the lack the of thermal NO_X formation observed in the air cases at high primary SR appears to be the reason for the lower sensitivity of oxy-fuel NO_X to primary SR.

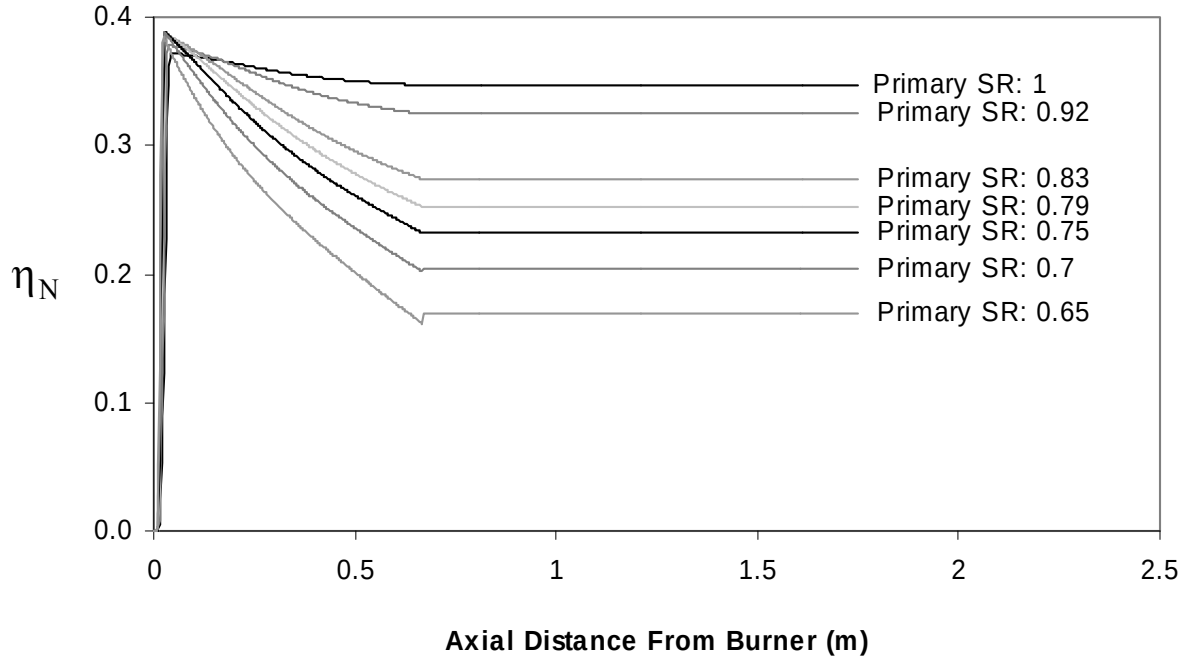

Figure 56. Axial profiles of predicted η_N in oxy-fuel (O30) combustion as a function of the depth of staging (or primary SR).

Close inspection of Figure 55 reveals that the model predicts lower initial NO_X formation with decreasing primary SR over most of the range of stoichiometries (primary SR = 0.92 is an exception). The available experimental data is consistent with this observation as illustrated in Figure 57. For oxy-fuel combustion the same trend is seen in the modeling results but was not observed experimentally. The effect is not as strong in the oxy-fuel model results as in the air cases.

The lower initial NO_X formation in air with lower primary SR may be due to lower nitrogen release from the coal, lower conversion of fuel-N to NO, or a combination. The model results for volatiles and nitrogen release were examined to help determine the relative significance of these reasons. Predictions shown in Table 11 indicate that nitrogen release is not expected to change significantly with primary SR. In general, volatiles and nitrogen release increase with particle heating rate, but with diminishing returns. At the high heating rates used the volatiles and nitrogen release is at or near the maximum attainable value. This points to lower conversion of fuel-N to NO as the explanation for lower initial NO_X formation at lower primary SR. Lower amounts of oxygen in these cases is probably the cause of the observation.

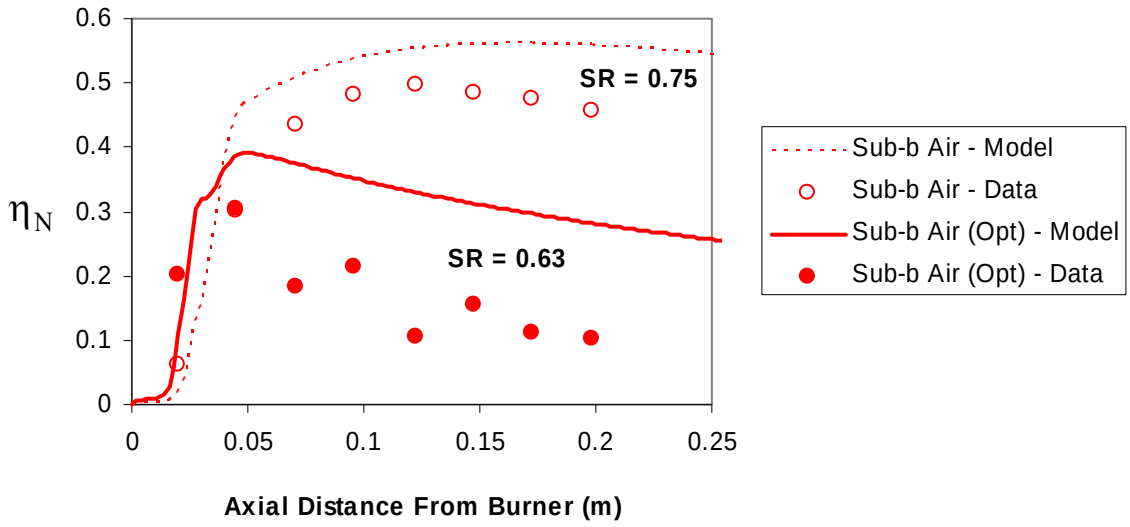

Figure 57. Model predictions and data comparison of initial NO_X formation for Sub-b Air and Sub-b Air (Opt) cases.

Table 11. Fractional volatiles and nitrogen release predictions for the sub-bituminous coal experiments.

Modeled Case	Volatiles Release	Nitrogen Release
Sub-b Air	67.6 %	62.2 %
Sub-b Air (Opt)	67.6 %	62.5 %
Sub-b O30	67.6 %	62.5 %
Sub-b O30 (Opt)	67.6 %	62.3 %

Model-Data Comparison: CO

A comparison of the experimental data and model predictions for the Illinois #6 Air and O30 CO concentrations is shown in Figure 58. The model does predict the trend of higher CO levels for the oxy-fuel case as seen in the data, but the magnitude of the model prediction is in poor agreement with the data. For the sub-bituminous data and model predictions shown in

Figure 59, the predictions are more accurate for the Air and O25 cases but too high for the O30 case. The model includes an empirical heat transfer parameter to account for heat lost through the reactor walls. Knowing that CO should follow equilibrium concentrations, the heat transfer parameter was tuned to force agreement between model predictions of CO and CO data from the Sub-b Air experiment, which explains the good agreement in that case. The chosen value obviously works well for O25 also, but not for the Illinois #6 coal and the Sub-b O30 experiment.

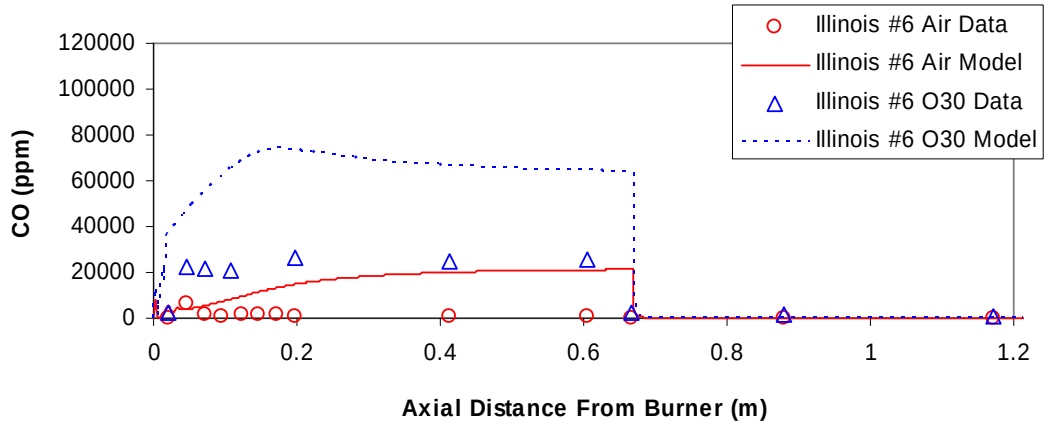

Figure 58. Model predictions and data comparison for CO in Illinois #6 staged combustion.

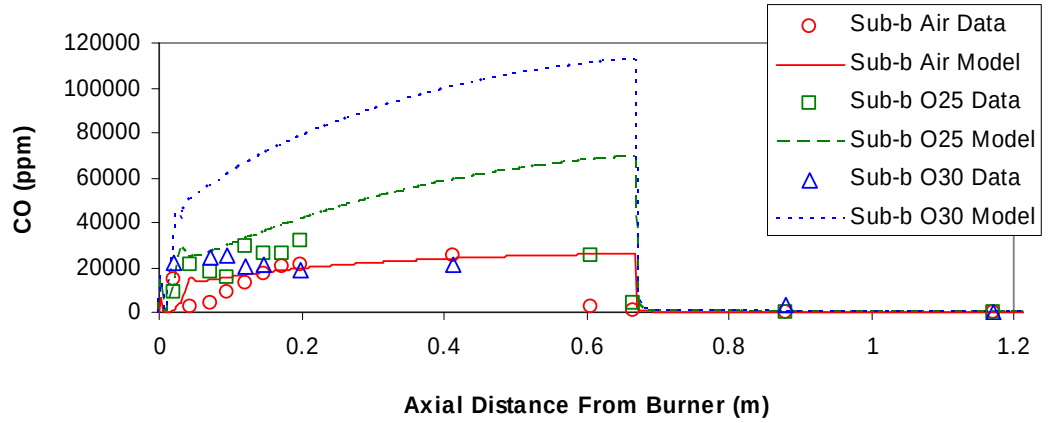

Figure 59. Model predictions and data comparison for CO in Sub-bituminous coal staged combustion.

The same model-data comparison for the sub-bituminous experiments at lowest effluent NO_X conditions is shown in Figure 60. At these markedly different levels of available oxygen in the primary combustion zone CO is similar between the air and oxy-fuel cases in both the model and the experiments.

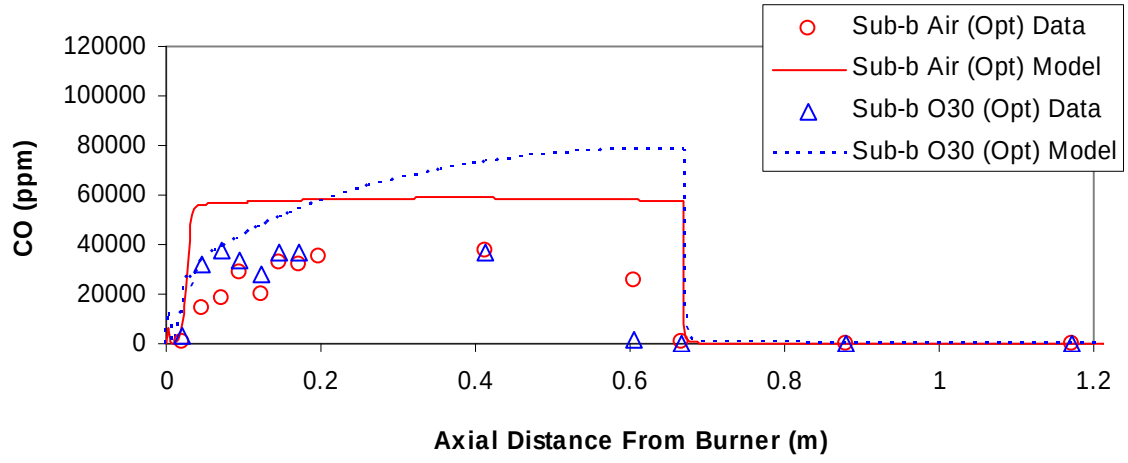

Figure 60. Model predictions and data comparison for CO in Sub-bituminous coal staged combustion at minimum effluent NO_X stoichiometries.

Effect of CO_2 Gasification of the Char on CO Concentrations

Early in the experimental work the high levels of CO observed in the reducing zone for oxy-fuel conditions combined with lower wall temperatures 0.4 m from the burner led to questions as to the cause of the high CO concentrations. Endothermic gasification of the char by CO_2 under oxy-fuel conditions was hypothesized as a possible explanation and this was investigated using the model.

Figure 61 presents model predictions for the same experiments considered in Figure 60 with and without inclusion of the CO_2 gasification reactions. The difference made to the CO levels is not insignificant, but it is small compared to the high level of CO. It appeared from these modeling results and equilibrium calculations for the same model cases presented in Figure 39 that gasification of the char by CO_2 does affect the level of CO, but the effect is minor compared with the CO quantities formed by thermal dissociation of CO_2 as equilibrium is maintained.

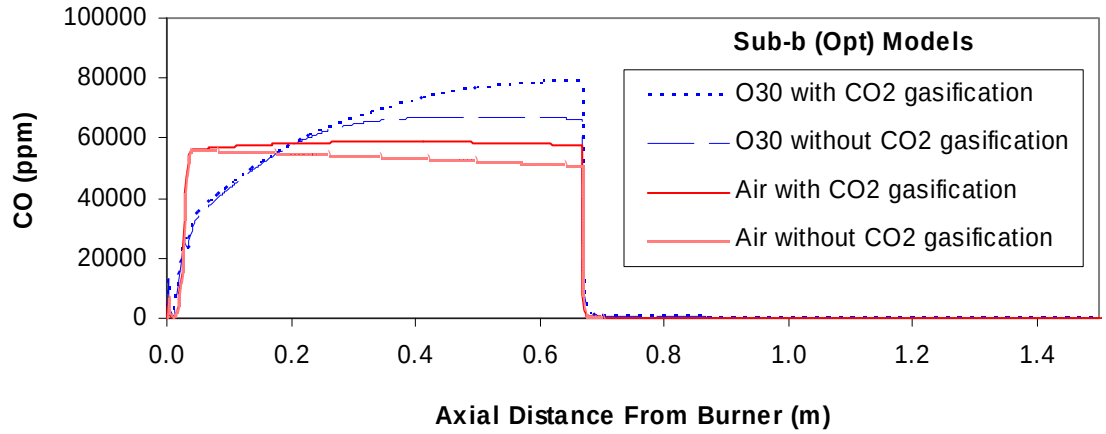

Figure 61. Effect of CO_2 gasification on CO levels in air and oxy-fuel model prediction.

The reasons that enabling or disabling the CO_2 gasification reactions in the model can change the predicted level of CO are that (1) The temperature is slightly lowered by the endothermic reactions; and (2) the production of CO added to the gas phase alters the elemental composition of the gas.

Effect of CO_2 Gasification of Char on η_N

In the literature review it was noted that moist oxidation of CO may produce radicals that are required by NO_X reduction reactions. As CO_2 gasification of the char is predicted to affect the CO concentration, it is also of interest to determine the effect of char gasification on NO_X. This model prediction is shown in Figure 62 and indicates little effect of the gasification reaction on η_N.

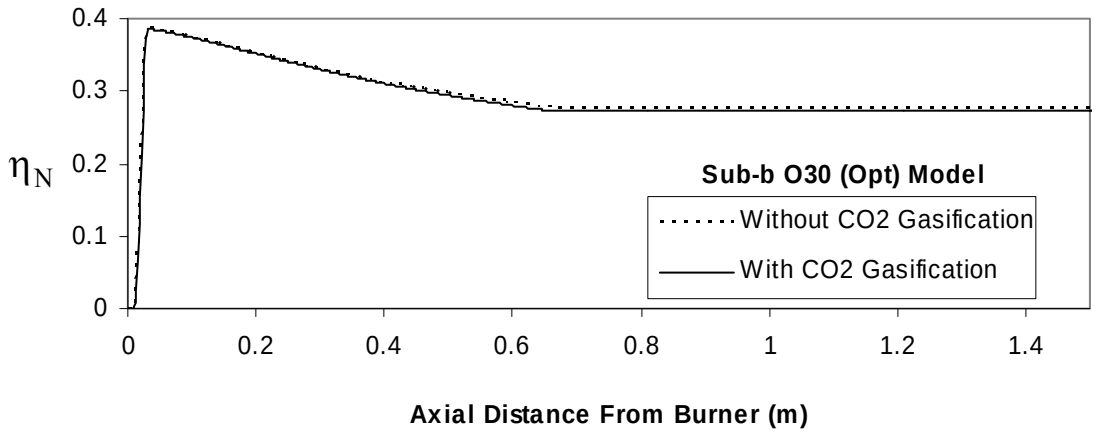

Figure 62. Predicted effect of CO_2 gasification reactions on nitrogen conversion efficiency for the Sub-b O30 (Opt) experiment.

Model-Data Comparison: NH_3 and HCN

As was done earlier for η_N, all three gas-phase mechanisms were compared to the experimental data for HCN and NH_3 prediction accuracy and as before the GRI-Mech 3.0 mechanism was most often closest to the experimental data. All predictions shown in this section were made using the GRI-Mech 3.0 reaction set.

Figure 63 shows model predictions compared to data for sub-bituminous coal staged combustion. The same qualitative trends seen in the data are followed by the model predictions, specifically the rise in NH_3 with distance from the burner, and the higher NH_3 concentration in oxy-fuel relative to air at the same primary SR, and the trend of increasing NH_3 as primary SR decreases for each oxidizer.

In spite of this qualitative agreement, the magnitude of the predicted levels of NH_3 is generally two orders of magnitude too low. The predictions for the Sub-b Air (Opt) case at significantly lower primary SR are also too low, but closer to the data.

In the model predictions the sharp narrow peak in NH_3 near the burner is associated with volatiles release, and the rise in NH_3 downstream is associated with homogeneous nitrogen chemistry. Nitrogen release from char is not modeled. These features appear distinct in the model but not in the experimental data, perhaps because the coal particle size distribution causes overlap of the physical processes in the measured data while a monodisperse distribution is assumed in the model, as will be discussed in more detail below.

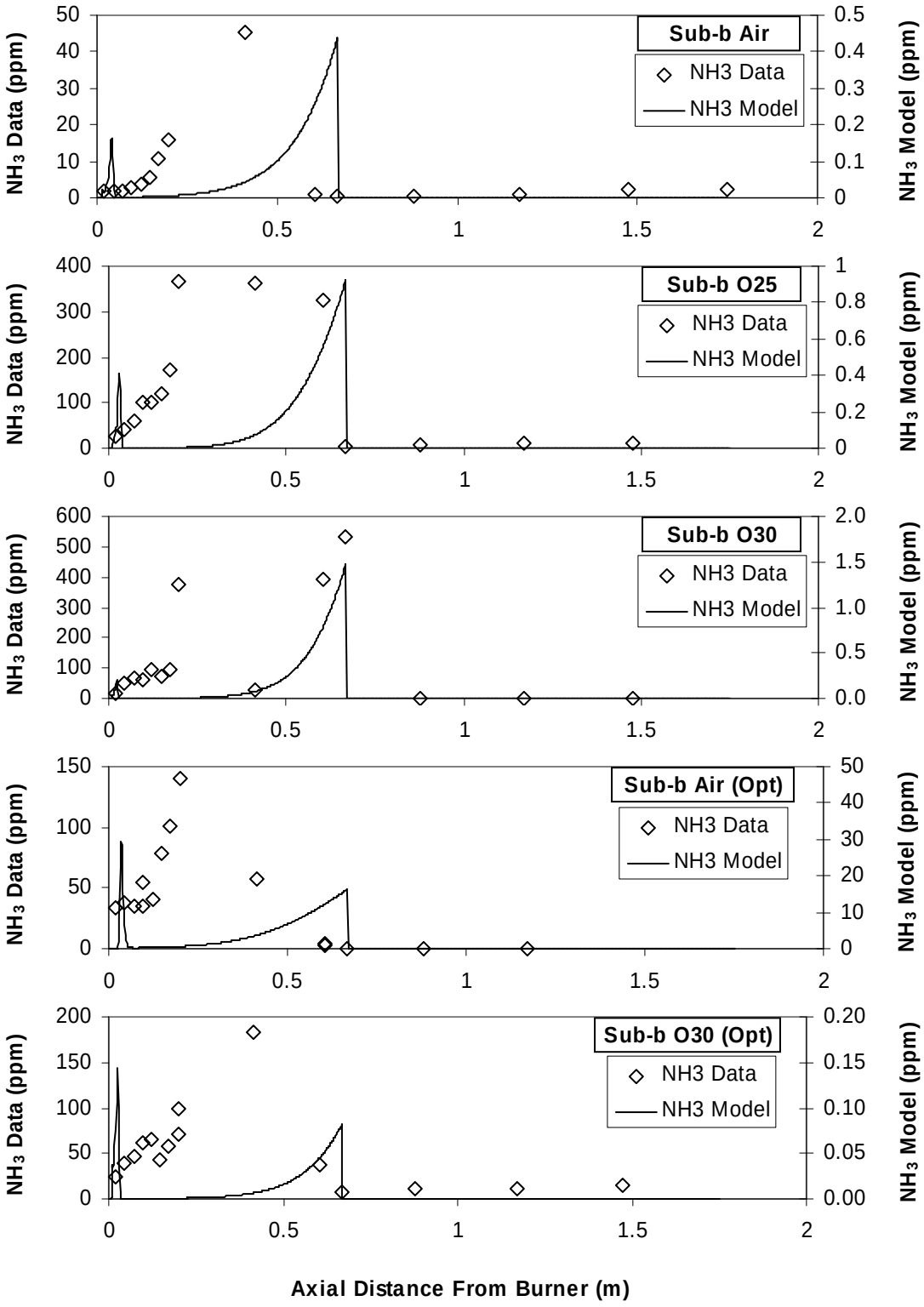

Figure 63. NH_3 model predictions and data for sub-bituminous coal staged combustion.

As observed experimentally, the model predicts lower NH_3 levels for the Illinois #6 coal than for the sub-bituminous coal, but the agreement between the model and data is still poor (Figure 64).

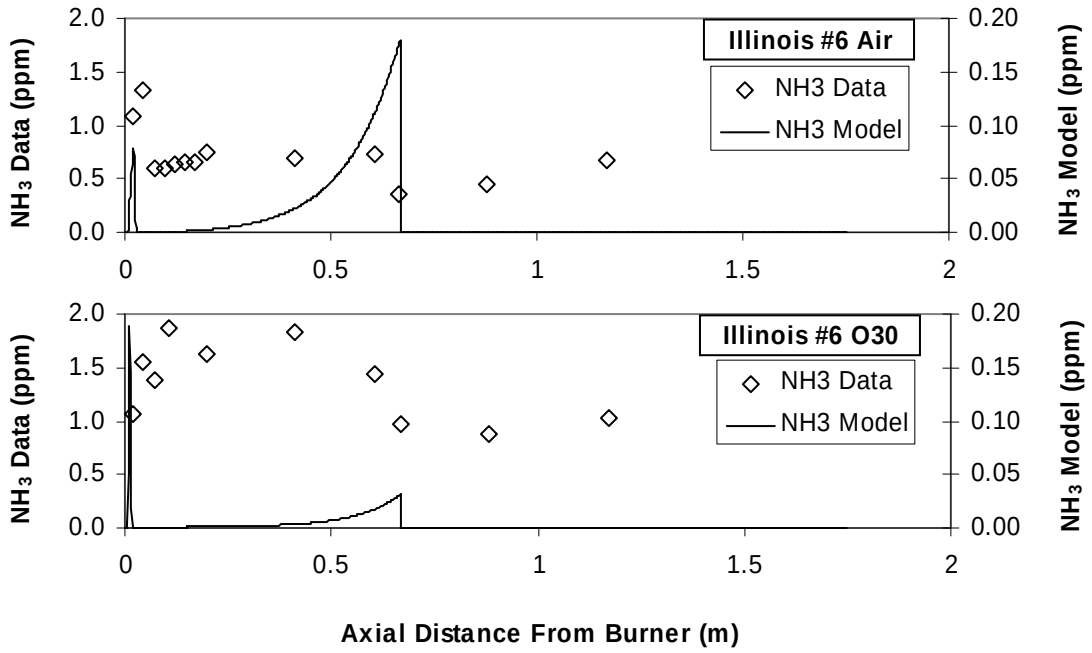

Figure 64. NH_3 model predictions and data for Illinois #6 staged combustion.

The HCN data for the sub-bituminous coal already presented above showed HCN present throughout the reducing zone. The model predictions for this coal however exhibit a sharp peak in HCN near the burner with no significant HCN elsewhere. The results in Figure 65 are qualitatively representative of all the sub-bituminous cases.

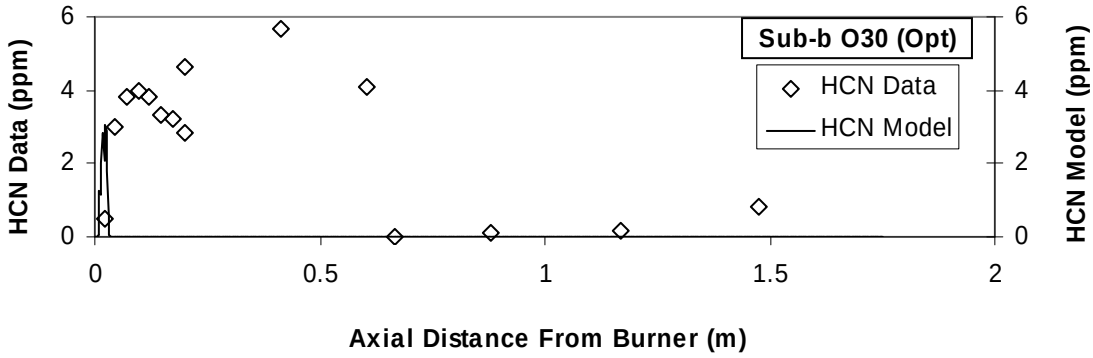

Figure 65. Comparison of HCN model predictions and experimental data for Sub-b O30 (Opt).

For the Illinois #6 coal the model again predicts only a sharp peak in HCN near the burner. As is seen in Figure 66 the model trend somewhat matches the Illinois #6 Air data with a rapid rise and fall in HCN, but not the Illinois #6 O30 data where the model shows a rapid rise and fall but the data shows a small but lingering concentration of HCN.

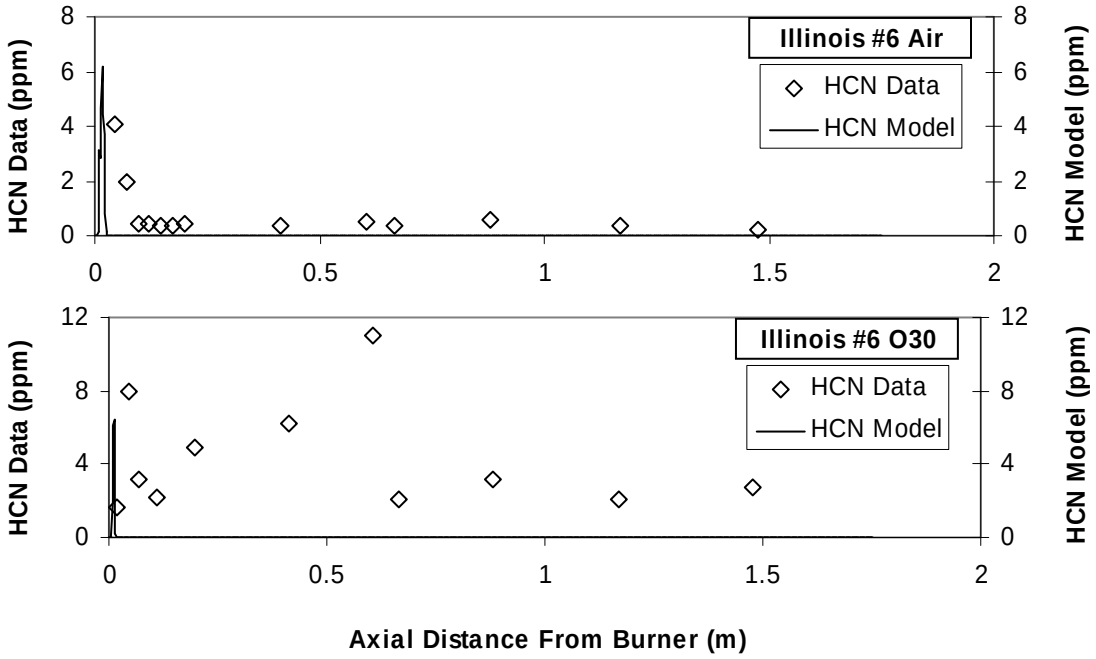

Figure 66. HCN experimental data and model predictions for the Illinois #6 experiments.

Model-Data Comparison: Hydrocarbons

Experimental data and model predictions for CH_4 in the Sub-b Air and Sub-b Air (Opt) cases appear in Figure 67. Similar information for C_2H_4 is in Figure 68.

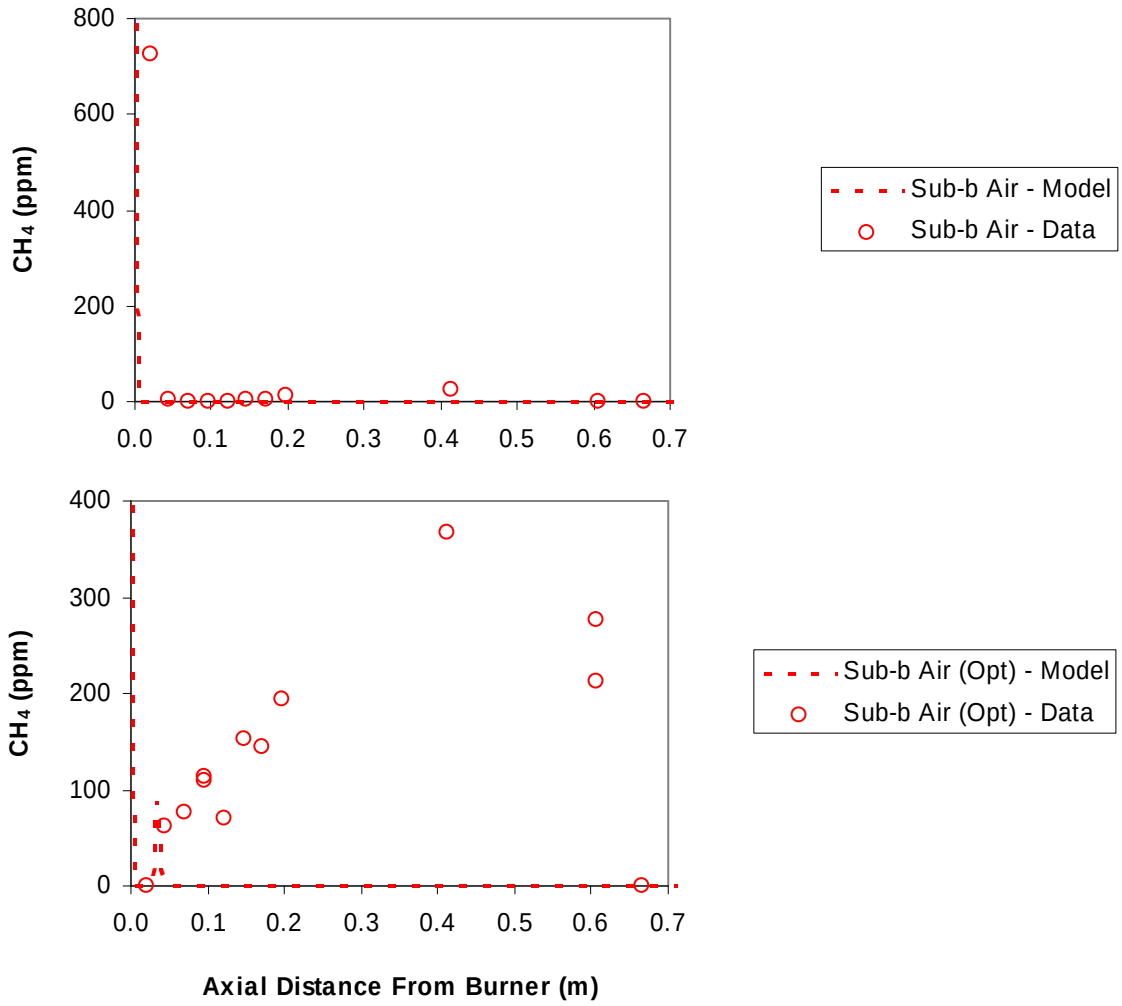

Figure 67. Comparison of model predictions and experimental data for CH_4 in the Sub-b Air and Sub-b Air (Opt) cases.

In these two figures the Sub-b Air case has high levels of both hydrocarbons near the burner. In the model this is associated with the natural gas flame. This high initial hydrocarbon level does not appear in the experimental data for the Sub-b Air (Opt) cases. A possible reason is that the lower flow rate through the burner moves the flame to a location upstream of the first gas sampling location.

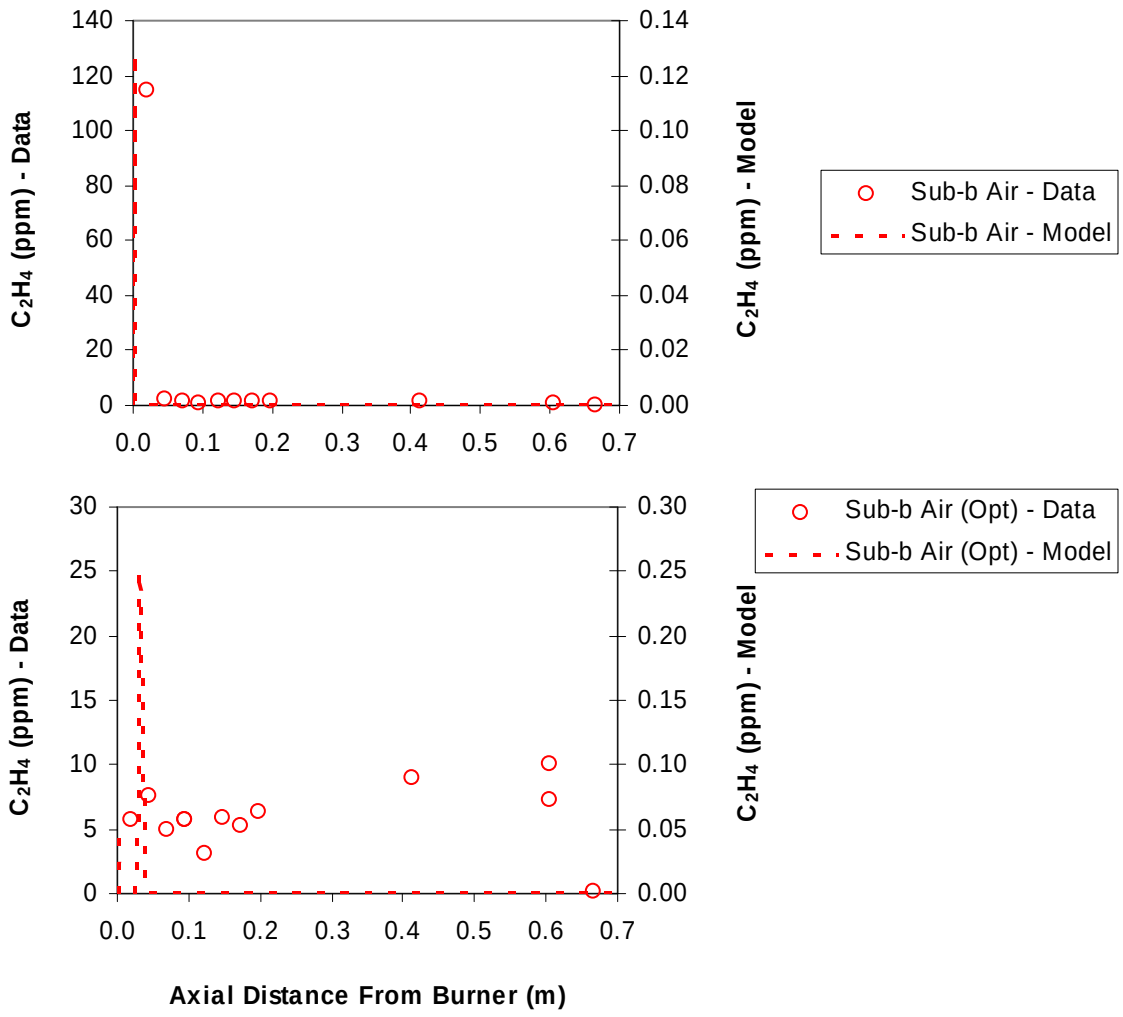

Figure 68. Comparison of model predictions and experimental data for C_2H_4 in the Sub-b Air and Sub-b Air (Opt) cases.

In the model predictions only, the hydrocarbon levels peak again just downstream of the initial high levels. These downstream peaks are associated with the predicted volatiles release from the coal. The size of these peaks is very small in the Sub-b Air case, probably due to high oxygen availability, but they are still present (Figure 69). The peak width is small and followed by near-zero levels of hydrocarbons, whereas the experimental data has higher levels of hydrocarbons over a broad region.

The Sub-b Air (Opt) case has higher hydrocarbon concentrations than the Sub-b Air case, consistent with the lower primary SR.

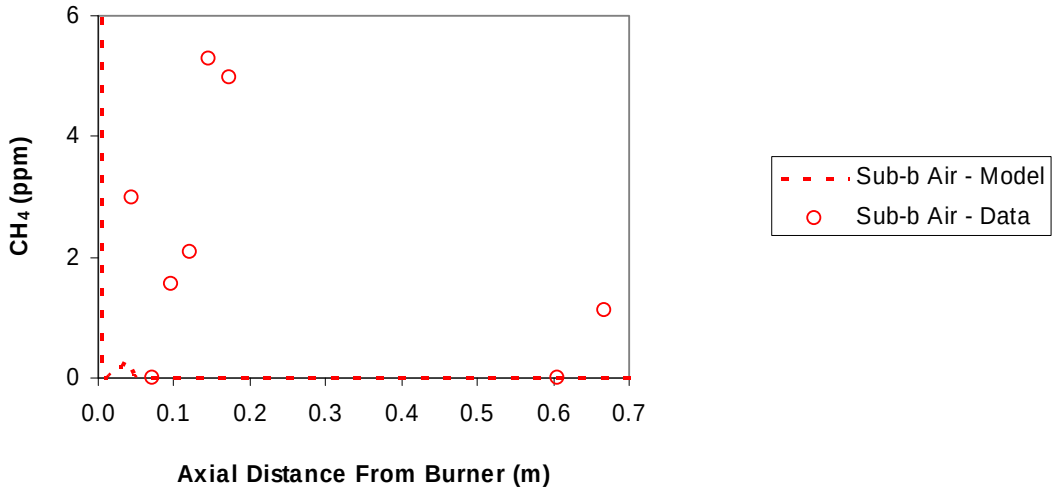

Figure 69. The same data and model predictions shown in the upper plot of Figure 67 but with the vertical axis limits changed to reveal small details in the model prediction near the burner.

The comparison between model predictions of hydrocarbons and experimental data for the Sub-b O30 and Sub-b O30 (Opt) cases displays similar trends to the Air combustion cases shown above. Other hydrocarbons predicted by the model for which there are no experimental measurements (such as CH_3, CH_2, CH, and HCCO) show the same behavior as CH_4 and C_2H_4.

A significant simplifying assumption made in the model is that of a single particle size representing the size distribution in the experiment. To investigate effects of this assumption, two model cases were run for the Sub-b Air (Opt) case using different particle sizes. The first case followed the standard modeling procedure used in this work of using the mean particle size from the measured particle size distribution (121 μm). The second case assumed 300 μm diameter particles to represent particles near the upper end of the size distribution. A plot of the predicted CH_3 profiles is shown in Figure 70. CH_3 was chosen as a representative hydrocarbon, as most of the hydrocarbons followed similar behavior.

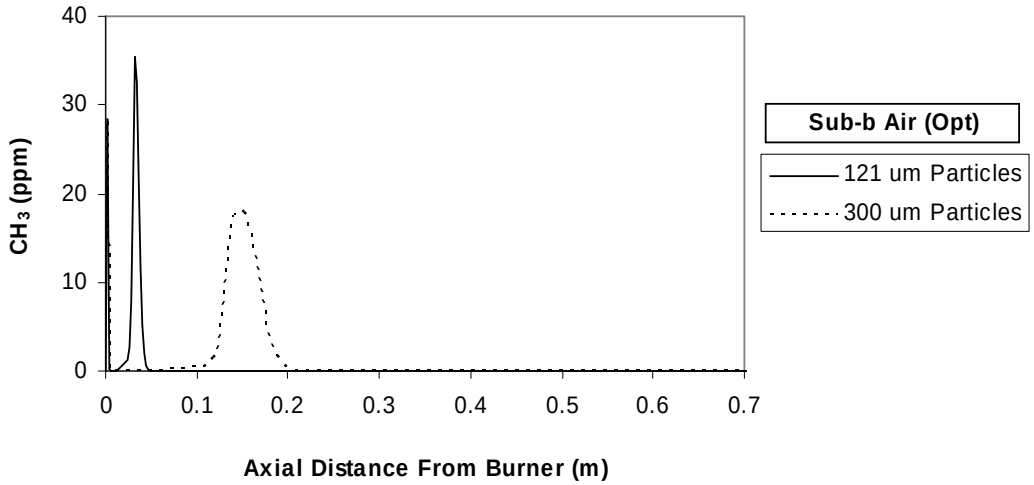

Figure 70. Plot of the predicted CH_3 profile for the Sub-b Air (Opt) case using two different particle sizes.

As is seen in the figure, the CH_3 profiles have two peaks each. A sharp, narrow peak near the burner is associated with the methane flame and further downstream is a wider peak spatially coincident with the modeled release of volatiles. These predictions suggest that if a particle size distribution was included in the model that volatiles would be released over a broad region from 0-0.2 m from the burner for the Sub-b Air (Opt) case, rather than in the first 0.05 m from the burner predicted when only one representative particle size is used. Smaller particles completing devolatilization early would be expected to consume oxygen by heterogeneous char oxidation while larger particles are still evolving volatiles. Volatiles evolved late from the larger particles would be released under reducing conditions and would probably result in the persistence of hydrocarbons throughout the primary combustion zone as observed in the experimental data.

An additional explanation for poor agreement between the model and the data is the lack of a model for mixing of coal and oxidizer. In the model, the coal is assumed to be perfectly mixed within the oxidizer. In reality, the coal may clump during the feed process and produce spatial or temporal pockets of rich products that require some amount of mixing before reaching the average stoichiometry of the mixture. This would also tend to broaden the region of volatiles release and produce local zones of lower SR in which HCN, NH_3, and hydrocarbons could survive.

NO_X Reaction Pathways

The MixMaster application was used to evaluate the pathways through which NO is destroyed in the model. For the GRI-Mech 3.0 mechanism, representative pathway diagrams for modeled NO destruction in the Sub-b Air (Opt) and Sub-b O30 (Opt) cases are shown in Figure 71 and Figure 72. It should be noted that these diagrams only show the most significant pathways since there are too many pathways in the mechanism to show all in a practical figure.

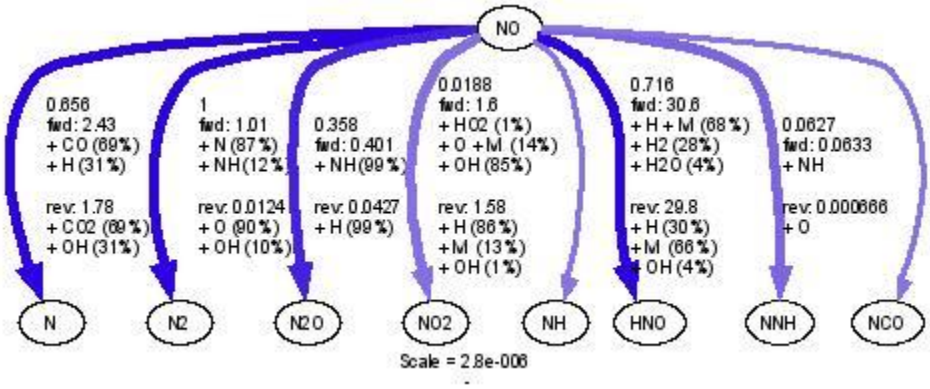

Figure 71. Major modeled NO reaction pathways for the Sub-b Air (Opt) case 152 mm from the burner using GRI-Mech 3.0.

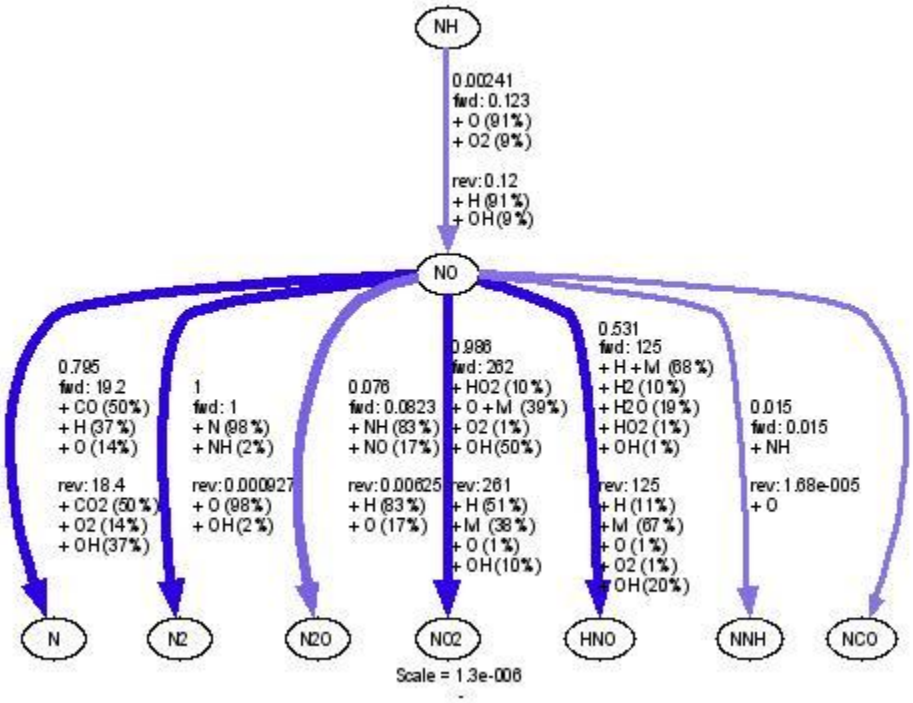

Figure 72. Major modeled NO reaction pathways for the Sub-b O30 (Opt) case 152 mm from the burner using GRI-Mech 3.0.

An important feature of these pathway diagrams is the absence of hydrocarbons in the reactants listed next to the pathway arrows even though the GRI-Mech 3.0 mechanism does include reactions of NO with hydrocarbons. Reaction 2 is an example.

$$CH_3 + NO \longleftrightarrow HCN + H_2O \qquad \text{[Reaction 2]}$$

The reason that the reburning reactions do not produce significant NO reduction in the model is a result of the hydrocarbon concentration predictions being near-zero over most of the reactor. As mentioned in connection with Figure 43 in Section 0 the SKG03 mechanism displays a unique feature in the predictions for the Sub-b Air (Opt) case. The narrow peak in hydrocarbons associated with the modeled volatiles release occurs at just the right place for reburning reactions to cause a sudden drop in NO. A reaction pathway diagram for this case is shown in Figure 73. The dominant NO destruction pathway here involves reaction of NO with hydrocarbons to produce HCN.

It is reasonable to expect that if the model used a range of particle sizes as discussed in Section 0 the hydrocarbon concentrations would be lower than predicted at the single narrow peak and spread over a larger region in space. The resulting NO destruction rate should then decrease relative to that in Figure 43 and also occur over a wider region.

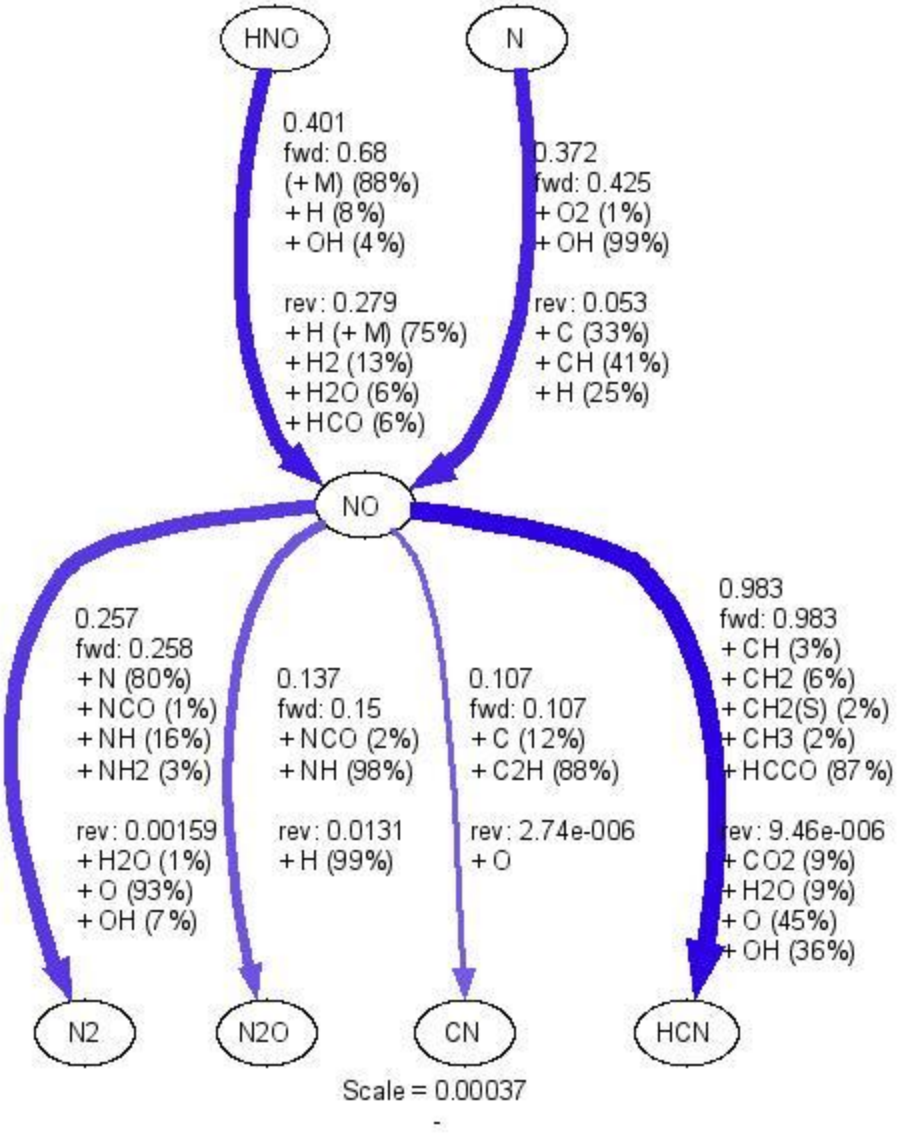

Figure 73. Major modeled NO reaction pathways for the Sub-b Air (Opt) case 32 mm from the burner using the SKG03 mechanism.

Flat Flame Burner Results

Experimental work was performed to simulate nitrogen release at enhanced temperatures in an oxy-fuel combustion environment using a flat flame burner (FFB) facility. Normal operation of the FFB includes a mixture of air, O_2, CO, and H_2. The oxy-fuel environment was provided by replacing the N_2 with CO_2.

Suite of Coals

Three coals (Illinois 6, Pittsburgh 8, Caballo) were originally designated for use in this project. Unfortunately, the Caballo Powder River Basin coal was not available, and the MFR group used

a coal identified as Black Thunder from a different PRB mine, although the exact history of this coal is not clear. This coal was used as a replacement in the FFB experiments.

The average mass mean particle diameter was measured using a LS series Coulter Counter. Each coal was run through the machine eight times and the measured diameters were averaged to obtain a mass mean diameter for each coal. Mass mean diameters were 70 μm for the Ill #6 coal, 80 μm for the BT coal, and 50 μm for the Pittsburgh #8 coal.

Gas Temperature Profiles in the FFB

It was desired to perform experiments at 1600, 1700, 1800 and 1900 K, tracking the nitrogen content of the coal over that range. Gas temperature in the FFB is changed by adjusting the flow of CO, H_2, O_2, and N_2 or CO_2 to the burner. Oxycombustion setting used CO_2 as the diluent gas while traditional combustion setting used N_2. Both settings used N_2 as the carrier gas to entrain the coal. Since the flow of carrier gas was 0.0367 standard liters per minute, it was considered negligible compared to the 30 slpm gas flow to the burner.

The constraints on the system were to have a fuel-rich flame in order to perform coal pyrolysis experiments, and to have a stable flame. After using a chemical equilibrium code to help search for appropriate conditions, four burner settings were identified. Gas temperature profiles were then obtained, with corrected centerline peak temperatures of 1580, 1699, 1789 and 1896 K. All gas temperatures were measured with a type B thermocouple, coated with SiO_2 to prevent catalytic reactions on the bead. The 1896 K setting caused the burner tubes to clog in part of the burner after a short period of running. To remedy this problem, a profile with a corrected peak of 1909 K was obtained by operating the burner with inverted settings. The inverted settings on the flat flame burner are created when the fuel feed and the oxidizer feed are switched, so that the oxidizer runs through the fuel tubes and the fuels runs through the honeycomb. The recorded temperature profiles used for the oxy-fuel experiments are shown in Figure 74-Figure 77.

Temperature profiles were also collected for N_2 diluted pyrolysis conditions in the same manner as explained for the CO_2 diluted conditions. The corrected centerline peak temperatures for these conditions are 1546, 1628, 1712, 1886 K respectively. While the peak temperatures are not exact matches to the CO_2 diluted conditions they allow a point of reference at similar positions. The gas temperature profiles from the experiments with the N_2 background are displayed in Figure 78-Figure 81.

The centerline gas temperature profile was collected by placing the thermocouple bead over the coolest point at the surface in the center, then lowering the burner to change vertical distance. The north, south, east and west readings were obtained by moving the thermocouple in a straight line from each of these directions and finding the peak temperature for that side. Gas temperature measurements were taken at the burner surface and at vertical heights above the burner surface ranging from 0.5 to 5.0 inches. Peak gas temperatures sometimes occurred closer to the burner surface when using inverted settings, so measurements were taken at 0.25 inches for the 1909 K

profile. The reading from the thermocouple was entered into a spreadsheet where the temperature was corrected for radiation effects.

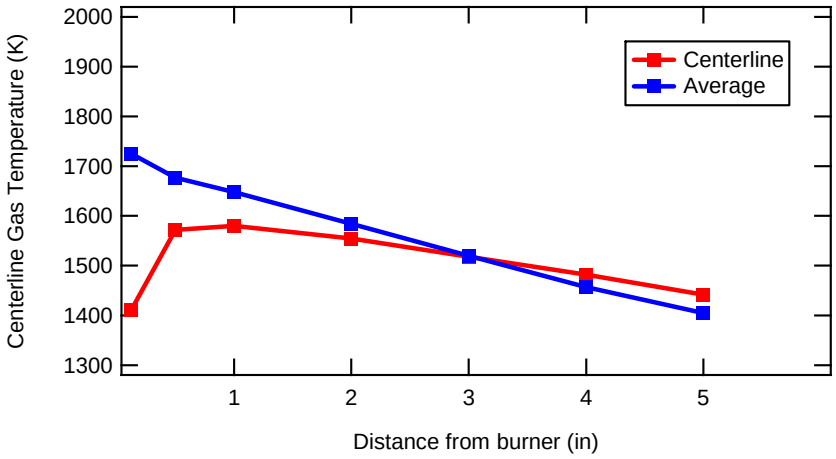

Figure 74. Vertical gas temperature profiles for the 1600 K CO_2 diluted pyrolysis condition in the FFB.

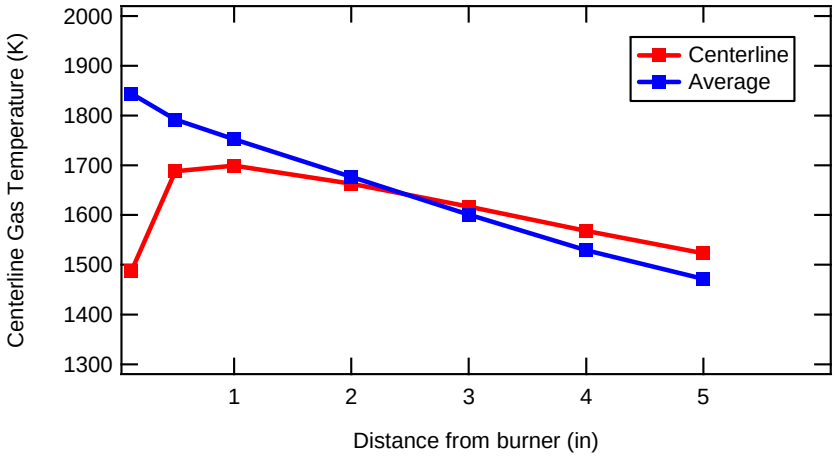

Figure 75. Vertical gas temperature profiles for the 1700 K CO_2 diluted pyrolysis condition in the FFB.

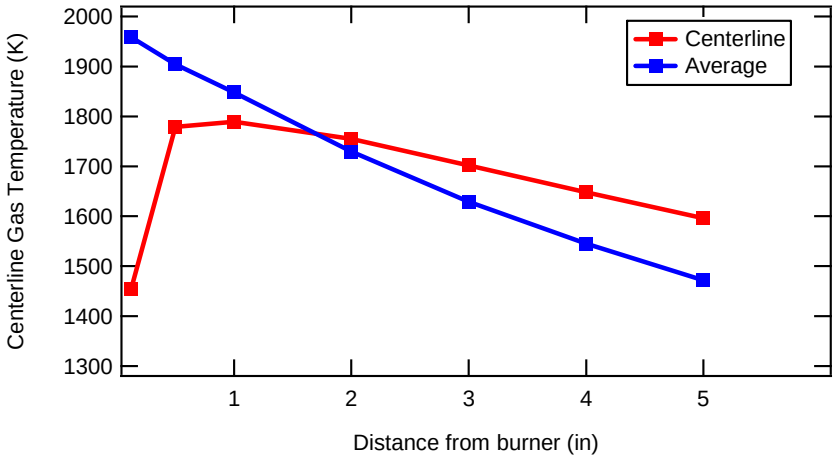

Figure 76. Vertical gas temperature profiles for the 1800 K CO_2 diluted pyrolysis condition in the FFB.

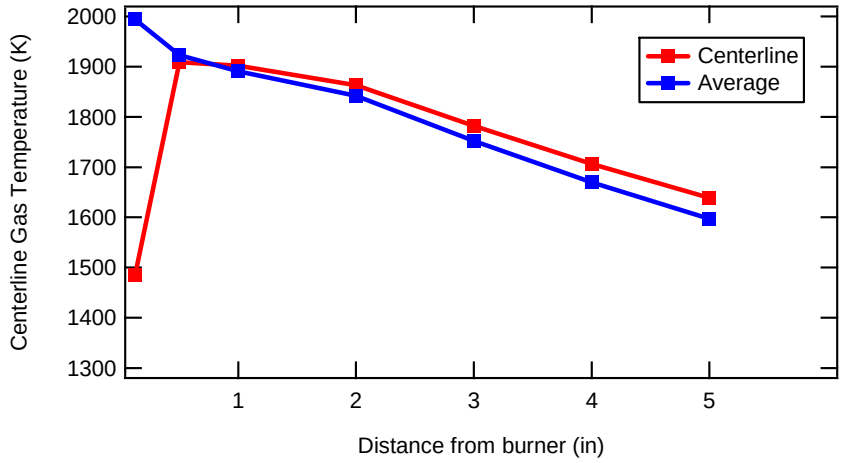

Figure 77. Vertical gas temperature profiles for the 1900 K CO_2 diluted pyrolysis condition in the FFB.

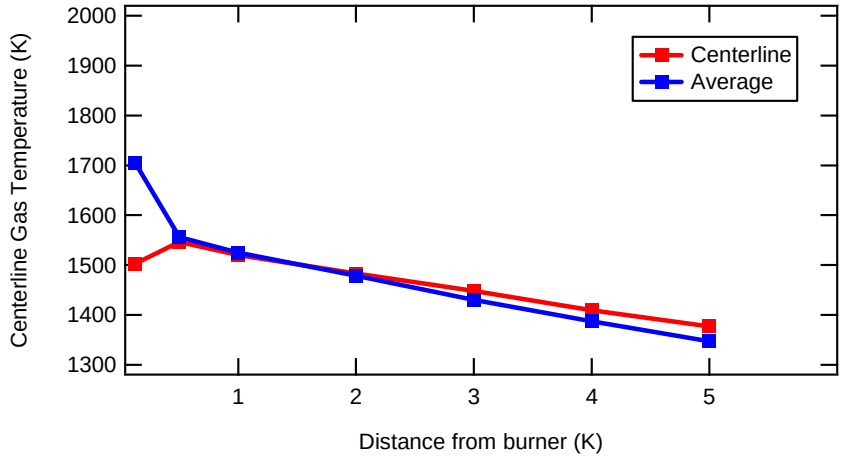

Figure 78. Vertical gas temperature profiles for the 1600 K N_2 diluted pyrolysis condition in the FFB.

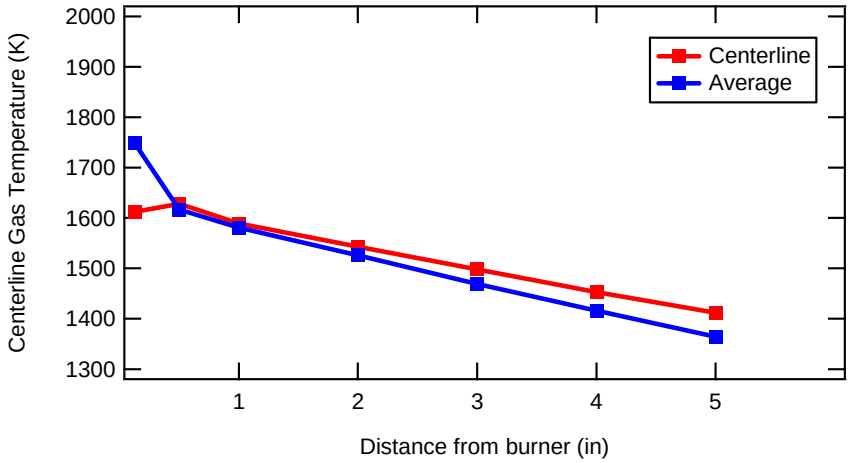

Figure 79. Vertical gas temperature profiles for the 1700 K N_2 diluted pyrolysis condition in the FFB.

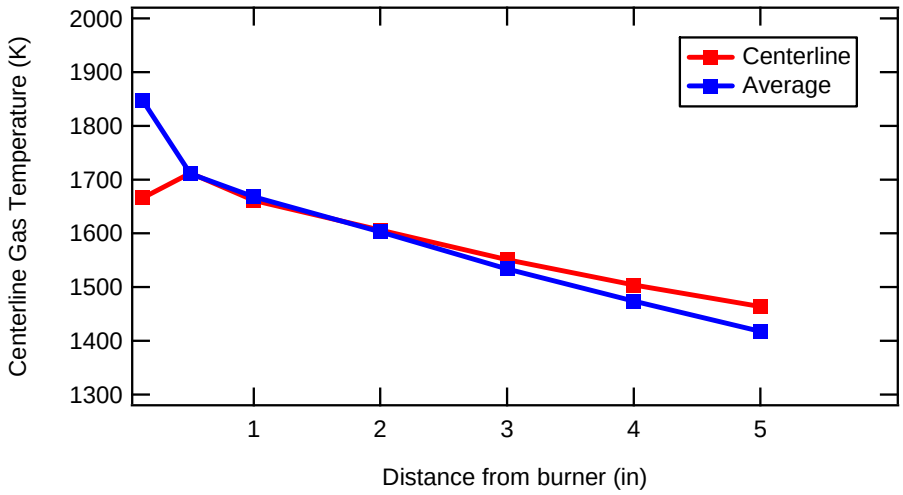

Figure 80. Vertical gas temperature profiles for the 1800 K N_2 diluted pyrolysis condition in the FFB.

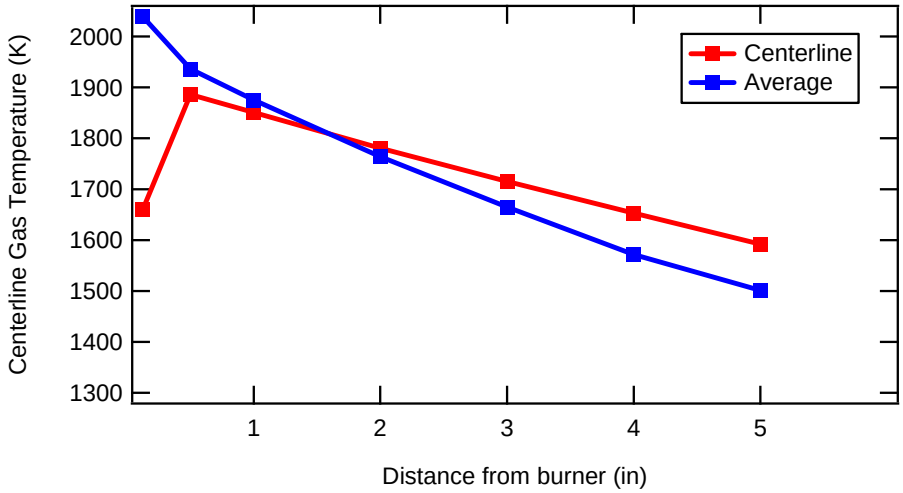

Figure 81. Vertical gas temperature profiles for the 1600 K N_2 diluted pyrolysis condition in the FFB.

Experiments Conducted

Coal pyrolysis experiments were conducted at each of the four temperature conditions with each of the three coals, collecting approximately 600 mg of char from each coal at each condition. Most of the char samples were sent to Huffman labs in Golden, CO for ultimate and ICP analysis. While placing the coal under Ar for storage in the refrigerator, the Pitt 8 sample at 1700 K was mixed with some of the sample from 1800 K. The contaminated 1700 K sample was therefore discarded, and fresh char was generated in repeat experiments. The experiments using the Black Thunder coal showed potential differences from the model and the previous results, therefore conditions were found in a N_2 rich environment to compare the data. Replicates were run at a sample probe heights of 1 and 2 inches as will be discussed later.

Devolatilization Results

The char samples were analyzed by inductively-coupled plasma atomic absorbtion (ICP) for the percentage of Al, Ti, and Si. The mass released as volatiles was determined using Al, Si, and/or Ti as tracers, assuming that none of these elements were released from the char. The total ash content was also used as a tracer, but with little confidence since some elements are known to be released from coal and char at high temperature. Upon analyzing the data, it became clear that in many cases, one of the elements did not give good results compared to the other elements. The "bad" element was not always the same element. For instance, the Si tracer analysis did not yield good results for the Black Thunder coal, but the Al tracer seemed to give poor results for the Pitt#8 coal. The results of the tracer analysis to determine the fraction of the daf coal that became volatiles are shown in Figure 82.

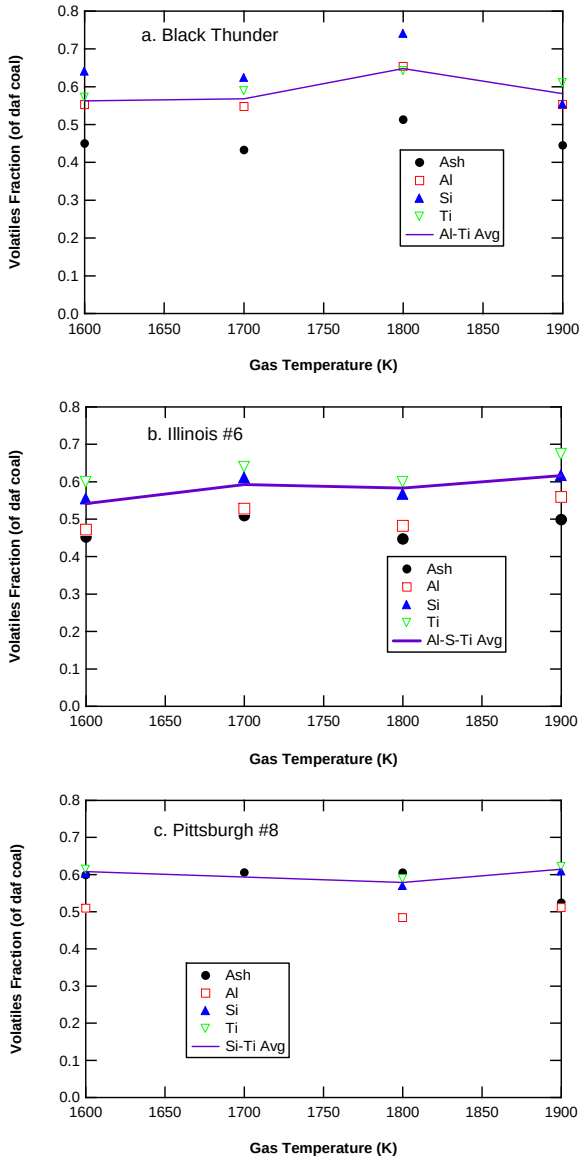

Figure 82. Volatiles fraction measured as a function of temperature for (a) Black Thunder, (b) Illinois #6 coal, and (c) Pittsburgh #8 coal.

It is clear from the volatiles release results that there is no significant increase in mass release at increased temperatures, as expected.

The ultimate analysis was converted to a dry ash free basis for both the coal and char samples. These data are presented in Table 12 - Table 16. Two samples were analyzed for the Illinois #6 char at the 1800 K condition. The cases were averaged in the calculations. Mass release data were reported previously. The nitrogen release was calculated at each temperature using Equation 5.

$$\%\ \text{N release (daf)} = 1 - \left(1 - MR_{daf}\right)\left(\frac{x_{N,daf\ char}}{x_{N,daf\ coal}}\right) \qquad \textbf{Equation 5}$$

where $x_{N,daf\ \text{char}}$ is the mass fraction of nitrogen in the char, $x_{N,daf\ \text{coal}}$ is the mass fraction of nitrogen in the coal and MR_{daf} is the mass release calculated on a dry ash free basis. This calculation was repeated at each temperature (1600, 1700, 1800 and 1900 K) and the nitrogen release values are displayed in Table 12 - Table 16 along with the mass release data.

Table 12. Ultimate Analysis for Ill #6 coal and chars in CO_2 at 1 inch from the probe on a dry ash free basis

	Coal	1600 K	1700 K	1800 K	1800b K	1900
C (wt% daf)	75.08	88.61	91.41	87.77	82.12	94.17
H	5.55	2.52	1.74	2.51	3.39	1.31
N	1.28	1.38	1.39	1.43	1.30	1.30
O (diff)	15.33	5.87	3.84	6.83	11.74	1.57
S	2.77	1.61	1.62	1.46	1.45	1.66
Mass Release (wt % of daf coal)						
Ash Tracer		49.65%	53.30%	50.37%	47.13%	58.59%
Ti Tracer		55.57%	61.13%	56.59%	56.59%	64.23%
Si Tracer		54.99%	60.57%	56.21%	56.21%	61.17%
Al Tracer		59.43%	63.43%	59.43%	59.43%	66.82%
MR Average (not ash)		56.66%	61.71%	57.41%	57.41%	64.07%
St. Dev. (not ash)		2.4%	1.5%	1.8%	1.8%	2.8%
Nitrogen Release		53.00%	58.32%	52.32%	56.70%	63.49%

Table 13. Ultimate Analysis for Pitt #8 coal and chars in CO_2 at 1 inch from the probe on a dry ash free basis

	Coal	1600 K	1700 K	1800 K	1900 K	
C (wt% daf)	81.60	91.94	87.68	87.91	95.15	
H	5.79	2.21	1.97	5.24	0.93	
N	1.33	1.37	1.37	1.30	1.31	
O (diff)	7.23	0.90	5.02	2.72	-0.17	
S	4.05	3.59	3.96	2.83	2.78	
Mass Release (wt % of daf coal)						
Ash Tracer		60.94%	58.54%	48.51%	53.20%	
Ti Tracer		61.56%	60.22%	59.05%	61.78%	
Si Tracer		60.58%	60.05%	57.28%	61.21%	
Al Tracer		61.72%	60.08%	59.22%	62.50%	
MR Average (not ash)		61.29%	60.12%	58.51%	61.83%	
St. Dev. (not ash)		0.6%	0.1%	1.1%	0.6%	
Nitrogen Release		60.20%	59.03%	59.50%	62.41%	

Table 14. Ultimate Analysis for Black Thunder coal and chars in CO_2 at 1 inch from the probe on a dry ash free basis

	Coal	1600 K	1700 K	1800 K	1900 K	1900 K
C (wt% daf)	71.19	88.96	92.34	86.93	86.75	90.85
H	5.30	1.54	1.40	2.16	2.00	1.60
N	1.02	1.13	1.20	1.19	1.20	1.26
O (diff)	21.91	8.06	4.74	9.34	9.69	5.83
S	0.58	0.31	0.33	0.39	0.36	0.46
Mass Release (wt % of daf coal)						
Ash Tracer		43.23%	49.64%	42.03%	43.28%	53.30%
Ti Tracer		61.68%	61.16%	71.68%	61.68%	67.12%
Si Tracer		63.65%	62.00%	73.60%	55.04%	66.84%
Al Tracer		56.83%	58.53%	63.87%	60.62%	64.72%
MR Average (not ash)		60.72%	60.56%	69.72%	61.15%	65.92%
St. Dev. (not ash)		3.5%	1.8%	5.2%	3.6%	1.3%
Nitrogen Release		56.59%	53.75%	64.84%	54.31%	58.05%

Table 15. Ultimate Analysis for Black Thunder coal and chars in N_2 at 2 inches from the probe on a dry ash free basis

	Coal	1600 K	1700 K	1800 K	1900 K	
C (wt% daf)	71.19	92.03	89.57	86.93	86.75	
H	5.30	1.10	1.67	2.16	2.00	
N	1.02	1.32	1.28	1.19	1.20	
O (diff)	21.91	5.21	7.10	9.34	9.69	
S	0.58	0.35	0.39	0.39	0.36	
Mass Release (wt % of daf coal)						
Ash Tracer		51.80%	49.21%	51.75%	60.01%	
Ti Tracer		65.89%	62.69%	61.16%	67.12%	
Si Tracer		65.68%	62.00%	61.13%	64.69%	
Al Tracer		64.72%	64.72%	60.12%	64.72%	
MR Average (not ash)		65.43%	63.14%	60.80%	65.92%	
St. Dev. (not ash)		0.6%	1.4%	0.6%	1.4%	
Nitrogen Release		55.56%	54.09%	54.48%	59.91%	

Table 16. Ultimate Analysis for Black Thunder coal and chars in N_2 at 1 inch from the probe on a dry ash free basis

	Coal	1600 K	1700 K	1800 K	1900 K	
C (wt% daf)	71.19	83.30	85.38	88.53	89.99	
H	5.30	2.70	2.43	1.67	1.24	
N	1.02	1.46	1.70	1.40	1.62	
O (diff)	21.91	12.12	10.01	7.93	6.72	
S	0.58	0.42	0.47	0.46	0.43	
Mass Release (wt % of daf coal)						
Ash Tracer		38.23%	45.98%	51.10%	45.57%	
Ti Tracer		50.82%	55.80%	57.19%	56.73%	
Si Tracer		37.59%	56.71%	59.40%	43.33%	
Al Tracer		48.76%	51.95%	55.91%	57.82%	
MR Average (not ash)		49.79%	53.88%	56.55%	57.28%	
St. Dev. (not ash)		1.5%	2.5%	1.8%	0.8%	
Nitrogen Release		27.18%	22.19%	39.59%	31.56%	

The bulk densities of the coal and char were measured using a tap density technique, yielding the mass of particles per volume of graduated cylinder. Assuming a packing factor of 0.5, the ratio of the char density to the coal density was determined. The result is the ratio of the apparent density of the char to that of the coal. These data are shown in Figure 83. These data show no real trend with temperature, as expected, and are consistent with the volatiles release data shown in Figure 82. The density ratio and the mass release ratio are related by Equation 6.

$$\%\ \text{N release (daf)} = 1 - \left(1 - MR_{daf}\right)\left(\frac{x_{N,daf\ char}}{x_{N,daf\ coal}}\right) \qquad \textbf{Equation 6}$$

The diameter ratios are shown in Figure 84, indicating a slight degree of shrinkage (rather than swelling) for all coal chars collected under these conditions.

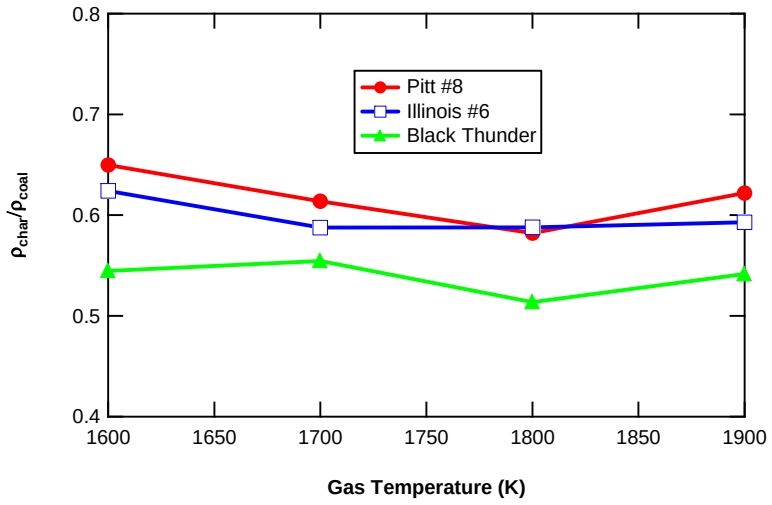

Figure 83. Apparent density ratios measured for the coal chars as a function of temperature.

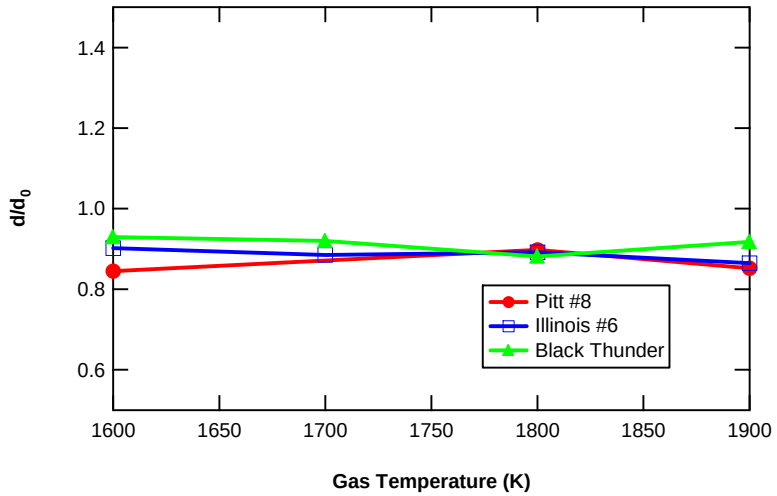

Figure 84. Diameter ratios measured for the coal chars as a function of temperature.

CPD Modeling and N_2 Environment Comparison

The mass release and nitrogen release calculated in the Oxyfuel environment were compared to an N_2 environment in two ways for the bituminous coals and three for the subbituminous coal. Previous experiments were conducted in the flat flame burner system by Zhang (Zhang and Fletcher, 2001). Data were collected between 1534 K and 1850 K. for the Black Thunder and Illinois #6 coals. A mass mean diameter of 60 μm was reported for the Illinois #6 coal, however no mass mean diameter was reported for the Black Thunder coal. No Pitt #8 coal experiments were conducted by Zhang. These data are represented in Figures la-b and le-f by the green diamonds.

The Chemical Percolation Devolatilization (CPD) model was used to predict both nitrogen and mass release. The CPD model was developed by Dr. Fletcher (Fletcher et al. 1992) and is currently used in programs such as Fluent. The CPD model uses coal data including the mass mean diameter, NMR data, ultimate and proximate analysis to predict mass release, gas speciation and nitrogen partitioning. This model has been quite successful in predicting coal devolatilization behavior over a large range of coal types, heating rates, temperatures, and pressures. All of the preceding coal specific data were input into the CPD code along with a temperature and velocity profile for each burner condition. The version of the CPD model used here was developed to run in an N_2 environment. Therefore, CPD model predictions in a way provide another contrast with the experimental data obtained in an Oxyfuel environment. The CPD predictions are displayed in the charts with the blue lines.

After analyzing the Black Thunder coal using the methods above, it was decided that the coal was not fully pyrolyzed in Zhang's experiments. Figure 85 shows the CPD predicted mass release curve with the newly measured data at both 1 and 2 inches for the given condition. Since the coal was not fully pyrolyzed at 1 inch for this condition, further N_2 diluted experiments were conducted at 2 inches for the four previously mentioned temperatures. The complete results for the Black Thunder coal are shown in Figure 86 e-f with the titles of N_2 - 2 inch and N_2 - 1 inch and represented by yellow diamonds and purple squares respectively. The Oxycombustion conditions are represented by red triangles and called CO_2 rich in the charts.

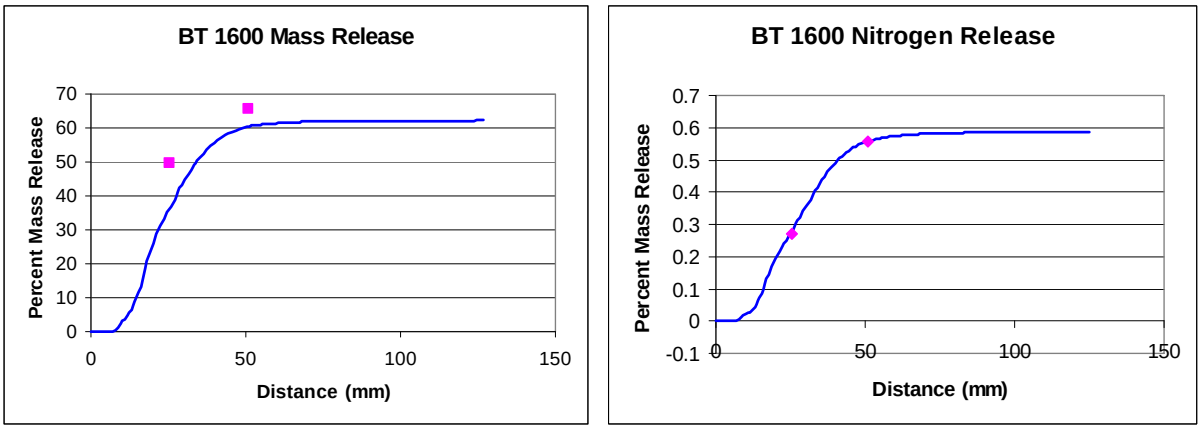

Figure 85. Measured and predicted mass and nitrogen release for the BT coal in the 1600 K temperature condition in the N_2 background.

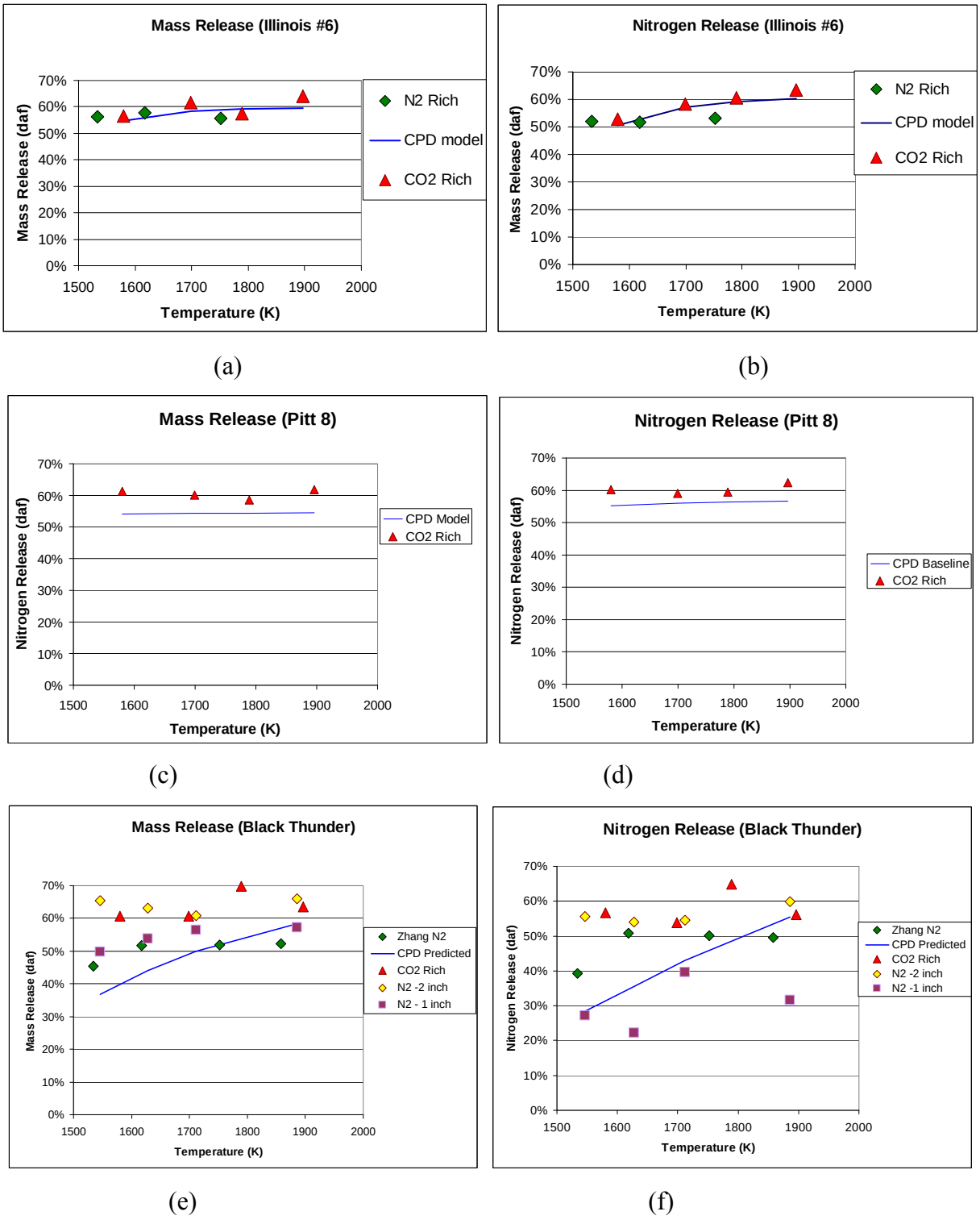

Figure 86. Predicted and Measured Nitrogen Release and Mass Release as a function of temperature

Discussion of Results

The mass release for the Illinois #6 coal during pyrolysis remained relatively constant after 1700 K, while the nitrogen release increased slightly with temperature throughout the temperature range. Little difference was seen between the mass release or nitrogen release data in either the N_2 or oxyfuel environment. The CPD model predictions for the Illinois #6 coal were in great agreement with both the mass release and the nitrogen release data. The mass release and nitrogen release for the Pittsburgh #8 coal did not show much change with temperature in these experiments; a slight trend might be indicated, but it seems to be within the scatter of the data. The lack of change in mass and nitrogen release at these temperatures was computed accurately by the CPD model. However, the CPD model predictions of both mass release and nitrogen release were slightly below the experimental values for this Pittsburgh #8 coal.

The data for the Black Thunder coal are a little more scattered. The mass release for the Black Thunder coal was higher in the oxyfuel case than in Zhang's experiments or in the 1 inch N_2 environment. However, in the 2 inch N_2 environment the mass release matched the oxyfuel case taken at 1 inch. The CPD model seems to match the mass release data in the 1 and 2 inch N_2 environments at higher temperatures. CPD model calculations have been performed for the gas temperature profiles in the CO_2 environments, but the thermodynamic data to help solve the particle energy equation was not changed to reflect the CO2 environment, so these calculations are being redone. It is possible that CO_2 may react with the char at these temperatures when the CO_2 concentration is high, which has been suggested in the literature. The difference in gas properties of N_2 and CO_2 seems to be causing the coal to lose its mass faster in the CO_2 environment. Molina and Shaddix (2007) reported that the different gas properties change the rates of ignition and devolatilization. Since experiments were not performed in the CO_2 environment at a 2 inch height it is unknown whether volatile and nitrogen yield would show a similar increase to the N_2 environment or remain the same. CPD predictions in the CO_2 environment are underway.

The CPD model predictions of the Black Thunder coal reported an error in predicting the species distribution of the light volatile gases. This error is due to an unfamiliar coal composition for interpolating from known pyrolysis data. It is likely that the ultimate analysis performed at the Huffman lab might be suspect, due to the high oxygen content (which is obtained by difference). A second ultimate analysis showed the O_2 content to vary by 13%.

The nitrogen release data for the Black Thunder coal in the oxyfuel environment were scattered, but higher on average than in Zhang's data and the 1 inch N_2 environment. The 2 inch N_2 environment data matched the 1 inch oxyfuel numbers, meaning that at least the mass release achieved some sort of asymptotic yield for these two conditions. The 1 inch N_2 environment data showed that the asymptote had not yet been reached. Upon further investigation, the measured amount of N in the char was higher for these Black Thunder samples than the chars from other coals, which accounted for the lower nitrogen release rates. These char analyses are being repeated. The data from Zhang in the N_2 environment seem to indicate a plateau in nitrogen release after 1600 K, while the CPD model predicts increasing mass release. This seems to be more of a residence time issue, as indicated in Figure 85. As with the mass release it is not know whether the CO_2 environment would yield a greater nitrogen release with longer residence time. If the nitrogen release is assumed to be a plateau then the change in gas properties can be assumed to make the difference.

The end result of these experiments seems to be that the reactions occur earlier in the CO_2 environment than in the N_2 environment. This is likely due to the higher heat capacity and thermal conductivity of the CO_2, causing the particles to heat up faster. We hope to confirm this in the near future with detailed CPD calculations in the CO_2 environment. These conclusions are consistent with the observations of Molina and Shaddix (2007).

Conclusions

Pulverized coal was burned in a down-fired, laminar flow reactor with and without oxidizer staging. Air or mixtures of O_2 and CO_2 were used as oxidizers, and nitrogen and combustion gas species concentrations were measured to gain insight into the differences between NO_X formation in air and oxy-fuel combustion. Additional understanding was obtained by modeling the reactor as a series of ideal reactors with detailed kinetics. Coal volatiles were predicted using the CPD-NLG coal devolatilization model. The following conclusions can be drawn from the results:

- In unstaged premixed combustion, air and oxy-fuel combustion produced similar levels of fuel nitrogen conversion to NO_X. Low NO_X emissions from oxy-fuel combustion are therefore not achieved without staged mixing of oxidizer and fuel as is the case for conventional air combustion.
- Wall temperature and other data indicated higher reaction rates under oxy-fuel conditions than in air.
- While effluent CO levels were comparable between air and oxy-fuel combustion, higher CO concentrations in fuel-rich, oxy-fuel flames were often measured. The computational model suggests that high CO levels observed in oxy-fuel combustion are due to thermodynamic equilibrium. Thermal dissociation of CO_2 becomes significant at about 1500 K which is expected to lead to strong temperature sensitivity of CO concentrations around this temperature. In oxy-fuel combustion, CO levels are higher than air combustion above 1500 K because of the greater amount of CO_2 available for dissociation reactions. CO may indirectly influence the NO_X chemistry through reactions that increase the concentration of radicals important to NO_X reduction.
- Gasification of char by CO_2 under oxy-fuel conditions has some influence on the level of CO through the thermal effects of the gasification reactions and the effect of additional fuel conversion on the elemental composition of the combustion gases. These gasification reactions may not be insignificant in oxy-fuel conditions as is often assumed to be the case in air combustion but the amount of CO appears to be dominated by equilibrium considerations, not gasification reactions.
- A detailed model of nitrogen evolution under pulverized coal air and oxy-fuel conditions was assembled using existing sub-models from the literature. The CPD-NLG devolatilization model was modified for use in oxy-fuel environments. The CPD-NLG model treats devolatilization as a purely thermal process. Interaction with the N_2 or CO_2-based surroundings is based on gas transport properties and not chemistry. The experimental data obtained are consistent with this model being adequate to describe the devolatilization process under oxy-fuel conditions.
- The homogeneous chemistry used in the model correctly predicts certain qualities of oxy-fuel combustion observed experimentally and shows promise of greater quantitative

accuracy with further development. The success achieved with the model suggests that NO_X formation in oxy-fuel combustion can be described with the existing knowledge base. Further model development is required to determine if the same may be said of NO_X destruction. As is the case with air combustion (Bose et al., 1988), heterogeneous chemistry is believed to be of minor importance to NO_X in pulverized coal oxy-fuel conditions.

- Initial formation of NO_X in the flames was predicted by the model to be controlled by finite rate chemistry for both air and oxy-fuel combustion. Model predictions and experimental data showed good qualitative agreement (good quantitative agreement was thought to be fortuitous).
- Measured values of NO_X formed in oxy-fuel were far above equilibrium. The extremely low equilibrium levels of NO_X in oxy-fuel gas mixtures have little effect on the finite rate NO_X chemistry.
- Thermal NO_X formation was insignificant in the oxy-fuel conditions studied however, it is predicted by the kinetic model to be the primary pathway for NO_X formed from trace amounts of N_2 present (from air infiltration and other sources).
- Destruction of NO_X by the reverse reactions of the thermal NO_X mechanism was predicted by the model to be important under both air and oxy-fuel conditions.
- Destruction of NO_X by reburning reactions was not predicted by the computational model and this was attributed to inaccuracies in hydrocarbon level predictions. Based on measured hydrocarbon, HCN, and NH_3 data, this pathway is believed to be the dominant means of rapid NO_X destruction observed in the experiments.
- NO_X destruction rates in the fuel-rich zone increased with increased inlet NO concentration caused by supplying NO to the oxidizer. This means that a greater amount of NO_X may be destroyed in a combustion zone supplied with recycled NO_X than in a once-through process. There was insufficient spatial resolution in the experimental data to measure suppression of NO_X formation by increased inlet NO levels, however others have observed this phenomenon (Okazaki and Ando, 1997) and the result is consistent with if not conclusively derived from the data.
- Air combustion shows greater sensitivity to changes in primary SR than oxy-fuel combustion as the SR is increased. This sensitivity is mostly due to the onset of thermal NO_X formation in air as more oxygen becomes available in the primary combustion zone.
- Both air and oxy-fuel combustion have an optimum level of oxidizer staging for low-NO_X emissions that arises from a trade off between NO_X formation and destruction in the primary combustion zone, and NO_X formation as additional oxidizer is mixed into fuel-rich products.
- The optimum primary SR for oxidizer-staged oxy-fuel combustion for low-NO_X is higher than that for air partially because thermal NO_X formation is not significant under oxy-fuel conditions. The higher optimum primary SR found here is consistent with pilot scale tests in turbulent combustion (Farzan et al., 2005) and has the advantages of more of the recycle stream passing through the fuel-rich zone for NO_X reburning, a less intense combustion that may form NO_X at the location of burnout oxidizer mixing, and improved burnout of the fuel.
- At the same primary SR oxy-fuel flames have higher CO, NH_3, HCN, and hydrocarbons than air flames which likely leads to more rapid reburning of NO_X in oxy-fuel. The high levels of nitrogen intermediates increases the potential to form NO_X as burnout oxidizer is added, providing further reason to use higher primary SR under oxy-fuel conditions.

- In the absence of N_2 to form thermal NO_X in oxy-fuel, high temperatures and higher primary SR can be used to benefit NO_X reduction kinetics without some of the trade-offs inherent in air combustion.
- Due to differences in thermal NO_X, reburning rates, and NO_X formation at burnout oxidizer injection, NO_X emissions from a once-through combustor can be lower in oxy-fuel than air combustion, however a further important factor in lower NO_X emissions from oxy-fuel is that a flue gas recycle system only releases a fraction of the furnace exit NO_X to the environment (or CO_2 capture process) while the remainder is sent back to the combustion chamber.

Future Work

Although the objectives of this work have been accomplished, there are still several areas of related research that are of significant interest related to NO formation in oxy-combustion and oxy-combustion in general.

This work was completed in a laminar, steady-flow reactor which was valuable in separating the processes involved in NO_X formation and destruction. Data from a swirl-stabilized, turbulent flame would be valuable for two reasons: 1. To demonstrate that NO_X trends in industrial coal flames will behave similar to those seen in the laminar flow reactor. 2. A detailed data set useful for comprehensive coal combustion modeling and validating oxy-combustion models is needed. Industrial pilot scale measurements have been completed but more detailed data are needed as well as data that can be shared in the public domain.

This work shows modeling results and some data that suggest oxy-combustion can produce lower NO if combustion temperatures are increased. This trend is opposite of what is known to happen in air combustion and therefore may require more complete data in order to be accepted. The theoretical basis is sound but additional experimental evidence is needed. Leakage of air containing nitrogen into the system will jeopardize this approach because of the higher nitrogen content. Data demonstrating this strategy and investigating the amount of air leakage that could be tolerated would be valuable.

While a detailed NO_X model was completed in this project, the large mechanisms investigated are not suitable for comprehensive CFD based models. A simplified model using a reduced mechanism is needed. Unfortunately, this work suggests reburning reactions are important and therefore large portions of the mechanism must be considered. While this task does not appear to be easy, the modeling of NO_X in oxy-combustion continues to be of considerable interest.

Several additional issues continue to be critical to understanding oxy-combustion. These include heat transfer, soot formation, deposition, and corrosion. The higher levels of CO_2 and potentially lower soot levels will increase the importance of gas phase heat transfer. The changes in heat transfer caused by oxy-combustion need to be understood but the increased CO_2 and H_2O concentrations cannot currently be modeled accurately. The higher concentrations of all gasses caused by flue gas recycle is expected to alter deposition and corrosion rates. Experiments with controlled recycled temperature are needed to help determine the best strategy for flue gas recycle and to measure the influence of recycled gasses on corrosion.

Cost Status

The total project costs were spent almost precisely according to budget. The travel budget was slightly overspent with student wages and supplies slightly underspent. The extra travel budget was used to send a student to conferences where he gained valuable experience presenting papers.

Completion of Scheduled Tasks

Several new objectives have been added to the project since the beginning of the contract. As a result, the list of milestones was separated into two categories, original and new milestones. The list of milestones is reviewed for completeness below.

Original Milestones

1. Modification of the FFB to run using simulated oxy-fuel combustion, Jan 2006 – Completed
2. Modification of the MFR to run with simulated oxy-fuel combustion, Feb 2006 – Completed
3. Completion of initial FFB char and gas analysis matrix, Aug. 2006 – Completed
4. Completion of the initial MFR temperature, NO and, ash collection, Aug. 2006 –Completed
5. Completion and shake-down of the NMFR reactor, Jan. 2007 – Completed
6. Complete air and oxy-combustion NO_x profiles with 500 ppm NO added to the reactants to determine the extent of reburning in oxy-combustion, March 2008 – Completed
7. Collection of oxy-fuel data in the NMFR, Aug. 2007, Cancelled, No reason to switch reactors, more data can be acquired in the old reactor at this time.
8. Supply Air Liquide with reduced mechanism and boundary conditions to model the BYU MFR. (Added March 2007) – Completed
9. Modification of the NMFR for non-premixed experiments, Cancelled, More can be learned from the premixed experiments at this time.
10. Final Report, Sept. 2008

New Milestones

1. Complete a staged combustion experiment of NOx and major gas species profiles in the MFR reactor. Completed April 2007
    a. Repeat experiments planned with additional fuels – Completed
2. Produce a full kinetic mechanism model of oxy-fuel combustion. Gas phase completed September 2007.
3. Add a char oxidation model with gasification reactions – Completed March 2008
4. Add a model of NO reduction at the char surface – Cancelled as literature search reveals this mechanism is probably insignificant at temperatures relevant to PC combustion.
5. Measure NH_3 and HCN and increase the spatial resolution of the staged combustion data – High resolution sampling ports completed March 2008, improved for centerline access April 2008, HCN and NH_3 measurements completed May 2008.
6. Repeat data for sub-bituminous coal – Completed May 2008
7. Improve the particle size aspect of the model to improve burnout predictions – Unable to complete this added task.
8. Try the SKG03 gas-phase kinetic mechanism (Skreiberg et al., 2004) to determine if more accurate NOx destruction rates are predicted – Completed

Table 17. Original project tasks by quarter. Scheduled "o" and Completed "x"

Tasks/Time	Q1	Q2	Q3	Q4	Q5	Q6	Q7	Q8	Q9	Q10	Q11	Q12
Flat Flame Burner Experiments												
Sieve and prepare coal	xx											
Modify FFB for CO_2		x										
Shake-down facility with CO_2/O_2		x										
Collect Sample in Air		x										
Learn to run the FFB	xxx											
Learn to use the FTIR		oo										
Collect coal/char samples		xx	xxx	ooo				xxx				
Analyze FTIR Data			ooo	ooo					xxx	Xxx		
Analyze char samples			ooo	ooo					xxx			
Repeat data where needed				xxx	xxx	o						
Multi-Fuel Reactor Experiments												
Modify reactor to run on CO_2/O_2		xx										
Shake-down modified reactor		xx										
Learn to operate FTIR analyzer		oo				xxx		xxx				
Collect Gas, temp., and ash data			xxx	xxx	xxx	xxx	xxx	xxx	xxx			
Take and analyze SEM images			oox	ooo	xxx	ooo						
Analyze data			xxx	ooo	xxx	ooo			xxx	Xxx		
Repeat selected experiments				xxx	xxx	ooo			xxx	Xxx		
Set up reactor for doped NO test				x	ooo				oox			
Collect NO profiles for doped NO test					oo	ooo				Xxx		
Set up reactor for staged combustion					xxx							
Collect staged combustion NO profiles					oox	ooo	xxx	xxx	xxx	Xxx		
NMFR Experiments												
Complete Construction of Sections			oox	xxx								
Add fuel feed system			ooo	ooo								
Add and shake-down preheater			ooo	ooo	xxx	xxx						
Convert flows from MFR to NMFR						xxx						
Convert DAQ from MFR to NMFR						ooo	oo					
Shake-down NMFR with coal firing						ooo	oo					
Add a second coal feed system						xxx						
Repeat MFR tests						ooo	ooo	ooo				

Table 18. New Project Tasks

Tasks/Time	Q1	Q2	Q3	Q4	Q5	Q6	Q7	Q8	Q9	Q10	Q11	Q12
Staged NO Profile Measurements						xxx			xxx			
Full Kinetic Mechanism Model								xxx				
Char oxidation & gasification model									ooo	oox		
Increased Resolution of near burner region										xxx		
Measurement of NH_3 and HCN										xxx		
Repeat Measurements on sub-bituminous coal										xxx		

Technology Transfer

Two journal articles are underway to document this work. One will deal with the measurements and a second the model.

Air Liquide has been in regular contact with BYU regarding this project and is now interested in a follow up project related to oxy-combustion. Dr. Nicolas Doquier visited BYY in October 2008 to attend the dissertation defense of Andrew Mackrory and internalize the information obtained.

References

Allam, R. J., R. S. Panesar, V. White, D. Dillon (2005) *Optimising the design of an Oxyfuel-Fired Supercritical PF Boiler*, The 30th International Technical Conference on Coal Utilization and Fuel Systems, April 17-21, 2005, Clearwater, FL.

Andersson, K. (2007) *Combustion Tests and Modeling of the Oxy-fuel Process, An Overview of Research Activities at Chalmers University*, 2nd IEAGHG International Oxy-combustion Workshop, January 25-26, 2007, Windsor, CT.

Asay, B. W. (1982) *Effects of Coal Type and Moisture Content on Burnout and Nitrogeneous Pollutant Formation*, Ph.D. Dissertation, Brigham Young University, Provo, UT.

Bose, A. C., K. M. Dannecker, J. O. L. Wendt (1988) *Coal Composition Effects on Mechanisms Governing the Destruction of NO and Other Nitrogenous Species during Fuel-Rich Combustion*, Energy and Fuels 2:301-308.

Bowman, C. T. (1997) *Mechanisms and Modeling of Gas-Phase Aftertreatment Methods for NO Removal from Combustion Products*, Physical and chemical aspects of combustion; a tribute to Irvin Glassman, 29-68, Edited by F. L. Dryer and R. F. Sawyer, Gordon and Breach.

Brown, B. W., L. D. Smoot, P. J. Smith, P. O. Hedman (1988) *Measurement and Prediction of Entrained-Flow Gasification Processes*, AIChE Journal, Vol. 34, No. 3, 435-446.

Buhre, B. J. P., L. K. Elliott, C. D. Sheng, R. P. Gupta, T. F. Wall (2005) *Oxy-fuel combustion technology for coal-fired power generation*, Progress in Energy and Combustion Science, Vol. 31, 283-307.

De Soete, G. G. (1975) *Overall Reaction Rates of NO and N_2 Formation from Fuel Nitrogen*, Fifteenth Symposium (International) on Combustion, pages 1093-1102, The Combustion Institute.

Dhungel, B., J. Maier, G. Scheffknecht (2007) *Emission Behaviour During Oxy-Coal Combustion*, AIChE 2007 Annual Meeting, November 4-9, Salt Lake City, UT.

Farzan, H., S. J. Vecci, F. Châtel-Pélage, P. Pranda, A. C. Bose (2005) *Pilot-Scale Evaluation of Coal Combustion in an Oxygen-Enriched Recycled Flue Gas*, The 30th International Technical Conference on Coal Utilization and Fuel Systems, April 17-21, 2005, Clearwater, FL.

Fletcher, T. H., A. R. Kerstein, R. J. Pugmire, M Solum, D. M. Grant (1992) *A Chemical Percolation Model for Devolatilization: Milestone Report*, Sandia Report SAND92-8207, available through National Technical Information Service, May 1992.

Fletcher, T. H., A. R. Kerstein, R. J. Pugmire, M. S. Solum, and D. M. Grant, "A Chemical Model of Coal Devolatilization: 3. Direct Use of ^{13}C NMR Data to Predict Effects of Coal Type," *Energy and Fuels,* 6(4), 414-431 (1992).

Genetti, D., T. H. Fletcher (1999) *Modeling Nitrogen Release during Devolatilization on the Basis of Chemical Structure of Coal*, Energy and Fuels, Vol. 13, 1082-1091.

Glarborg, P., A. D. Jensen, J. E. Johnsson (2003) *Fuel nitrogen conversion in solid fuel fired systems*, Progress in Energy and Combustion Science, Vol. 29, 89-113.

Goetz, G. J., N. Y. Nsakala, R. L. Patel, T. C. Lao (1982) *Combustion and Gasification Characteristics of Chars from Four Commercially Significant Coals of Different Rank*, Combustion Engineering, Inc., Windsor, CT.

Goodwin, D. G. (2003), *An open-source, extensible software suite for CVD process simulation*, Chemical Vapor Deposition XVI and EUROCVD 14, M. Allendorf, F. Maury and F. Teyssandier, editors, Electrochemical Society, 155-162.

Gordon, S., B. J. McBride (1994) *Computer Program for Calculation of Complex Chemical Equilibrium Compositions and Applications I. Analysis*, NASA Reference Publication 1311, October 1994.

Grant, D. M., R. J. Pugmire, T. H. Fletcher, A. R. Kerstein (1989) *A Chemical Model of Coal Devolatilization Using Percolation Lattice Statistics*, Energy and Fuels, Vol. 3, 175-186.

Hjärtstam, S., K. Andersson, F. Johnsson (2007) *Combustion Characteristics of Lignite-Fired Oxy-Fuel Flames*, The 32nd International Technical Conference on Coal Utilization and Fuel Systems, June 10-15, Clearwater, FL.

Hu, Y. Q., N. Kobayashi, M. Hasatani (2001) *The reduction of recycled-NO_X in coal combustion with O_2/recycled flue gas under low recycling ratio*, Fuel, Vol. 80, 1851-1855.

Hu, Y. Q., N. Kobayashi, M. Hasatani (2003) *Effects of coal properties on recycled-NO_X reduction in coal combustion with O_2/recycled flue* gas, Energy Conversion and Management, Vol. 44, 2331-2340.

Kajitani, S., N. Suzuki, M. Ashizawa, S. Hara (2006) *CO_2 gasification rate analysis of coal char in entrained flow coal gasifier*, Fuel, Vol. 85, 163-169.

Khare, S. P., T. F. Wall, R. P. Gupta, L. K. Elliott, and B. J. P. Buhre (2005) *Retrofitting of Air-Fired pf Plant to Oxy-Fuel: Combustibility and Heat Transfer Impacts*, The 30th International Technical Conference on Coal Utilization and Fuel Systems, April 17-21, 2005, Clearwater, FL.

Kimura, N., K. Omata, T. Kiga, S. Takano, S. Shikisima (1995) *The Characteristics of Pulverized Coal Combustion in O_2/CO_2 Mixtures for CO_2 Recovery*, Energy Conversion and Management, Vol. 36, 805-808.

Molina, A., E. G. Eddings, D. W. Pershing, A. F. Sarofim (2000) *Char nitrogen conversion: implications to emissions from coal-fired utility boilers*, Progress in Energy and Combustion Science, Vol. 26, 507-531.

Molina, A., C. Shaddix (2007) *Ignition and devolatilization of pulverized bituminous coal particles during oxygen/carbon dioxide coal combustion*, Proceedings of the Combustion Institute, Vol. 31, 1905-1912.

Nakayama, S., Y. Noguchi, T. Kiga, S. Miyamae, U. Maeda, M. Kawai, T. Tanaka, K. Koyata, H. Makino (1992) *Pulverized coal combustion in O_2/CO_2 mixtures on a power plant for CO_2 recovery*, Energy Conversion and Management, Vol. 33, 379-386.

Niksa, S. (1996) *Flashchain Theory for Rapid Coal Devolatilization Kinetics. 7. Predicting the Release of Oxygen Species from Various Coals*, Energy and Fuels, Vol. 10, 173-187.

Nozaki, T., S. Takano, T. Kiga (1997) *Analysis of the Flame Formed During Oxidation of Pulverized Coal by an O_2-CO_2 Mixture*, Energy, Vol. 22, 199-205.

Okazaki K., T. Ando (1997) *NO_X Reduction Mechanism in Coal Combustion with Recycled CO_2*, Energy, Vol. 22, 207-215.

Sangras, R. et al. (2004) *Oxycombustion process in pulverized coal-fired boilers: a promising technology for CO_2 capture*, The 29th International Technical Conference on Coal Utilization and Fuel Systems, April 18-22, 2004, Clearwater, FL.

Sarofim, A. F. (2007) *Oxy-fuel Combustion: Progress and Remaining Issues*, 2nd IEAGHG International Oxy-Combustion Workshop, January 25-26, Windsor, CT.

Scheffknecht, G. J. Maier, B. Dhungel, P. Mönckert (2007) *Investigation of Oxy-Coal Combustion in Semi-technical Test Facilities*, Third International Conference on Clean Coal Technologies for our Future, May 15-17, Cagliari, Sardinia, Italy.

Shaddix, C. R., J. J. Murphy (2003) *Coal Char Combustion Reactivity in Oxy-Fuel Applications*, Twentieth Annual International Pittsburgh Coal Conference, September 15-19, Pittsburgh, PA.

Shaddix, C. (2007) *Coal Particle Ignition, Devolatilisation & Char Combustion Kinetics During Oxy-Combustion*, 2nd IEAGHG International Oxy-Combustion Workshop, January 25-26, Windsor, CT.

Shaddix, C., A. Molina (2007) *Effect of CO_2 on Coal Char Combustion Rates in Oxy-fuel Applications*, Pittsburgh Coal Conference, September 10-14, Johannesburg, South Africa.

Skreiberg, Ø., P. Kilpinen, P. Glarborg (2004) *Ammonia chemistry below 1400 K under fuel-rich conditions in a flow reactor*, Combustion and Flame, Vol. 136, 501-518.

Smith, K. L., L. D. Smoot, T. H. Fletcher, R. J. Pugmire (1994) *The Structure and Reaction Processes of Coal*, The Plenum Chemical Engineering Series, Springer, (book).

Smith, G. P., D. M. Golden, M. Frenklach, N. W. Moriarty, B. Eiteneer, M. Goldenberg, C. T. Bowman, R. K. Hanson, S. Song, W. C. Gardiner, Jr., V. V. Lissianski, and Z. Qin (2000) *GRI-Mech 3.0*, http://www.me.berkeley.edu/gri_mech/

Smoot, L. D., P. J. Smith (1985) *Coal combustion and gasification*, The Plenum Chemical Engineering Series, Plenum Press, NY (book).

Smoot, L. D., Editor and co-author (1993) *Fundamentals of Coal Combustion for Clean and Efficient Use*, Elsevier, The Netherlands, (book).

Tan, Y., E. Croiset (2005) *Emissions from Oxy-fuel Combustion of Coal with Flue Gas Recycle*, The 30th International Technical Conference on Coal Utilization & Fuel Systems, April 17 - 21, 2005, Clearwater, FL.

Xu, H., L. D. Smoot, D. R. Tree, S. C. Hill (2001) *Prediction of Nitric Oxide Destruction by Advanced Reburning*, Energy and Fuels, vol. 15, 541-551.

Zabielski, M. F., D. J. Seery, L. G. Dodge (1984) Influence of Mass Transport and Quenching on Nitric Oxide Chemiluminescent Analysis, Environ. Sci. Technol. 18:88-92.

Zhang, H. and T. H. Fletcher, "Nitrogen Transformations during Secondary Coal Pyrolysis," *Energy and Fuels,* **15,** 1512-1522 (2001).

Zevenhoven, R., P. Kilpinen (2002) *Control of pollutants in flue gases and fuel gases*, 2nd ed., ISBN 951-22-5527-8.